

GAMBIT and its Application in the Search for Physics Beyond the Standard Model

Anders Kvellestad^{a,b}, Pat Scott^{a,c}, Martin White^d

^a*Department of Physics, Imperial College London, Blackett Laboratory, Prince Consort Road, London SW7 2AZ, UK*

^b*Department of Physics, University of Oslo, N-0316 Oslo, Norway*

^c*School of Mathematics and Physics, The University of Queensland, St. Lucia, Brisbane, QLD 4072, Australia*

^d*Department of Physics, University of Adelaide, Adelaide, SA 5005, Australia*

Abstract

The Global and Modular Beyond-Standard Model Inference Tool (**GAMBIT**) is an open source software framework for performing global statistical fits of particle physics models, using a wide range of particle and astroparticle data. In this review, we describe the design principles of the package, the statistical and sampling frameworks, the experimental data included, and the first two years of physics results generated with it. This includes supersymmetric models, axion theories, Higgs portal dark matter scenarios and an extension of the Standard Model to include right-handed neutrinos. Owing to the broad spectrum of physics scenarios tackled by the **GAMBIT** community, this also serves as a convenient, self-contained review of the current experimental and theoretical status of the most popular models of dark matter.

Keywords: Supersymmetry, Axions, Global fits, Right-handed neutrinos, Higgs portal dark matter

1. Introduction

The core of the scientific method in the physical sciences is the identification of mathematical theories that describe some aspect of our Universe in terms of a number of free parameters. The use of global statistical fits, in either a Bayesian or frequentist framework, allows us to find the preferred parameter values of a candidate theory given experimental data, and to compare the abilities of different models to describe that data. Our current

knowledge of particle physics is enshrined in the Standard Model (SM), and global fit techniques are routinely used to provide the most accurate estimates of the parameters of the neutrino sector [1–3], the CKM matrix [4], and the electroweak sector [5, 6].

Despite its incredible successes in explaining experimental data, the SM still faces a number of experimental and theoretical challenges. Many if not all of these can be explained by new physics Beyond the Standard Model (BSM). Such physics could show up in a number of experiments, including direct searches for new particles at high energy particle colliders [7–9], measurements of rare Standard Model processes [10–12], direct searches for dark matter [13–15], indirect astroparticle searches for distant annihilation or decay of dark matter [16–18], and cosmological observations [19–21]. Unfortunately, despite the existence of many candidate theories beyond the SM, there is no unambiguous prediction of what we expect to observe, or in which experimental field we expect to observe it. It is therefore highly likely that the next theory of particle physics will have to be pieced together by combining clues from a number of disparate fields and experiments. In the process, it is essential to also consistently combine *null* results in experiments that had the potential to discover a given candidate theory, but failed to do so. Even in the complete absence of positive discoveries in the near future, it is essential to determine which candidate BSM theories are now comfortably excluded, and which regions of which candidate theories are now the most amenable to future discovery.

Global fits of BSM theories have thus been a very active area of research for well over a decade [22–25], with increases in computing power opening the option of exploring models with larger and larger parameter spaces. Nevertheless, it remains a considerable challenge to efficiently explore the high-dimensional parameter spaces of candidate theories whilst rigorously calculating likelihoods for a large range of experiments, each of which may require a costly simulation procedure. To further complicate matters, one must consistently handle systematic uncertainties that may be correlated across different datasets, resulting from either instrumental effects, or our imprecise knowledge of the nuclear, astro- or particle physics relevant to a given set of experiments. Prior to 2017, most global fits were focussed on supersymmetric theories, involving dedicated software that was built from the ground up with a knowledge of the supersymmetric parameters [22–95]. These results typically covered low-dimensional subsets of the minimal supersymmetric SM (MSSM) or, in some cases the next-to-minimal variant, with relatively few

global studies of other theories completed [96–109].

In 2017, the **GAMBIT** collaboration released the Global and Modular Beyond-Standard Model Inference Tool (**GAMBIT**) [110], an open-source package able to produce results in both the Bayesian and frequentist statistical frameworks, and easily extendible to new BSM models and new experimental datasets. A fully modular design enables much of the code to be reused when changing the theoretical model of interest. **GAMBIT** includes a wide variety of efficient sampling algorithms for posterior evaluation and optimisation, and ensures computational efficiency through massive, multi-level parallelisation, both of the sampling algorithms and individual likelihood calculations.

The purpose of this article is to give a brief introduction to the **GAMBIT** software and science programme, reviewing the most important results obtained with **GAMBIT** in the first few years since its initial release. These serve to illustrate the versatility of the code in attacking completely different BSM models, and the constraining power of the highly detailed and rigorous simulations of different particle and astroparticle datasets in **GAMBIT**. Given the centrality of dark matter (DM) in the current search for BSM physics, this review also serves as a convenient summary of the status of the most widely-studied DM candidates.

In Section 2, we describe the structure and design of the **GAMBIT** package, including the core framework, the means by which **GAMBIT** supports generic BSM models, the sampling and statistics module, and the various physics modules able to produce theoretical predictions and experimental likelihoods. In Section 3, we summarise the results of recent **GAMBIT** global fits of various supersymmetric theories, Higgs portal and axion DM models, and a right-handed neutrino extension of the SM. We then conclude in Section 4.

2. The **GAMBIT** software

The core **GAMBIT** software is written in C++11, but interfaces seamlessly with extensions and existing physics codes written in Python, Mathematica, Fortran and C. Since the release of **GAMBIT** 1.0.0 in 2017 [110], the most notable updates have been versions 1.1 (adding support for Mathematica) [111], 1.2 (adding support for Python and higher-spin Higgs portal models) [112], 1.3 (adding support for axion and axion-like particles) [113] and 1.4 (adding support for right-handed neutrinos) [114]. The current public release is v1.4.2. The source code is openly available from <http://gambit.hepforge.org> under the 3-clause BSD license.

2.1. Core design

The core principles of **GAMBIT**'s software design are modularity and flexibility. All theoretical predictions and experimental likelihood evaluations are separated into a series of smaller, self-contained sub-calculations, with each sub-calculation represented by a single function. Each function is assigned a metadata string that identifies the physical quantity that the function is able to calculate. Examples might be the mass of the lightest Higgs boson, or the likelihood for the latest run of the LUX direct detection experiment. Functions are further tagged with additional metadata strings indicating any other physical inputs required for them to run. In the case of the Higgs mass, one might require e.g. the SM electroweak vacuum expectation value and the masses and couplings of various other particles. In the case of the LUX likelihood, one might require the number of events observed by LUX, its detector efficiency as a function of nuclear recoil energy, and the theoretically predicted event rate. At runtime, **GAMBIT** identifies which functions are actually required for the analysis of a given theory, and connects them dynamically in order to enable the calculation in the most efficient manner possible.

The individual functions are grouped together according to physics theme, into seven different **physics modules**. We describe these specific modules in Section 2.4 below. Individual functions are thus referred to as **module functions**. The module functions are the true building blocks of a **GAMBIT** analysis, allowing the code to automatically adapt itself to incorporate new observables, likelihoods, theories and experimental datasets. The metadata string associated with the output of a module function is referred to as its **capability**, and the metadata associated with the required inputs are referred to as **dependencies**. The process of dynamically connecting the outputs of module functions to the inputs of others at runtime thus consists of matching dependency strings to the capability strings of other functions (and ensuring that their C++ types also match). This process is known as **dependency resolution**, and is performed by the **GAMBIT** dependency resolver.

The result is a (potentially extremely large) directed graph connecting the outputs and inputs of different module functions, known as a **dependency tree**. The module functions themselves constitute graph nodes, and their resolved dependencies graph edges. An example of such a graph is shown in Fig. 1. For such a graph to constitute a viable computational pathway to all theoretical predictions and experimental likelihoods of interest, two things are required. The first is for the actual numerical values of some dependencies to

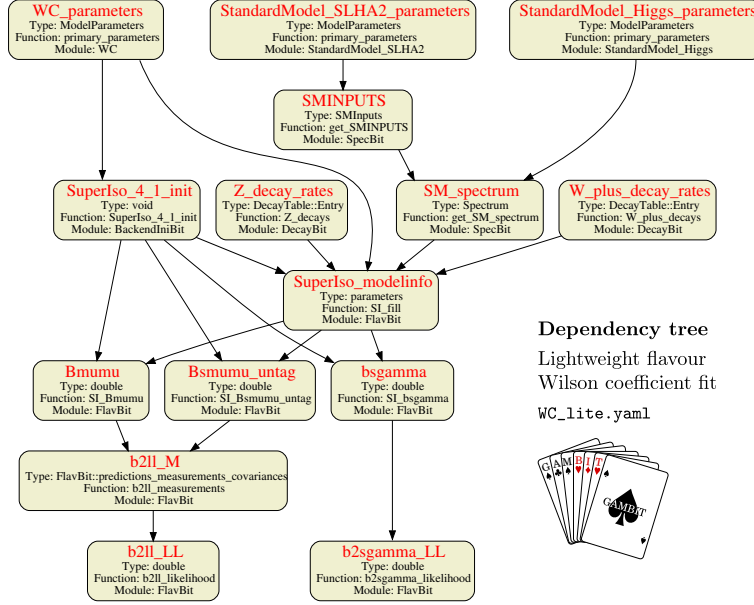


Figure 1: An example GAMBIT dependency tree for a simple fit of flavour Wilson coefficients to $b \rightarrow s\gamma$ and $B \rightarrow ll$ data. Boxes (graph nodes) correspond to single module functions. Function capabilities are marked in red, and return types of the functions, their actual function names and enveloping modules are indicated in black. Arrows (graph edges) indicate the direction of information flow, from the capability (output) of one function to the dependencies (inputs) of others. The input file used to instigate this fit (`WC_lite.yaml`) is one of the example files distributed with GAMBIT. This particular fit makes use of the GAMBIT modules FlavBit, SpecBit and DecayBit, as well as the backend (external package) SuperIso 4.1 [115–117].

be known in advance. These are the parameters of the theory that the user wishes to analyse, and must be chosen ‘from on high’ before the dependency tree can be evaluated. These are selected by the user’s chosen statistical parameter sampling algorithm, discussed below in Section 2.3.

From the values of a model’s parameters, all other intermediate quantities can be obtained, as long as the second criterion is also met. This condition is that no closed loops exist in the graph, i.e. there are no dependencies of any module function upon things that can only be computed by knowing the result of the function. Many algorithms exist within graph theory for taking such a directed acyclic graph and obtaining a linear ordering of its

nodes that respects the underlying structure of the graph. **GAMBIT** uses the **Boost::Graph** library to obtain such an ordering, and then employs that ordering to evaluate the module functions in turn. This ensures that all module functions run before any other functions that depend upon their results. Within topologically equivalent subsets of the ordering, **GAMBIT** also further dynamically optimises the module function evaluation order for speed, according to previous function evaluation times and likelihoods.

Module functions may also make use of functions provided by external packages, or **backends**. These are also connected dynamically at runtime to module functions by the dependency resolver, in much the same way as it ensures that dependencies upon the results of other module functions are fulfilled. This layer of abstraction allows **GAMBIT** to provide its module functions with seamless and interchangeable access to functions from external codes written in C, C++, Python 2, Python 3, Mathematica and all variants of Fortran. The **GAMBIT** build system allows users to select and automatically download, configure and build whatever combination of backends they prefer to use, and the dependency resolver automatically adapts to the presence or absence of different backends when selecting which functions to connect to others. Backends presently supported in version 1.4.2 of **GAMBIT** are Capt’n General [112], DarkSUSY [118, 119], DDCalc [112, 120], FeynHiggs [121–125], gamLike [120], GM2Calc [126], HiggsBounds [127–129], HiggsSignals [130], micrOMEGAs [131–137], nulyke [18, 41], Pythia [138, 139], SPheno [140, 141], SuperIso [115–117], SUSYHD [142] and SUSY-HIT [143]. Many more are also already supported in the current development version, which will be released in 2020.

Actual runs of **GAMBIT** are driven by a single input file, in **YAML** format. In this file, the user selects the model(s) to analyse, gives details of which algorithms to use in order to sample the models’ parameters, and provides a list of all likelihoods and physical observables that should be calculated in the scan. The model parameter values constitute one boundary condition for dependency resolution (the dependency tree must begin from the parameters), and the target likelihoods and observables the other (the final outputs of the tree must be the required likelihoods and observables). The dependency resolver is then responsible for identifying and filling in all the required steps in between. To help direct this process and break degeneracies in the valid choices available to the dependency resolver at each step, the **YAML** input file may also set rules that the dependency resolver must respect. These may be e.g. restrictions about which functions should be selected to fill which

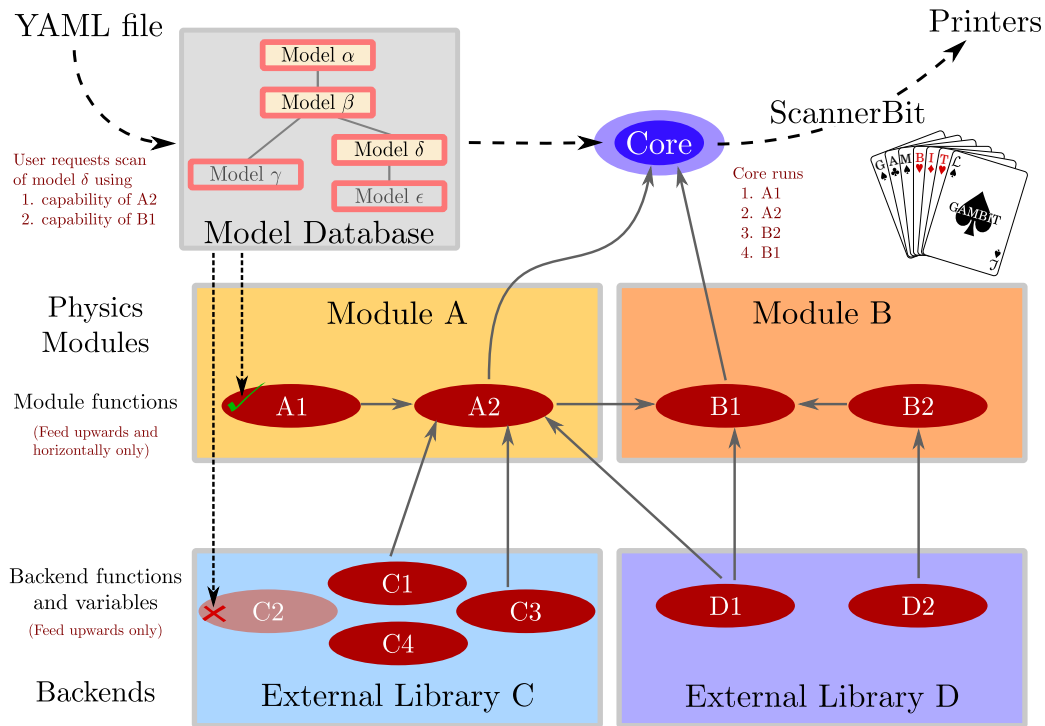


Figure 2: The overall structure of a GAMBIT run, illustrating the roles of the input YAML file, modules, module functions, capabilities, dependencies, backends, backend functions, dependency resolver, hierarchical model database and the sampling machinery. The user specifies one or more models to scan in the input YAML file, and chooses likelihoods and observables to compute in the scan, making their choice by capability rather than by choosing specific functions. The dependency resolver automatically identifies and connects appropriate module and backend functions in order to facilitate the computation of the requested likelihoods and observables, and the scanning machinery (**ScannerBit**) selects parameter combinations to pass through the resulting dependency tree. From [110].

specific dependencies, or which version of a given backend should be used throughout the run. These rules can be arbitrarily complicated, general or specific. A rule can also contain explicit keyword options that will be passed to all module functions that fulfil the rule, allowing enormous control to be exercised over the details of the individual calculations from a single input file.

The core design elements of **GAMBIT** described so far in this section are module functions, backend abstraction, dependency resolution, and an input format that borders on its own programming language. Together, these combine to provide an extremely flexible and extendible framework for performing global analyses of theories for BSM physics. Fig. 2 illustrates how all of these features work together to enable a **GAMBIT** scan. Further technical details can be found in Ref. [110].

2.2. Model support

Another feature illustrated in Fig. 2 is the **GAMBIT** hierarchical model database. Models are defined both in terms of their parameters, and in terms of their relationships to each other via parameter translation routines. Models may descend from one another, meaning that a parameter combination in a child model can be translated ‘up’ its family tree to a point in an appropriate subspace of its parent model, or in any other more distant ancestor model. Cross-family ‘friend’ translation pathways can also be defined. These pathways allow module functions to be designed to work with one model, but to be used with another model without further alteration, so long as a translation pathway exists from one model to the other.

Module functions, backend functions and all rules set in **YAML** files can be endowed with model-specific restrictions. This allows the model-dependence of every sub-calculation to be tracked explicitly, and for the dependency resolver to explicitly ensure that the entire dependency tree of every scan is validated for use with the model under investigation.

The complete model database of **GAMBIT** 1.4.2 is shown in Fig. 3.

2.3. Sampling and statistics

In carrying out a global statistical analysis of a BSM theory, one may be interested in determining which parameter combinations are able to explain the totality of observed data within a given model, and to what extent – or one may be more interested in using the experimental data to choose between entire theories. The first of these tasks is parameter estimation, whereas the

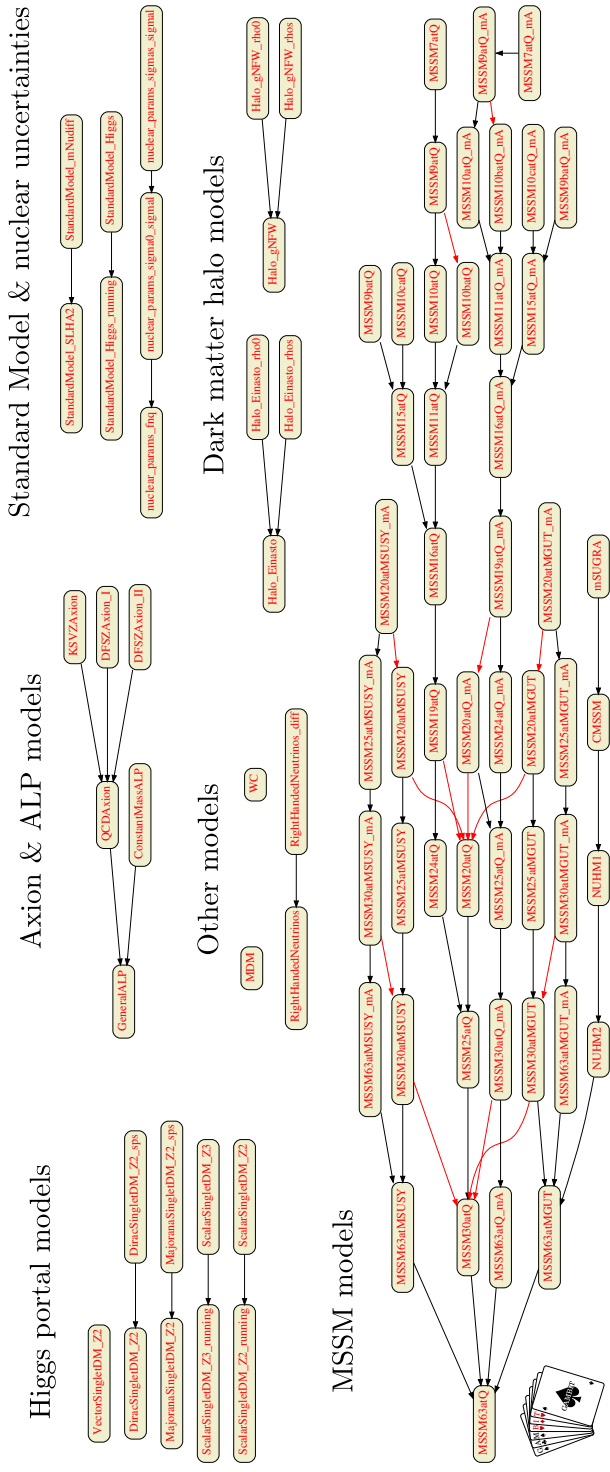


Figure 3: Hierarchical model database of GAMBIT 1.4.2. Models are shown as boxes, child-to-parent translations as black arrows, and friend translations as red arrows.

second is model comparison. There are two philosophically distinct ways of posing both these questions:

1. How probable is it that we would have observed the data that we have, if a model and a specific combination of its parameters were true?
2. How probable is it that a model (or a specific combination of its parameters) is true, given the data that we have observed to date?

Question 1 concerns frequentist statistics, whereas Question 2 is fundamentally Bayesian.

In the context of parameter estimation, the choice of question dictates whether the appropriate quantity to consider is the frequentist profile likelihood, or the Bayesian posterior. The profile likelihood for some parameters of interest $\boldsymbol{\theta}$ is the maximum value of the likelihood at each parameter combination $\boldsymbol{\theta}$, regardless of the values of any other parameters $\boldsymbol{\alpha}$:

$$\hat{\mathcal{L}}(\boldsymbol{\theta}) = \max_{\boldsymbol{\alpha}} \mathcal{L}(\boldsymbol{\theta}, \boldsymbol{\alpha}), \quad (1)$$

where the parameters $\boldsymbol{\alpha}$ are other ‘nuisance’ parameters not of direct interest. Conversely, the Bayesian posterior probability distribution for the parameters $\boldsymbol{\theta}$ is given by Bayes’ Theorem as the integral of the likelihood over $\boldsymbol{\alpha}$, weighted by ones prior belief $\pi(\boldsymbol{\theta}, \boldsymbol{\alpha})$ as to the plausibility of different values of $\boldsymbol{\theta}$ and $\boldsymbol{\alpha}$:

$$\mathcal{P}(\boldsymbol{\theta}) = \int \mathcal{P}(\boldsymbol{\theta}, \boldsymbol{\alpha}) d\boldsymbol{\alpha} = \frac{1}{\mathbb{Z}} \int \mathcal{L}(\boldsymbol{\theta}, \boldsymbol{\alpha}) \pi(\boldsymbol{\theta}, \boldsymbol{\alpha}) d\boldsymbol{\alpha}. \quad (2)$$

Here $\mathbb{Z} \equiv \int \mathcal{L}(\boldsymbol{\theta}, \boldsymbol{\alpha}) \pi(\boldsymbol{\theta}, \boldsymbol{\alpha}) d\boldsymbol{\alpha} d\boldsymbol{\theta}$ is a normalisation factor referred to as the model evidence; taking ratios of evidences of different models is the most common method of Bayesian model comparison. In contrast, frequentist model testing typically involves building up the distribution of the likelihood or other test statistic by simulation, in order to determine the precise probability of obtaining the observed (or worse-fitting) data if the model is assumed to be correct.

The choice of Bayesian posterior or profile likelihood has strong implications for the required design of the algorithm with which to sample the model parameters: efficiently obtaining converged estimates of profile likelihood and posterior distributions requires drastically different sampling distributions. In neither case is random sampling at all sufficient nor correct, whether for accurate estimation of statistical properties nor for making statements about what is ‘typical’ or ‘normal’ within the parameter space of a given

theory. Efficient profile likelihood evaluation requires fast location of and convergence towards the maximum likelihood, whereas efficient posterior and evidence evaluation requires samples obtained with a density approximately proportional to the value of the posterior itself (as indeed is the case in most other numerical integration problems).

Sampling and statistical considerations in **GAMBIT** are handled mostly by the **ScannerBit** module [144]. It contains all the tools necessary to transform the likelihood function provided by the dependency resolver into converged profile likelihoods and Bayesian posteriors. It also facilitates Bayesian model comparison by calculating evidences (see e.g. Refs. [112, 113] for recent examples), and frequentist model testing by providing information that can be used to perform statistical simulations (see Ref. [145] for a detailed example).

For Bayesian analyses, **ScannerBit** provides a series of different prior transformations, allowing the user to choose what assumptions to make about the probabilities of different model parameter at the beginning of a run, and to sample accordingly.

ScannerBit contains interfaces to various built-in and external implementations of a number of leading sampling algorithms. These include algorithms optimised for profile likelihood evaluation, and algorithms optimised for posterior and evidence calculations. Amongst these are **T-Walk** [144], a built-in ensemble Markov Chain Monte Carlo (MCMC) well suited to posterior evaluation, **GreAT** [146], a regular MCMC, **Diver** [144], a differential evolution optimiser able to efficiently map profile likelihoods, and **MultiNest** [147, 148] and **polychord** [149], nested samplers well suited to evidence and posterior evaluation. Detailed performance comparisons between the different samplers can be found in Ref. [144].

For consistency and the convenience of module function writers, **GAMBIT** also provides a series of relatively simple pre-profiled and pre-marginalised likelihood functions [110]. These functions provide likelihoods where the influence of one or more Gaussian or log-normally distributed nuisance parameters is profiled or integrated out without the assistance of explicit sampling by **ScannerBit**.

2.4. Physics modules

The physics content of **GAMBIT** currently resides in seven modules, which contain the module and backend functions relevant for all necessary theoretical calculations, simulations of particle astrophysics experiments and likelihood calculations. Future **GAMBIT** updates will both refine the code in each module,

and add new modules for new branches of physics (such as the forthcoming CosmoBit module).

2.4.1. *SpecBit*

BSM physics theories necessarily introduce new particles. The first step in evaluating the likelihood of any parameter combination in a new theory is typically to calculate the masses and decay branching fractions of the new particles. These calculations get very complicated once one moves beyond tree level, as loop corrections can involve any number of new states in the theory, and loop corrections that shift the masses and decays of the existing SM particles must also be taken into account.

Particle mass and coupling calculations are handled in the **SpecBit** module, which includes module functions for obtaining the pole masses and mixings of all new physical states in a model, scheme-dependent quantities such as those defined in the \overline{DR} and \overline{MS} schemes, and SM masses and couplings (e.g. couplings of the SM-like Higgs). Generally, this information is obtained by running an appropriate spectrum generator but, in the simple case that the pole masses of a model are specified as input parameters, **SpecBit** simply formats the information to match that expected from a spectrum generator. In any case, it is important to realise that a spectrum cannot be stored simply as a set of numbers, since different experimental likelihoods may require predictions of running particle properties at different physical scales. Thus, **SpecBit** facilitates the passing of a spectrum object to module functions that contains knowledge of the renormalisation group equations of a model, allowing module functions in other parts of the **GAMBIT** code to locally run the \overline{DR} or \overline{MS} parameters to the appropriate scale. Although **SpecBit** can be extended to include any model, its development has tended to proceed through updates that add functionality for the specific models targeted in **GAMBIT** physics papers. To date, this includes functions for GUT-[150] and weak-scale [145, 151] parameterisations of the MSSM, singlet DM models with either a scalar, fermion or vector DM candidate [112, 152, 153], minimal electroweak triplet and quintuplet DM [154, 155], and a low-energy object that holds SM-like particle information. A range of backends is used to supply the **SpecBit** calculations, including **SPheno** [140, 141] and **FlexibleSUSY** [156] for BSM mass spectrum calculations. The latter is typically used for all spectrum generation requirements outside of the MSSM, including for the scalar singlet model examples described in this review. The Higgs and W masses can also be calculated via the **FeynHiggs** [121–125, 157] backend.

2.4.2. *DecayBit*

Particle decay calculations are handled by the **DecayBit** module, after accepting the masses and couplings of particles from **SpecBit**. These are used to calculate decay widths and branching fractions for each particle, which are stored in a single decay table entry for each particle. The collection of entries is then gathered into a full **GAMBIT** decay table, which is passed on to other **GAMBIT** modules.

DecayBit includes known SM particle decays, modifications of SM particle decays through new physics effects, and the decays of BSM particles. For the SM, **DecayBit** contains the Particle Data Group results for the total widths for the W , Z , t , b , τ and μ (plus antiparticles), and for the most common mesons π^0 , π^\pm , η , ρ^0 , ρ^\pm and ω [158]. In addition, partial widths to all distinct final states are provided for W , Z , t , b , τ , μ , π^0 and π^\pm . These “pure SM” decays are used in **GAMBIT** whenever an SM decay acquires no BSM contribution in a model, or when the only effect of the BSM physics is to introduce a new decay channel, in which case the pure SM decays can be appended to the new list of decay channels. For the pure SM Higgs boson, the user can decide whether to calculate the partial and total decay widths at the predicted value of the Higgs mass with **FeynHiggs**, or to use pre-computed tables provided in **DecayBit**, sourced from Ref. [159].

BSM decays are handled on a model-by-model basis. For Higgs portal DM models, **DecayBit** contains analytic expressions for the partial width for a Higgs decay to two DM particles, and this decay is added to the list of SM Higgs partial widths, before rescaling the decay branching fractions and the total width. For MSSM variants, **DecayBit** calculates both the decays of all sparticles and additional Higgs bosons, and the SUSY corrections to the decays of the SM-like Higgs boson and the top quark. Higgs decay results may be sourced from either **HDECAY** via **SUSY-HIT**, or **FeynHiggs**, whilst top quark decays are only available via **FeynHiggs**. Sparticle decays are obtained from **SDECAY** via **SUSY-HIT**, but we note that a patch to the code is required to allow **GAMBIT** to call functions from a shared library, and to solve problems with negative decay widths for some models due to large and negative 1-loop QCD corrections. Full details are given in [160]; the patch is applied automatically when **SUSY-HIT** is retrieved and built from within **GAMBIT**.

A recent update of **DecayBit** has seen the addition of routines for observables relating to right-handed neutrino studies. This includes the in-

visible decay width of the Z boson Γ_{inv} , and the leptonic W boson decay widths $\Gamma_{W \rightarrow e\bar{\nu}_e}$, $\Gamma_{W \rightarrow \mu\bar{\nu}_\mu}$ and $\Gamma_{W \rightarrow \tau\bar{\nu}_\tau}$. Measurements and uncertainties are taken from Ref. [161], whilst theoretical results are taken from Refs. [162, 163, 163, 164, 164–168].

2.4.3. *PrecisionBit*

Some of the most severe constraints on BSM physics scenarios come from precision measurements of the electroweak sector, and other SM quantities. In **GAMBIT**, these are handled by the **PrecisionBit** module, which provides nuisance likelihoods for SM quantities such as the top quark mass and strong coupling constant, which have been measured with high precision. A related function is the calculation of the BSM corrections to SM observables such as the mass of the W boson and the weak mixing angle, and the provision of likelihood functions that compare these predictions with experimental data.

A schematic representation of **PrecisionBit** is shown in Fig. 4, providing our first interesting example of the interaction between **GAMBIT** modules. Standard Model parameters that do not require BSM correction calculations are provided directly by the **GAMBIT** SM model, and are used in the calculation of SM nuisance likelihoods. The BSM parameters, meanwhile, are first used by **SpecBit** in the calculation of particle masses, couplings and precision Higgs properties. **PrecisionBit** then updates the results to form a precision-updated spectrum (including a dedicated calculation of the W mass) which is used for calculating Higgs and W mass likelihoods, in addition to a suite of electroweak precision observables (EWPO).

Likelihoods exist for the Fermi coupling constant (G_F), the fine-structure constant (α_{em}), the \overline{MS} light quark (u, d, s) masses at $\mu = 2$ GeV, the charm ($m_c(m_c)$) and bottom ($m_b(m_b)$) masses, and the W , Z and Higgs boson masses. There are also calculations and likelihoods for other precision observables such as the anomalous magnetic moment of the muon $a_\mu = \frac{1}{2}(g - 2)_\mu$, the effective leptonic weak mixing angle $\sin^2\theta_{W,eff}$, and the departure from 1 of the ratio of the Fermi constants implied by the neutral and weak currents $\Delta\rho$. Note that, for the full suite of observables, calculations are currently only included for the MSSM; calculations for other models will be added as the corresponding models are implemented in **GAMBIT**.

Like **DecayBit**, **PrecisionBit** has also recently been updated to include observables for right-handed neutrino studies. These consist of right-handed neutrino contributions to m_W and $\sin^2\theta_{W,eff}$.

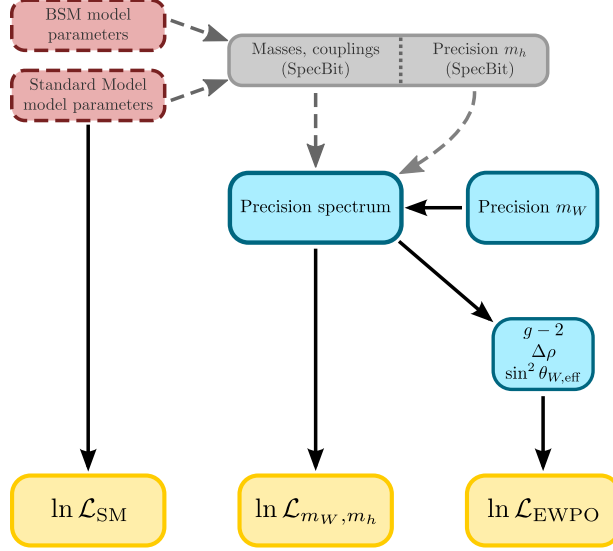


Figure 4: Schematic representation of the structure of **PrecisionBit**. From [160].

2.4.4. *DarkBit*

BSM physics models that include particle DM candidates can potentially give rise to observable consequences in a wide range of astrophysical DM experiments.

In gamma-ray indirect detection, the **DarkBit** module contains a dedicated signal yield calculator, along with an interface to **gamLike**, a likelihood calculator for current and future gamma-ray experiments. This combination can cope with signatures that result from an arbitrary mixture of final states, which significantly extends previous tools.

Further indirect detection constraints come from an interface to the **nulike** neutrino telescope likelihood package [18].

Direct DM search experiments are handled by the dedicated **DDCalc** package, which can be extended to include the effects of generic interactions between Weakly Interacting Massive Particles (WIMPs) and nucleons, as parameterised through effective operators. This includes both spin-dependent and spin-independent scattering. The package models a wide range of direct search experiments including Xenon100, SuperCDMS, SIMPLE, LUX, PandaX, PICO-60 and PICO-2L.

Finally, the relic density of dark matter can be computed via interfaces to **DarkSUSY** and **micrOMEGAs** [119, 169], and used to constrain models by

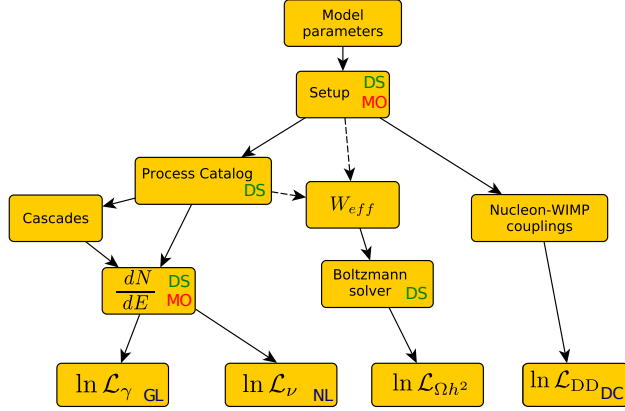


Figure 5: Schematic overview of the DarkBit module. The two-letter insets indicate what backend codes can be used: DarkSUSY (DS), micrOMEGAs (MO), gamLike (GL), nulyke (NL) and DDCalc (DC). From [120].

computing a likelihood based on the value observed by *Planck* [170].

The basic structure of **DarkBit** applicable to WIMP theories is sketched in Fig. 5, providing a good example of **GAMBIT**’s modular design principle. None of the likelihoods requires knowledge of the BSM physics parameters, instead only requiring knowledge of derived quantities that can be shared between likelihood calculations. The first step in **DarkBit** is to create a Process Catalogue containing information on particle annihilation processes, using the particle masses and couplings provided by **SpecBit**. For indirect detection calculations, this is used to create the gamma ray or neutrino spectrum of the annihilation products, via a weighted sum of individual contributions. For long decay chains, a native cascade decay Monte Carlo generator is used. This final annihilation spectrum is then passed to the likelihood calculators for gamma ray and neutrino telescope experiments. The Process Catalogue is also used to provide the effective annihilation rate for relic density calculations, which is then passed to a Boltzmann solver, followed by the relic density likelihood calculator. For direct detection signatures, the model parameters are used to set the WIMP-nucleon couplings, which are then used in the calculation of the direct detection likelihood via the **DDCalc** package.

A recent update of **DarkBit** has added various module functions required for the calculation of axion observables and likelihoods. The included observables are detailed in Section 3.3.2.

An important additional function of **DarkBit** is to constrain nuisance

parameters for various astrophysical unknowns that strongly affect direct and indirect searches for DM. **DarkBit** contains likelihoods for the parameters of the local DM spatial and velocity distributions, plus the nuclear matrix elements that enter direct search WIMP-nucleon scattering calculations.

2.4.5. *FlavBit*

A very powerful indirect probe of BSM physics comes from the measurement of flavour physics processes, as theoretical predictions for these observables would be shifted by loop corrections from new particles. The excellent precision of flavour physics measurements allows them to be sensitive to much higher energy scales than direct searches for new particles. Indeed, recent measurements from the LHCb experiment [171–177] and from B factories [178–186] show tensions with the SM that are generating a considerable amount of theoretical interest.

FlavBit implements flavour physics constraints from rare decay observables using the effective Hamiltonian approach, in which the cross-sections for transitions from initial states i to final states f are proportional to the squared matrix elements $|\langle f | \mathcal{H}_{\text{eff}} | i \rangle|^2$. For example, an effective Hamiltonian for $b \rightarrow s$ transitions given by

$$\mathcal{H}_{\text{eff}} = -\frac{4G_F}{\sqrt{2}} V_{tb} V_{ts}^* \sum_{i=1}^{10} \left(C_i(\mu) \mathcal{O}_i(\mu) + C'_i(\mu) \mathcal{O}'_i(\mu) \right). \quad (3)$$

The local operators \mathcal{O}_i represent long-distance interactions. The Wilson coefficients C_i can be calculated using perturbative methods, by requiring matching between the high-scale theory and the low-energy effective theory, at some scale μ_W which is of the order of m_W . The Wilson coefficients can then be evolved to the characteristic scale for B physics calculations (μ_b , of the order of the b quark mass) using the renormalisation group equations of the *effective* field theory. A similar approach can be taken to $b \rightarrow d$ transitions, using a different basis of low-energy operators. The original list of observables in **FlavBit** was divided into four categories:

- **Tree-level leptonic and semi-leptonic decays:** includes decays of B and D mesons to leptons, including $B^\pm \rightarrow \tau \nu_\tau$, $B \rightarrow D^{(*)} \tau \nu_\tau$ and $B \rightarrow D^{(*)} \ell \nu_\ell$.
- **Electroweak penguin transitions:** includes measurements of rare decays of the form $B \rightarrow M \ell^+ \ell^-$ (where M is a meson with a smaller

mass than the parent meson), such as angular observables of the decay $B^0 \rightarrow K^{*0} \mu^+ \mu^-$.

- **Rare purely leptonic decays:** includes B decays with only leptons in the final state, such as $B_{(s)}^0 \rightarrow \mu^+ \mu^-$.
- **Other observables:** includes $b \rightarrow s$ transitions in the radiative decays $B \rightarrow X_s \gamma$, the mass difference (ΔM_s between the heavy B_H and light B_L eigenstates of the B_s^0 system, and kaon and pion decays (e.g. the leptonic decay ratio $\mathcal{B}(K^\pm \rightarrow \mu \nu_\mu) / \mathcal{B}(\pi^\pm \rightarrow \mu \nu_\mu)$).

Theoretical calculations for these processes are handled via an interface to **SuperIso** [115–117]. Experimental results used in the calculation of likelihoods come from a variety of sources, including the PDG, the BaBar and Belle experiments, the HFAG collaboration and the LHCb experiment. Full details are given in [187].

More recently, **FlavBit** has been updated with observables relevant to right-handed neutrinos. These include:

- **Lepton-flavour violating (LFV) muon and tau decay searches** performed by the MEG, BaBar, Belle, ATLAS, LHCb and SINDRUM collaborations [188–195]. LFV processes can also result in a neutrinoless $\mu - e$ conversion inside a nucleus, and these are included in the form of three results using Ti, Pb and Au nuclei obtained by the SINDRUM II experiment [196–198].
- **Tests of lepton universality violation** in the semileptonic decays of B mesons $B^{0/\pm} \rightarrow X^{0/\pm} l^+ l^-$, as performed by LHCb [174, 199].

A forthcoming major update to the **FlavBit** module will add an interface for **SuperIso 4**, with added support for theory uncertainty covariance matrices. The experimental likelihoods will also receive an update, via a new interface to the **HEPLike** package [200].

2.4.6. *ColliderBit*

A leading source of constraints on BSM physics models comes from high-energy collider searches for new particles, plus the relatively recent measurements of the Higgs boson mass and decay branching fractions. The **ColliderBit** module includes the most comprehensive list of recent LHC particle searches

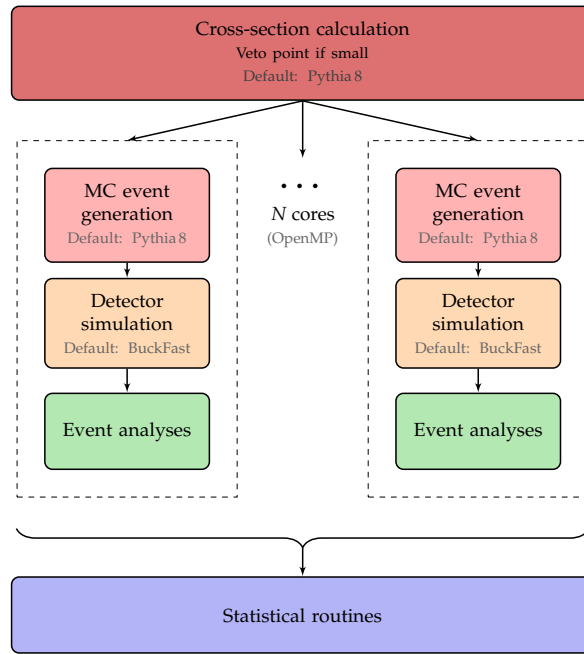


Figure 6: Schematic diagram of the ColliderBit processing chain for LHC likelihoods. From [201].

of any public package, alongside a new interpolation of LEP results for supersymmetric particle searches. Higgs signal strength and mass measurements (including limits on possible signatures arising from new Higgs bosons) are handled via an interface to the **HiggsSignals** [130] and **HiggsBounds** [127, 128] packages, which includes data from LEP, the Tevatron and the LHC.

LHC constraints are particularly difficult to model rigorously for general models. Searches for new particles are often optimised on, and interpreted in terms of, so-called “simplified models”, which feature only a few options from the much broader phenomenology of the parent model. For example, searches for supersymmetric particles might assume that only a particular pair of sparticles is ever produced, with decays fixed to a particular final state. The resulting exclusion limit will never apply directly to a more general model, although one can obtain approximate limits by scaling individual simplified model limits by the known cross-sections and branching ratios for each parameter point [202, 203].

In **ColliderBit**, we provide more rigorous limits by performing an actual reproduction of the ATLAS and CMS limit-setting procedures, as shown in Fig. 6. This includes a cross-section calculation for new particle production processes, followed by Monte Carlo simulation of LHC events for each parameter point using a custom parallelised version of the **Pythia 8** generator [138, 139]. The results can either be fed at the truth level into code that reproduces the kinematic selections of a wide range of LHC analyses, or passed through a custom detector simulation based on four-vector smearing before analysis. Cross-sections are currently taken at leading order (plus leading log) from **Pythia 8**, but a forthcoming update will allow user-specified cross-sections. The final step of the process is to calculate a combined likelihood by either taking the signal region in a given final state for each experiment that is expected to have the highest sensitivity to the model in question, or by using a covariance matrix for analyses in cases where this is published by the relevant experimental collaboration. The list of **ColliderBit** analyses is continually updated, and currently includes a broad selection of searches for supersymmetric particles, plus monojet searches for DM particles.

2.4.7. *NeutrinoBit*

The **NeutrinoBit** module contains a variety of module functions for calculating observables and likelihoods in the neutrino sector, both for SM(-like) neutrinos and for right-handed neutrinos (RHNs). RHNs could cause observable consequences in a number of experiments, although it should be

noted that the recent **GAMBIT** study focussed on models that are capable of explaining the light neutrino oscillation data, which excludes most sterile neutrino dark matter models. This is because long-lived RHNs would require very small couplings with SM matter, in which case their contribution to light neutrino mass generation is negligible.

NeutrinoBit currently contains likelihoods dealing with the following classes of experimental data:

- **Active neutrino mixing:** **NeutrinoBit** includes likelihoods for the 3-flavour SM-like active neutrino mixing observables θ_{12} , θ_{13} , θ_{23} (mixing angles), δ_{CP} (CP-phase) and Δm_{21}^2 and $\Delta m_{3\ell}^2$ (mass splittings) with $\ell = 1$ for normal mass ordering and $\ell = 2$ for inverted mass ordering. The likelihoods use the one-dimensional $\Delta\chi^2$ tables provided by the NuFIT collaboration [204, 205]. These in turn include results from the solar neutrino experiments Homestake (chlorine) [206], Gallex/GNO [207], SAGE [208], SNO [209], the four phases of Super-Kamiokande [210–212] and two phases of Borexino [213–215]. They also include results from the atmospheric experiments IceCube/DeepCore [216], the reactor experiments KamLAND [217], Double-Chooz [218], Daya-Bay [219] and Reno [220], the accelerator experiments MINOS [221, 222], T2K [223] and NO ν A [224], and the cosmic microwave background results from Planck [225].
- **Lepton universality:** **NeutrinoBit** contains likelihoods for lepton universality violation in fully leptonic decays of charged mesons, $X^+ \rightarrow l^+\nu$.
- **CKM unitarity:** The determination of the CKM matrix elements usually relies on the assumption that the active-sterile neutrino mixing matrix is zero. The presence of non-trivial mixing thus modifies the CKM matrix elements, and the experimentally-observed values can be used to simultaneously constrain the true CKM element values, and the active-sterile mixing matrix Θ . **NeutrinoBit** constructs a likelihood based on the deviations of the true values of $(V_{CKM})_{us}$ and $(V_{CKM})_{ud}$ from their experimentally-measured values.
- **Neutrinoless double-beta decay:** In a double-beta decay process, two neutrons decay into two protons, with the emission of two electrons and two anti-neutrinos. Majorana neutrinos would give rise to lepton number violation, resulting in neutrinoless double-beta decay

($0\nu\beta\beta$). In addition, the exchange of RHNs can modify the effective neutrino mass $m_{\beta\beta}$, which is constrained by half-life measurements of $0\nu\beta\beta$ decay. The best upper limits currently come from the GERDA experiment (Germanium) [226] with $m_{\beta\beta} < 0.15 - 0.33$ eV (90% CL), and KamLAND-Zen (Xenon) [227], $m_{\beta\beta} < 0.061 - 0.165$ eV (90% CL). **NeutrinoBit** uses these values to define one-sided Gaussian likelihoods, with theoretical calculations for RHN models taken from Refs. [228, 229]

- **Big Bang Nucleosynthesis:** RHNs can affect the abundances of the primordial elements if they decay shortly before BBN, as the typical energy of the decay products is significantly higher than the plasma energy at that time. This can lead to the dissociation of formed nuclei, or the creation of deviations from thermal equilibrium. The requirement that RHNs decay before BBN implies an upper limit on their lifetime which, in turn, results in a constraint on the total mixing with the active neutrinos. **NeutrinoBit** currently includes a basic BBN likelihood that uses decay expressions from Refs. [230, 231], and requires the lifetime of each RHN to be less than 0.1s [232]. A more comprehensive update will be released in future, associated with the new **CosmoBit** module.
- **Direct RHN searches:** Direct searches for RHNs can be performed by looking for peaks in the lepton energy spectrum of a meson decay, looking for evidence of production in beam dump experiments, and by studying the decay of vector bosons or mesons in e^+e^- or pp colliders. **NeutrinoBit** contains likelihoods for RHN searches at the PIENU [233], PS-191 [234], CHARM [235], E949 [236, 237], NuTeV [238], DELPHI [239], ATLAS [240] and CMS [241] experiments.

3. Applications to new physics

3.1. Supersymmetry

Supersymmetry (SUSY) has long been one of the leading candidates for BSM physics, owing to its potential for simultaneously answering several of the questions left open by the SM. In particular, the hierarchy problem and the dark matter “WIMP miracle” suggest the possible existence of SUSY states around the weak scale.

Most phenomenological explorations of SUSY take the MSSM as their starting point. On top of its minimal supersymmetrisation of the SM, the

MSSM effectively parameterises our ignorance about the high-scale mechanism responsible for breaking SUSY. This is done by including in the Lagrangian all gauge-invariant and renormalisable terms that break SUSY “softly”, that is, without re-introducing the quadratic Higgs mass divergences that gave rise to the hierarchy problem. In this way the MSSM provides a unified framework for exploring a wide range of possible manifestations of SUSY, but at the price of a vast parameter space: if no further assumptions are made the soft SUSY-breaking terms introduce more than one hundred free parameters.

Many different assumptions have been employed in the literature to reduce this parametric freedom and improve predictability. The resulting models broadly fit in two categories.

The first category consists of high-scale models that take inspiration from the fact that SUSY can provide gauge coupling unification at some high Grand Unified Theory (GUT) scale, typically around 10^{16} GeV. In these models a small number of unified mass and coupling parameters are defined at the GUT scale and then run down to the electroweak scale where phenomenological predictions are calculated. Thus, the assumption of high-scale unification constrains the model to a low-dimensional subspace of the full MSSM space, effectively imposing a set of characteristic correlations among the many MSSM parameters at the weak scale.

Probably the most studied SUSY model in this category is the Constrained MSSM (CMSSM) [242]. Here the parameter space is reduced to only four continuous parameters and a sign choice: the unified soft-breaking scalar mass, m_0 ; the unified soft-breaking gaugino mass, $m_{1/2}$; the unified trilinear coupling, A_0 ; the ratio of the vacuum expectation values for the two Higgs doublets, $\tan \beta \equiv v_u/v_d$; and the sign of the supersymmetric Higgsino mass parameter μ . The CMSSM has been studied in global fits for over a decade [22–25, 65–89], most recently in the GAMBIT analysis in [150].

Two much-studied generalisations of the CMSSM are the Non-Universal Higgs Mass models 1 and 2 (NUHM1 and NUHM2) [243–247]. These models loosen the tight link in the CMSSM between the Higgs sector and the sfermions by separating out the soft-breaking mass parameters of the Higgs sector from the common scalar mass parameter m_0 . This is achieved by introducing either one (NUHM1) or two (NUHM2) additional parameters at the GUT scale. In recent years the NUHM1 and NUHM2 have been studied in several global fit analyses [50, 67, 69, 70, 76, 84, 92]. GAMBIT global fits of the NUHM1 and NUHM2 were performed along with the fit of the CMSSM in [150]. In Section 3.1.1 we summarise the GAMBIT results for these GUT-scale SUSY

models.

The second category of MSSM sub-models are the weak-scale models. Here the focus is on exploring a broad range of weak-scale phenomenological scenarios in an economical manner, by varying only the MSSM parameters that most directly impact the observables under study. With all MSSM parameters defined near the weak scale, these models are mostly agnostic to questions concerning physics at very high scales, such as grand unification. The models are often labeled as **MSSM n** (or as **pMSSM n** for the *phenomenological MSSM n*), with n specifying the number of weak-scale MSSM parameters that are treated as free parameters.

Various such weak-scale models have been subjected to global fit analyses in the past few years [90–95]. The **GAMBIT** analyses in this category are [151], which looks at a seven-dimensional MSSM parameterisation (MSSM7), and [145], in which the fast LHC simulation capabilities of **ColliderBit** are used for a collider-focused fit of the four-dimensional MSSM “electroweakino” (chargino and neutralino) sector (EWMSSM). We summarise the **GAMBIT** results for the MSSM7 in Section 3.1.2 and for the EWMSSM in Section 3.1.3.

The phenomenological richness of the MSSM means that a wide range experimental results are relevant for constraining the parameter space. The mass and signal strength measurements for the 125 GeV Higgs boson and the measurement of the relic density of dark matter are of particular importance. We note that the impact of the relic density measurement depends strongly on whether the SUSY model is assumed to account for the full relic density, or, more conservatively, some arbitrary fraction of it. The **GAMBIT** studies reviewed here all take the latter approach.

Measurements of electroweak precision observables such as m_W and the muon $g - 2$, and of flavour observables like $BR(B \rightarrow X_s \gamma)$ and $BR(B_{(s)} \rightarrow \mu^+ \mu^-)$, introduce further important requirements on the SUSY parameter space. Finally, the null results from direct and indirect dark matter searches, and from collider searches for sparticles and additional Higgs bosons, essentially rule out some parts of SUSY parameter space. Though, to determine the exact implications of such null-result collider searches is far from trivial, as will be illustrated by the EWMSSM results discussed in Section 3.1.3.

3.1.1. Results for the CMSSM, NUHM1 and NUHM2

The **GAMBIT** global fits of the CMSSM, NUHM1 and NUHM2 in [150] are interpreted in terms of frequentist profile likelihood maps, identifying the

best-fit point and the 1σ and 2σ preferred regions relative to this point. As the results for **NUHM2** are qualitatively similar to those for **NUHM1**, we here focus on the **CMSSM** and **NUHM1** results.

The profile likelihood maps for the $(m_0, m_{1/2})$ planes of the **CMSSM** and **NUHM1** are shown in the left panels of Fig. 7. The **NUHM1** plane is clearly less constrained compared to the **CMSSM**. The underlying reason is the additional parametric freedom in the Higgs sector of the **NUHM1**, where the MSSM Higgs parameters $m_{H_u}^2$ and $m_{H_d}^2$ are not unified with m_0^2 at the GUT scale, but are rather set by an independent parameter m_H through the GUT-scale requirement $m_{H_u} = m_{H_d} \equiv m_H$. (In the **NUHM2**, m_{H_u} and m_{H_d} are taken as independent parameters at the GUT scale.) We note that as m_H is taken to be a real parameter, we have $m_{H_u}^2 = m_{H_d}^2 > 0$ at the GUT scale. The correct shape of the Higgs potential at the weak scale must therefore be generated through radiative corrections, as is the case for the **CMSSM**.

The right-hand panels in Fig. 7 help us understand the preferred parameter space in more detail. In these panels different sub-regions of the 2σ region are coloured according to which mechanism(s) contribute to keeping the DM relic density close to or below the observed value. The following criteria are used to define the DM mechanism regions in [150] and in the **MSSM7** study in [151]:

- stop co-annihilation: $m_{\tilde{t}_1} \leq 1.2 m_{\tilde{\chi}_1^0}$,
- sbottom co-annihilation: $m_{\tilde{b}_1} \leq 1.2 m_{\tilde{\chi}_1^0}$,
- stau co-annihilation: $m_{\tilde{\tau}_1} \leq 1.2 m_{\tilde{\chi}_1^0}$,
- chargino co-annihilation: $\tilde{\chi}_1^0 \geq 50\%$ Higgsino,¹
- A/H funnel: $1.6 m_{\tilde{\chi}_1^0} \leq (m_A \text{ or } m_H) \leq 2.4 m_{\tilde{\chi}_1^0}$,
- h/Z funnel: $1.6 m_{\tilde{\chi}_1^0} \leq (m_Z \text{ or } m_h) \leq 2.4 m_{\tilde{\chi}_1^0}$.

The coloured regions overlap for parameter points where more than one mechanism contributes.

¹For brevity we refer to this mechanism simply as “chargino co-annihilation”, though it also includes co-annihilations with the next-to-lightest neutralino. Further, for many points in this region the most important effect is simply enhanced $\tilde{\chi}_1^0\text{--}\tilde{\chi}_1^0$ annihilations, owing to the dominantly Higgsino $\tilde{\chi}_1^0$ composition.

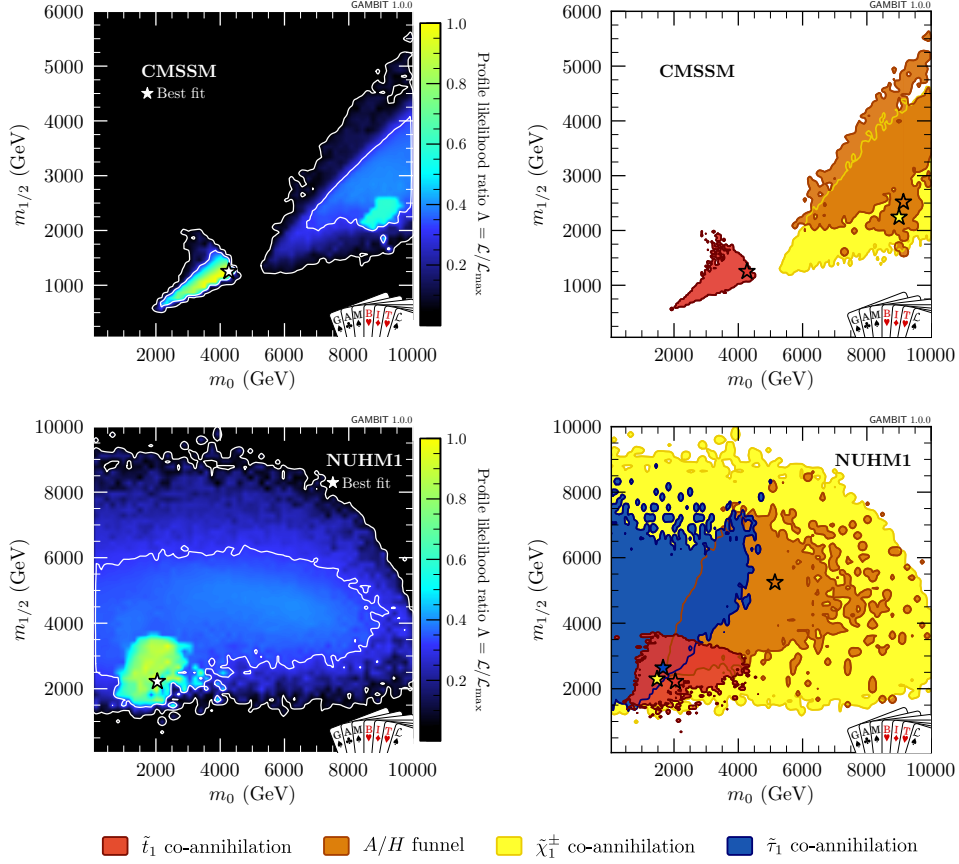


Figure 7: Profile likelihood in the $(m_0, m_{1/2})$ plane in the CMSSM (*top left*) and the NUHM1 (*bottom left*). The right-hand panels show the mechanisms that contribute to bringing the predicted DM relic density close to or below the observed value. The white contours show the 1σ and 2σ preferred regions relative to the best-fit point (white star). From [150].

In the CMSSM the overall highest-likelihood point is found in the stop co-annihilation region, at $m_0 \lesssim 4.5$ TeV. This region is associated with large, negative values for the trilinear coupling, $A_0 \lesssim -5$ TeV, and $\tan \beta \lesssim 16$. Only two other DM mechanisms are active within the best-fit parameter space, namely the A/H funnel and chargino co-annihilation. Thus, in contrast with earlier CMSSM fits, these results show that the stau co-annihilation region has fallen out of the preferred parameter space. This is mainly driven by the likelihood contribution from the LHC Higgs measurements, which penalise the lower- m_0 region where the lightest stau get sufficiently close in mass to the lightest neutralino.

As discussed above, the link between m_0 and the Higgs sector is relaxed in the NUHM1. This opens up the parameter space at lower m_0 , allowing the stau co-annihilation region back within the 2σ preferred region, as seen in the lower right panel of Fig. 7. A second consequence of m_0 being decoupled from the Higgs sector in the NUHM1 is that the allowed chargino co-annihilation region is extended to arbitrarily small m_0 values, compared to in the CMSSM. We can understand this by investigating the CMSSM case: the chargino co-annihilation DM mechanism is important when the MSSM Higgsino mass parameter μ is smaller than the bino mass parameter M_1 at the weak scale, as in that case the $\tilde{\chi}_1^0$ will be the lightest state in a triplet of near mass-degenerate Higgsinos (two neutralinos and one chargino).² In the CMSSM, the MSSM Higgsino mass parameter μ is strongly linked to m_0 via the conditions for EWSB; reducing m_0 effectively increases μ . The bino mass parameter M_1 is on the other hand controlled by $m_{1/2}$ via the GUT-scale relation $M_1 = M_2 = M_3 \equiv m_{1/2}$. For a fixed value of $m_{1/2}$, lowering m_0 therefore eventually leads to $M_1 \ll |\mu|$, resulting in a bino-dominated $\tilde{\chi}_1^0$ significantly lower in mass than the Higgsino-dominated neutralinos/chargino. In the NUHM1, on the other hand, the μ parameter is mostly controlled by m_H . This allows for $|\mu| < M_1$, and thus chargino co-annihilation, also in the low- m_0 region.

As mentioned above, in these fits the observed DM relic density is only imposed as an upper bound, to leave open the possibility for non-MSSM contributions in the observed DM density. While this choice broadens the

²In the general MSSM it is also possible to have chargino co-annihilation between a pair of wino-dominated $\tilde{\chi}_1^0$ and $\tilde{\chi}_1^\pm$, when $|M_2| < |M_1|, |\mu|$. However, this mechanism is not available in the models discussed here, as the GUT-scale relation $M_1 = M_2 = M_3 \equiv m_{1/2}$ leads to $M_2 \sim 2M_1$ at the weak scale.

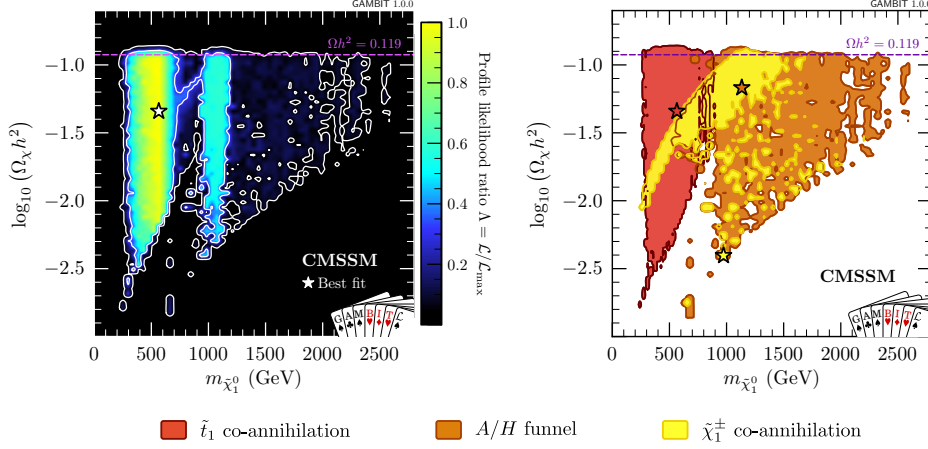


Figure 8: Profile likelihood in the $(m_{\tilde{\chi}_1^0}, \Omega_\chi h^2)$ plane of the CMSSM (*left*), and the mechanisms that bring the predicted relic density close to or below the measured value (*right*). The stars show the best-fit points, while the white contours outline the 1σ and 2σ regions. From [150].

allowed parameter space, it is worth noting that the parameter regions that fully explain the relic density can have equally high likelihoods as those with a lower predicted relic density. This can be seen in the left panel of Fig. 8, which shows the profile likelihood in the CMSSM plane of the neutralino mass $m_{\tilde{\chi}_1^0}$ and the predicted relic density $\Omega_\chi h^2$. For most $m_{\tilde{\chi}_1^0}$ values there is little variation in the profile likelihood when moving up to a point where the prediction saturates the observed value (dashed purple line).

The right-hand panel in Fig. 8 shows that, in the CMSSM, the lowest predicted neutralino masses are found within the stop and chargino co-annihilation regions, extending down to $m_{\tilde{\chi}_1^0} \sim 250$ GeV. In the NUHM1 and NUHM2, the chargino co-annihilation and stau co-annihilation regions extend further down, to $m_{\tilde{\chi}_1^0} \sim 150$ GeV. The chargino co-annihilation region in Fig. 8 also illustrates the well-known result that a dominantly Higgsino $\tilde{\chi}_1^0$ produces the entire observed relic density when $m_{\tilde{\chi}_1^0} \sim 1$ TeV. Moving along the observed relic density towards higher neutralino masses, additional contributions from resonant A/H -funnel annihilations become more and more important.

Direct detection DM searches seem the most promising experimental probe for the SUSY scenarios preferred in these fits. In Fig. 9 the preferred CMSSM (left) and NUHM1 regions are shown in the plane of the lightest

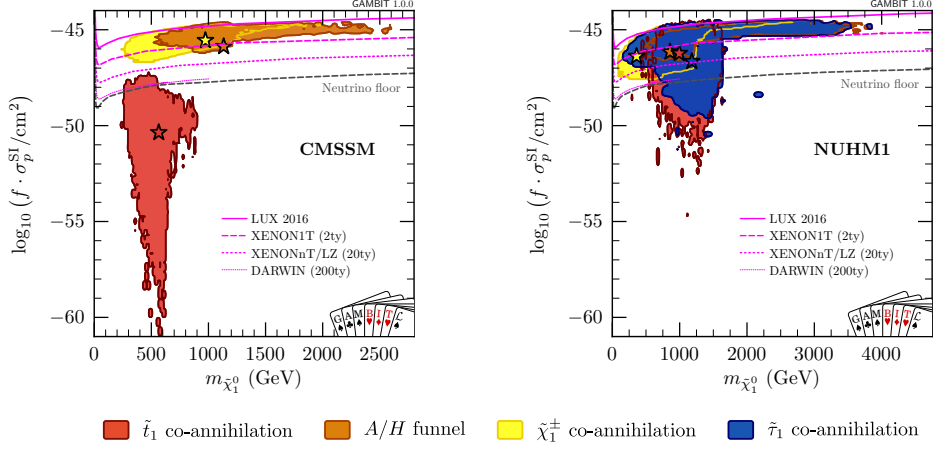


Figure 9: The 2σ preferred regions in the plane of the spin-independent neutralino-proton cross-section versus the neutralino mass for the CMSSM (*left*) and the NUHM1 (*right*), coloured according to the mechanism(s) that limit the predicted DM relic density. The pink lines show the observed 90% CL exclusion limit from LUX [248] and projected limits for XENON1T (two tonne-years of exposure), XENONnT/LZ (20 tonne-years of exposure) [249] and DARWIN (200 tonne-years of exposure) [250]. The 1σ and 2σ regions are shown as white contours; best-fit points are marked by stars. From [150].

neutralino mass versus the spin-independent neutralino-proton cross-section. The predicted cross-section is scaled by the fraction f of the full DM relic density that the given parameter point attributes to neutralinos. The solid pink line shows the 90% CL exclusion limit from the LUX 2016 result [248], which was included as a likelihood component in these fits. The dashed and dotted lines show projected 90% CL limits for the XENON and DARWIN experiments [249, 250]. While the stop co-annihilation regions will largely remain out of reach, as will much of the stau co-annihilation region in the NUHM1, both the chargino co-annihilation and the A/H funnel regions can be fully probed in future direct detection searches.

Finally, we note that the CMSSM, NUHM1 and NUHM2 fit results in [150] indicate that these models no longer hold much promise for resolving the observed discrepancy in the muon anomalous magnetic moment. The strong constraints on the low-mass parameter space – in particular from LHC sparticle searches, DM direct detection and the LHC Higgs measurements – push the fits towards heavier sfermion and electroweakino spectra, thus diminishing

the possible SUSY contribution to the muon ($g - 2$).

3.1.2. Results for the *MSSM7*

We now move on to the weak-scale parameterisations of the MSSM, starting with the **GAMBIT** analysis of the **MSSM7** in [151]. Here the free parameters are the wino mass parameter, M_2 ; the $(3, 3)$ elements of the \mathbf{A}_u and \mathbf{A}_d MSSM trilinear coupling matrices, $(\mathbf{A}_u)_{33} \equiv A_{u_3}$ and $(\mathbf{A}_d)_{33} \equiv A_{d_3}$ (the other trilinear couplings are set to 0); the soft-breaking Higgs mass parameters, $m_{H_u}^2$ and $m_{H_d}^2$; a common parameter m_f^2 for the sfermion soft-breaking mass parameters; and the ratio of the Higgs vacuum expectation values, $v_u/v_d \equiv \tan \beta$. All the parameters are defined at the scale $Q = 1 \text{ TeV}$, except $\tan \beta$, which is defined at $Q = m_Z$.

While this model is a weak-scale MSSM parameterisation, the GUT-inspired relation

$$\frac{3}{5} \cos^2 \theta_W M_1 = \sin^2 \theta_W M_2 = \frac{\alpha}{\alpha_s} M_3, \quad (4)$$

is imposed to limit the dimensionality of the parameter space. Equation 4 represents an expected weak-scale relation between M_1 , M_2 and M_3 if they originate from a common GUT-scale parameter, like $m_{1/2}$ in the **CMSSM**.

As in the GUT-scale models, the Higgsino mass parameter μ is determined from the input parameters – most importantly $m_{H_u}^2$ and $m_{H_d}^2$ – and the requirements for EWSB. Since Eq. 4 implies that $|M_1| < |M_2|$, we again have three *a priori* possibilities for the composition of the neutralino state: dominantly bino ($|M_1| < |\mu|$), dominantly Higgsino ($|\mu| < |M_1|$), or a bino-Higgsino mixture ($|M_1| \sim |\mu|$).

The global fit analysis in [151] finds that all these three neutralino scenarios are allowed within the 2σ preferred parameter space of the **MSSM7**. This can be seen in the top panels of Fig. 10, showing the profile likelihood in the (μ, M_1) plane (left) and the active mechanisms that bring the relic density close to or below the observed value (right). In the $\mu < |M_1|$ regions of the plane, corresponding to a mostly Higgsino $\tilde{\chi}_1^0$, the chargino co-annihilation and A/H funnel mechanisms dominate. Moving towards larger μ we enter the bino-Higgsino mixture scenario at $\mu \sim |M_1|$, before reaching the bino- $\tilde{\chi}_1^0$ scenario at $\mu > |M_1|$. Here the chargino co-annihilation mechanism is no longer relevant, so an acceptable relic density must be achieved either through efficient A/H funnel annihilations, co-annihilations with the lightest stop or

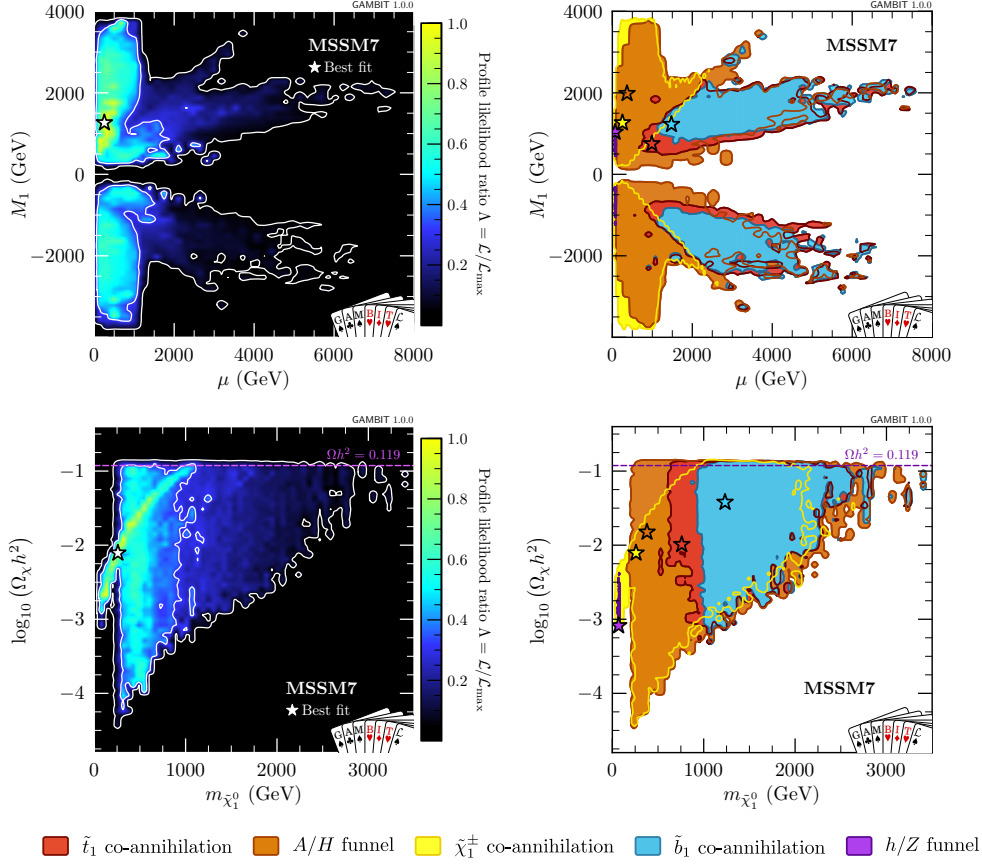


Figure 10: Profile likelihoods in the (μ, M_1) plane (*top left*) and the $(m_{\tilde{\chi}_1^0}, \Omega_\chi h^2)$ plane of the MSSM7. The right-hand panels show the 2σ preferred parameter regions coloured according to which mechanism(s) contribute to limit the relic density. The stars mark the best-fit points, while the white contours show the 1σ and 2σ preferred regions. From [151].

sbottom, or a combination of these mechanisms.³

The overall best-fit point in the **MSSM7** is found in the chargino co-annihilation region, with $m_{\tilde{\chi}_2^0} \approx m_{\tilde{\chi}_1^\pm} \approx m_{\tilde{\chi}_1^0} \approx 260$ GeV. As can be seen in the lower panels of Fig. 10, the predicted neutralino relic density at this point can only explain around 10% of the observed DM relic density. However, with only slightly heavier neutralino masses there are **MSSM7** scenarios that achieve close to the same likelihood values – well within the 1σ region – and account for the full relic density. These are scenarios with a mostly bino $\tilde{\chi}_1^0$ and efficient $\tilde{\chi}_1^0$ – $\tilde{\chi}_1^0$ annihilations through the A/H funnel.

The cutoff of this A/H funnel region at $m_{\tilde{\chi}_1^0} \sim 250$ GeV, corresponding to $m_{A/H} \sim 500$ GeV, is due to several independent likelihood contributions that penalize the lower-mass scenarios. In particular, the constraint on BSM contributions to $BR(B \rightarrow X_s \gamma)$ plays an important role here, as the A^0 mass is closely related to the H^\pm mass, and a light charged Higgs will induce sizable SUSY contributions to this decay. Further important constraints on this region come from the LHC Higgs measurements, and also from LHC gluino searches, as the gluino mass parameter M_3 is connected to M_1 via Eq. 4, giving $M_3 \sim 5M_1$.

We note that even the h/Z funnel mechanisms are present within the 2σ parameter regions, for $m_{\tilde{\chi}_1^0} \approx 45$ GeV and $m_{\tilde{\chi}_1^\pm} \approx 62$ GeV. However, the allowed scenarios in this low- $m_{\tilde{\chi}_1^0}$ region have an almost pure Higgsino $\tilde{\chi}_1^0$ anyway, so this alone ensures a predicted relic density far below the observed value, also explaining how the otherwise strong constraints from DM direct detection are avoided.

As for the GUT-scale models discussed in the previous section, direct DM searches seem the most promising probe of the **MSSM7** scenarios preferred by this fit. Figure 11 shows the profile likelihood (left) and the active DM mechanisms (right) across the plane of the neutralino mass and the spin-independent neutralino-proton cross-section. We see that future direct detection experiments will explore not only the full chargino co-annihilation

³The lack of a stau co-annihilation region in the **MSSM7** is related to the assumption of a common sfermion mass parameter defined at the low scale of $Q = 1$ TeV. The differences in sfermion masses are then mostly determined by the amount of L/R mixing in the sfermion mass matrices, rather than RGE running of mass parameters. Since the L/R mixing terms for both up-type and down-type sfermions are proportional to the corresponding Yukawa couplings, the light stop ends up being the lightest sfermion across much of parameter space, and the light sbottom is always lighter than then light stau.

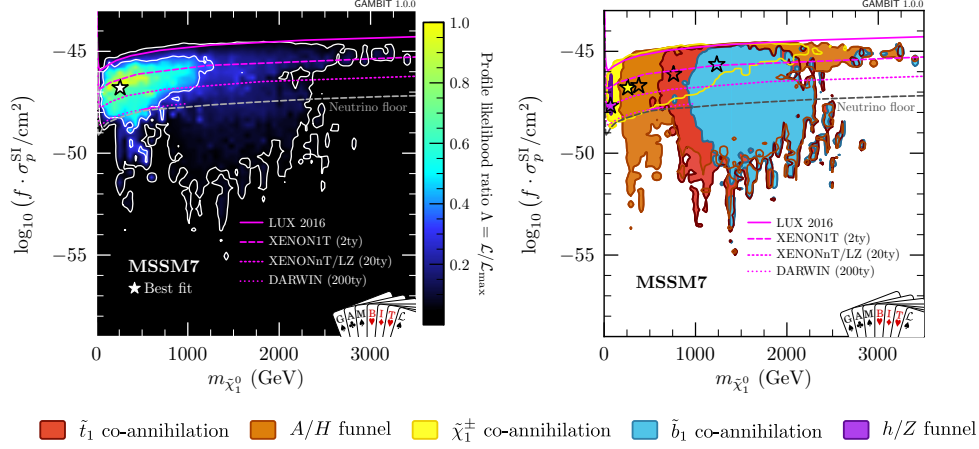


Figure 11: Profile likelihood in the plane of the neutralino mass versus the spin-independent neutralino-proton cross-section in the MSSM7 (left), and the relic density mechanisms that are active in different parts of the 2σ region (right). The predicted neutralino-proton cross-section is rescaled at each point by the fraction f of the observed DM relic density that the neutralino relic prediction accounts for. 90% CL exclusion limits are shown for the full LUX exposure [248] and the projected reach for for XENON1T (two tonne-years of exposure), XENONnT/LZ (20 tonne-years of exposure) [249] and DARWIN (200 tonne-years of exposure) [250]. The 1σ and 2σ regions are outlined by white contours. The stars mark the best-fit points. From [151].

region, but almost the entire 1σ region preferred in the GAMBIT fit.

Concerning the muon $(g - 2)$ discrepancy, the fit in [151] shows that there is little hope that the MSSM7 can provide an explanation. This is not particularly surprising: because the model dimensionality is kept low, relating all sfermion mass parameters to the common m_f^2 parameter at the weak scale, it is impossible to get sufficiently light smuons and muon sneutrinos without simultaneously causing significant tension with other observables such as LHC squark searches.

3.1.3. Results for the EWMSSM

Current SUSY searches by the ATLAS and CMS experiments at the LHC are usually optimised and interpreted assuming a simplified model. These models typically include only two or three different sparticles and assume 100% of decays occur to the signal processes. Such theory simplifications are a necessary compromise given the level of detail and complexity in experimental

searches. Nevertheless it leaves open an important question: what impact do the results from ATLAS and CMS SUSY searches have on the parameter space of more realistic models like the MSSM?

The **GAMBIT** analysis in [145] takes on this question in the context of LHC searches for neutralinos and charginos. The canonical simplified model for these searches is one that assumes production of a purely wino $\tilde{\chi}_2^0 \tilde{\chi}_1^\pm$ pair, with subsequent decays to a purely bino $\tilde{\chi}_1^0$ via $\tilde{\chi}_2^0 \rightarrow Z \tilde{\chi}_1^0$ and $\tilde{\chi}_1^\pm \rightarrow W^\pm \tilde{\chi}_1^0$. This gives motivation for a search for events with leptons, jets and missing energy (see e.g. [251, 252]). The **GAMBIT** study assumes a phenomenologically far richer model, referred to as the **EWMSSM**. This is the effective theory obtained when assuming that all sparticles except the MSSM electroweakinos are too heavy to affect current collider searches. The **EWMSSM** is thus a model with six sparticles – four neutralinos and two charginos – controlled by only four free MSSM parameters: M_1 , M_2 , μ and $\tan \beta$. Loosely speaking, the bino soft-mass M_1 controls the mass of one neutralino, the wino soft-mass M_2 controls the masses of one neutralino and one chargino, and the Higgsino mass parameter μ sets the masses of two neutralinos and one chargino.

In contrast to the global fits discussed in the previous two sections, the fit in [145] focuses exclusively on collider constraints. This choice allows the fit to explore the full range of possible collider scenarios in the **EWMSSM** without further enlarging the model parameter space. Keeping the dimensionality of the parameter space fairly low is of critical importance, due the large computational expense of this fit: for each sampled **EWMSSM** parameter point, **ColliderBit** is used to run full Monte Carlo simulations of the relevant ATLAS and CMS searches. While running full simulations at each point in a global fit is always computationally challenging, it is particularly so when simulating electroweakino searches due to the low signal acceptance rates in these searches.⁴

The analysis in [145] includes **ColliderBit** simulations of most of the 13 TeV electroweakino searches that were available at the time of the study [251, 253–259]. The combined likelihood obtained from these simulations is the main

⁴For most of the included LHC searches there is no public information on how background estimates are correlated across signal regions. In these cases the single signal region with the best expected sensitivity must be identified at each **EWMSSM** parameter point in the fit. This adds to the already substantial computational cost, as distinguishing between “competing” signal regions often requires higher Monte Carlo statistics than what is needed to get reasonable signal estimates for each individual signal region alone.

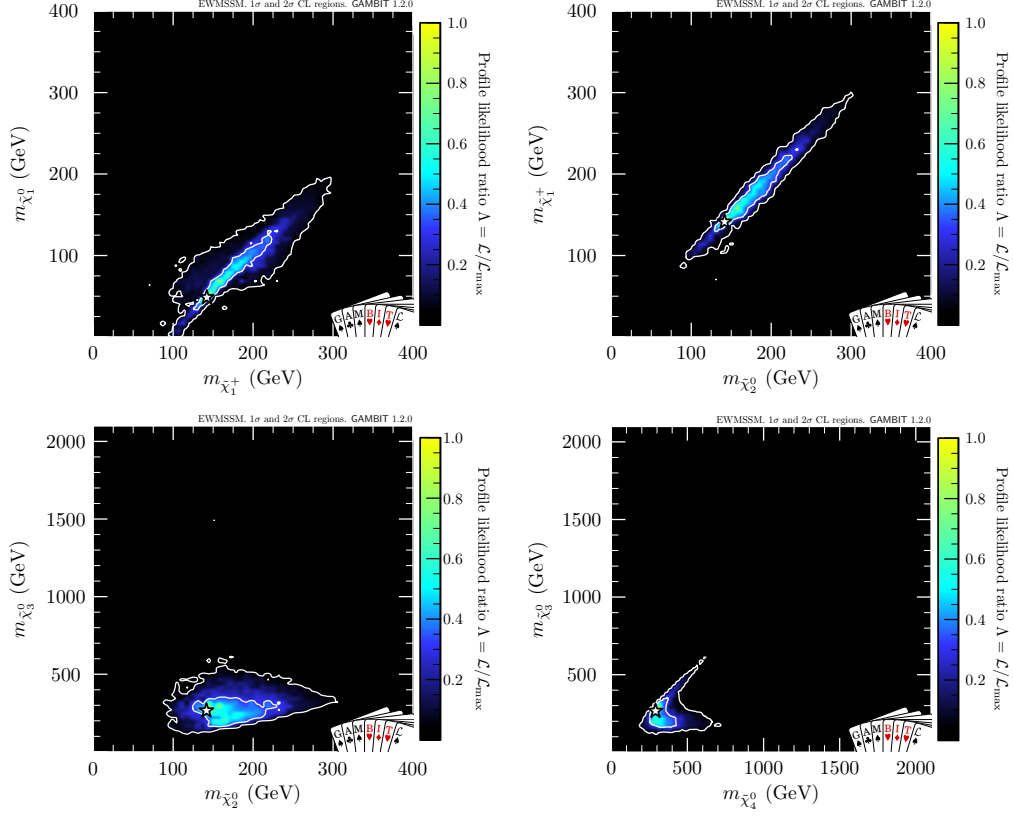


Figure 12: Profile likelihood in four different EWMSSM mass planes: the $(m_{\tilde{\chi}_1^\pm}, m_{\tilde{\chi}_1^0})$ plane (top left), the $(m_{\tilde{\chi}_2^0}, m_{\tilde{\chi}_1^\pm})$ plane (top right), the $(m_{\tilde{\chi}_2^0}, m_{\tilde{\chi}_3^0})$ plane (bottom left), and the $(m_{\tilde{\chi}_4^0}, m_{\tilde{\chi}_3^0})$ plane (bottom right). The white contours show the 1σ and 2σ preferred regions. The star marks the best-fit point. From [145].

component in the fit likelihood function. The other collider observables going into the total likelihood are a collection of SUSY cross-section limits from LEP and the invisible decay widths of the Z and the 125 GeV Higgs.

The main result from [145] is that, when combined, the ATLAS and CMS electroweakino results prefer EWMSSM scenarios with a distinct pattern of relatively light neutralino and chargino masses (Fig. 12). The preferred 2σ parameter region has all six neutralinos and charginos below ~ 700 GeV, with the lightest neutralino below ~ 200 GeV. The lightest neutralino is always dominantly bino, but it also has a non-negligible wino or Higgsino component. Further, the best-fit parameter region predicts two characteristic $\gtrsim m_Z$ gaps in

the mass spectrum: the first between the mostly bino $\tilde{\chi}_1^0$ and the mostly wino (Higgsino) $\tilde{\chi}_2^0/\tilde{\chi}_1^\pm$, and the second between $\tilde{\chi}_2^0/\tilde{\chi}_1^\pm$ and the mostly Higgsino (wino) $\tilde{\chi}_4^0/\tilde{\chi}_2^\pm$.⁵

At first sight this result may seem surprising. None of the included ATLAS and CMS searches have seen a convincing SUSY signal, yet when combined they prefer the low-mass region over the decoupling region, where all EWMSSM collider predictions would align with SM expectations. The reason is that the EWMSSM is able to simultaneously fit a pattern of small excesses across several of the simulated LHC searches, while at the same time avoiding generating too much tension with the other searches. The excesses that mostly drive this result come from searches for 2-, 3-, and 4-lepton final states in ATLAS [251, 253, 255], specifically in signal regions that target leptons from on-shell Z and W decays. This explains the preference in the fit for electroweakino mass spectra with two $\gtrsim m_Z$ mass gaps.

To understand the interplay between the analyses contributing to the excess, we can look at their individual likelihood contributions across the combined best-fit surface. This is done in Fig. 13, where the contributions from four ATLAS results are displayed across the preferred 3σ regions in three different mass planes. When reading these plots it is important to keep in mind that the plotted points are those parameter samples picked out by profiling the *total* likelihood. The sharp changes in analysis likelihood seen in some plots are due to abrupt changes in what scenarios are picked out by this profiling, which again changes which signal region is selected to set the analysis likelihood value.

One example of the interplay between analyses is seen by comparing the middle panels on the first and third rows. The first of these show the likelihood contribution from an ATLAS search for 4-lepton final states, with the leptons coming from two Z bosons [255]. We see that fitting a 4-lepton excess in the EWMSSM relies on having non-negligible production of $\tilde{\chi}_3^0$, as this allows for signal leptons from the decays $\tilde{\chi}_3^0 \rightarrow Z\tilde{\chi}_{1,2}^0$. The second of these panels is for an ATLAS search for 3-lepton final states [251], designed to target $\tilde{\chi}_2^0\tilde{\chi}_1^\pm$ production. For a given $m_{\tilde{\chi}_2^0}$, reducing $m_{\tilde{\chi}_3^0}$ to $\lesssim 600$ GeV (as preferred by the 4-lepton search) also improves the fit to this 3-lepton search, which for high $m_{\tilde{\chi}_3^0}$ sees some tension with the data. At lower $m_{\tilde{\chi}_3^0}$ production processes with

⁵In the preferred scenarios, $\tilde{\chi}_3^0$ is always mostly Higgsino and thus fairly close in mass to the other Higgsino-dominated states, i.e. either $\tilde{\chi}_2^0/\tilde{\chi}_1^\pm$ or $\tilde{\chi}_4^0/\tilde{\chi}_2^\pm$.

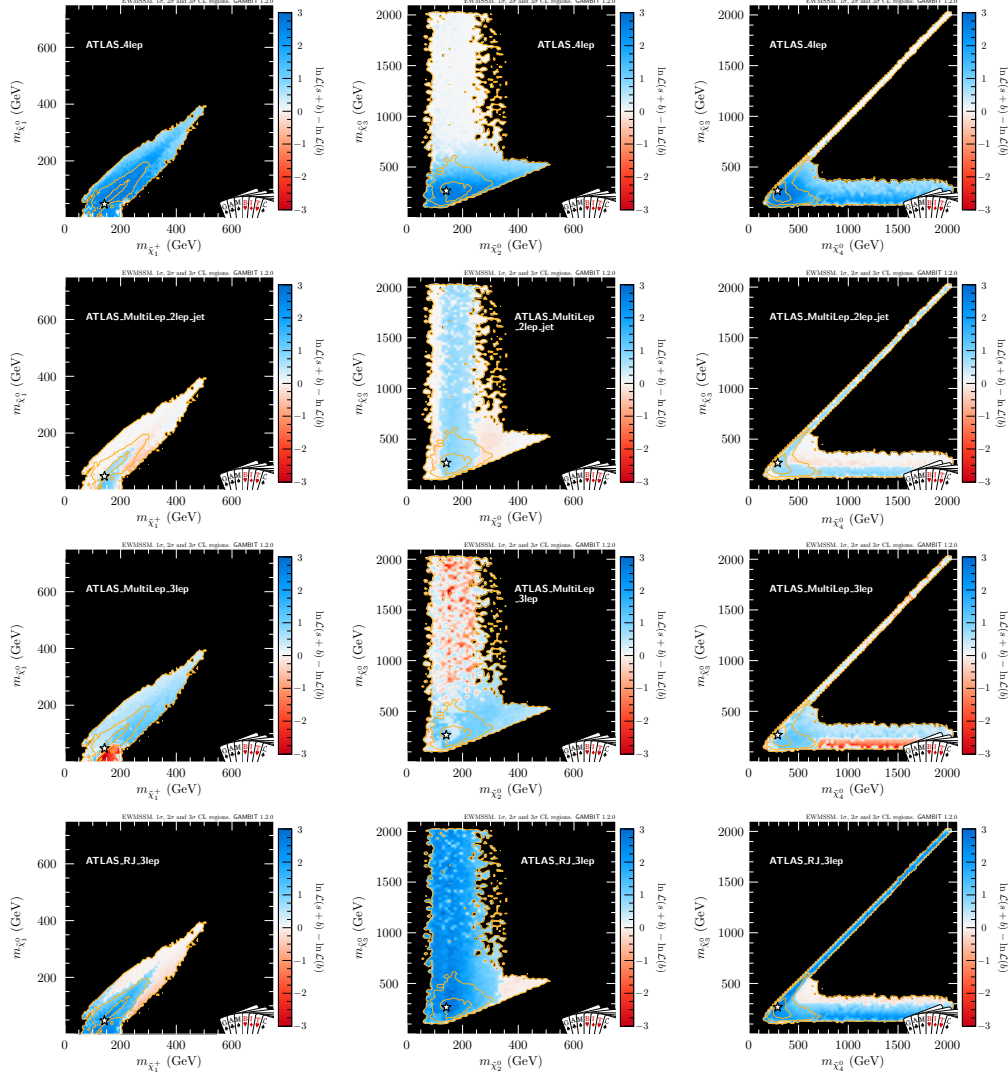


Figure 13: Contributions to the total fit likelihood from the ATLAS searches in Ref. [255] (top), Ref. [251] (second and third rows), and Ref. [253] (bottom), shown across the full 3σ regions in the $(m_{\tilde{\chi}_1^\pm}, m_{\tilde{\chi}_1^0})$ plane (left), the $(m_{\tilde{\chi}_2^0}, m_{\tilde{\chi}_3^0})$ plane (middle), and the $(m_{\tilde{\chi}_4^0}, m_{\tilde{\chi}_3^0})$ plane (right). In the blue regions a non-zero signal prediction in the given search improves the overall fit, while in red regions the signal prediction worsens the fit. In the white regions the given search is not sensitive. The orange contours outline the 1σ , 2σ and 3σ regions preferred in the fit. The white star marks the best-fit point. From [145].

$\tilde{\chi}_3^0$ come into play, involving more complicated event topologies. At the same time the production cross-section for the $\tilde{\chi}_2^0\tilde{\chi}_1^\pm$ pair is reduced somewhat, due to a higher Higgsino component. The combined effect is a change in which 3-lepton signal region is identified as having the best expected sensitivity.

The combined excess in the 13 TeV searches is estimated in [145] to have a local significance of 3.3σ . The impact of 8 TeV LHC results on the preferred low-mass scenarios is investigated by post-processing all parameter samples in the 1σ region with simulations of relevant ATLAS and CMS electroweakino searches at 8 TeV [260–263]. The result is an upwards shift in the best-fit mass spectrum, by ~ 20 GeV in all masses, and a small reduction of the estimated significance of the excess, to 2.9σ .

We also note that even though the EWMSSM fit did not include DM constraints, parts of the preferred parameter space do give acceptable relic density predictions while avoiding exclusion from current direct and indirect DM searches. This is possible for scenarios with $m_{\tilde{\chi}_1^0}$ close to $m_Z/2$ or $m_h/2$, where resonant annihilations via the Z/h funnel can bring the predicted relic density close to or below the observed value.

While the small excess seen in the EWMSSM fit is quite possibly due to background fluctuations, the fit demonstrates two important points. First, that LHC constraints on light SUSY can be significantly weaker in realistic SUSY such as the MSSM than in simplified models.⁶ Second, that proper statistical combinations of collider searches can be a powerful tool to uncover suggestive patterns in BSM parameter spaces.

3.2. Higgs Portal models for dark matter

No definitive evidence has yet been uncovered for non-gravitational interactions of DM with the SM. At some level however, such interactions must be inevitably generated by effective operators connecting Lorentz-invariant, gauge singlet combinations of SM particles to equivalently symmetric combinations of DM fields. The lowest-dimension such operator in the SM is the Higgs bilinear $H^\dagger H$. Depending on the spin and gauge representation of a DM candidate X , the lowest-order Lorentz- and gauge-invariant DM operator may be either the bilinear $X^\dagger X$, or a lone DM field. Operators linear in

⁶While not discussed here, the analysis in [145] shows that for every mass hypothesis in the $(m_{\tilde{\chi}_2^0}, m_{\tilde{\chi}_1^0})$ plane – not just for points in the best-fit region – there is a point in the EWMSSM parameter space that fits the *combined* collider results at least as well as the SM expectation.

X are only consistent if X is itself a Lorentz invariant (i.e. a scalar), and a gauge singlet. If it is to be a viable DM candidate however, X must be stable on cosmological timescales. The most straightforward way to achieve this is for X to hold a different charge to SM particles under some new unbroken (typically discrete) symmetry. This has the effect of forbidding terms linear in X , preventing the field from decaying.

The lowest-order operator connecting X to the SM guaranteed to exist at some level is therefore the so-called ‘Higgs portal’ operator $X^\dagger X H^\dagger H$. Following electroweak symmetry breaking, this operator gives rise to a mass term for X proportional to v_0^2 (with v_0 the vacuum expectation value of the Higgs field), a Higgs-DM-DM vertex proportional to v_0 , and a direct four-particle vertex between two Higgses and two DM particles. The new 3-particle and 4-particle interactions of X with the Higgs boson lead to DM annihilation (enabling thermal production and possible indirect detection), spin-independent DM-nucleon scattering (leading to possible direct detection), DM production at colliders (with the possibility for signals in e.g. monojet searches), and invisible decays of the Higgs to two DM particles when $m_X < m_h/2$.

Depending on the Lorentz representation of DM, $X^2 H^2$ may be a fully renormalisable dimension 4 operator (if X is a scalar), an effective dimension 4 operator (if X is a vector), or an effective dimension 5 operator (if X is a fermion). All three of these cases have been considered in detail in the literature, with a particular focus on models where X is itself a gauge singlet and the $X^2 H^2$ term is therefore the sole link between DM and the SM. The most commonly studied cases have been the \mathbb{Z}_2 -symmetric scalar [96, 104, 264–308; GAMBIT analyses 152, 153], vector [300–312; GAMBIT analysis 112] and fermionic [109, 298–308, 312–318; GAMBIT analysis 112] variants, along with the \mathbb{Z}_3 -symmetric scalar [319–323; GAMBIT analysis 153].

3.2.1. \mathbb{Z}_2 -symmetric scalar singlet

The simplest Higgs portal model for DM, and indeed probably the most minimal of all models for particle DM, is a single, real, gauge-singlet scalar field S , protected from decay by a \mathbb{Z}_2 symmetry. The only new renormalisable Lagrangian terms allowed by gauge, Lorentz and \mathbb{Z}_2 symmetry are

$$\mathcal{L}_{\mathbb{Z}_2} = \frac{1}{2}\mu_s^2 S^2 + \frac{1}{4}\lambda_s S^4 + \frac{1}{2}\lambda_{hs} S^2 |H|^2. \quad (5)$$

The model is fully specified by the S bare mass μ_s , the dimensionless S quartic self-coupling λ_s , and the dimensionless Higgs portal coupling λ_{hs} . For

the most part, the S quartic coupling has little impact on the phenomenology of the model, as it leads only to DM self-interactions, which are not sufficiently constrained by existing data to place strong limits on λ_s . A key exception, however, is the impact of λ_s on the running of gauge couplings under renormalisation group flow, which can have important implications for stability of the electroweak vacuum.

Denoting the physical SM Higgs field by h , following electroweak symmetry breaking $H \rightarrow [0, (v_0 + h)/\sqrt{2}]^T$. This generates new vertices of the form $v_0 h S^2$ and $h^2 S^2$, and induces a shift to the S bare mass, such that at tree level

$$m_s = \sqrt{\mu_s^2 + \frac{1}{2}\lambda_{hs}v_0^2}. \quad (6)$$

The interaction with the physical Higgs endows S with essentially all of the classic phenomenology of WIMP DM, via the diagrams shown in Fig. 14 – along with the added possibility of Higgs decays $h \rightarrow SS$ where $m_s \leq m_h/2$. The leading constraints on the model come from searches for gamma rays from dark matter annihilation in dwarf spheroidal galaxies [17], the observed relic density of dark matter [170], direct searches performed by the XENON1T [324] and PandaX [326] experiments, and searches for invisible Higgs decays at the LHC [327, 328].

The resulting preferred regions of parameter space are shown in Fig. 15. These results explicitly allow models where S is only a fraction of the observed DM, and include a fully self-consistent rescaling of the predicted signals at direct and indirect searches according to the fraction $f \leq 1$ of DM constituted by S at each point in the parameter space. The allowed parameter space splits into three regions: one at high masses where direct detection loses sensitivity, a second at intermediate mass where the 4-boson vertex boosts the annihilation cross-section and depletes the relic density, and another at and immediately below $m_s = m_h/2$, where S annihilates highly efficiently via an s -channel resonance mediated by the Higgs, depleting the relic density to below the observed value even for very small values of λ_{hs} .

The Higgs invisible width constraint rules out large couplings λ_{hs} at singlet masses below the resonance. The thermal relic density of S provides the lower limit of the low-mass and high-mass allowed regions. Indirect detection plays the leading role only on the high-mass edge of the resonance, where thermal effects in the early Universe push annihilation slightly off resonance but late-time annihilation remains strongly boosted. Direct detection plays

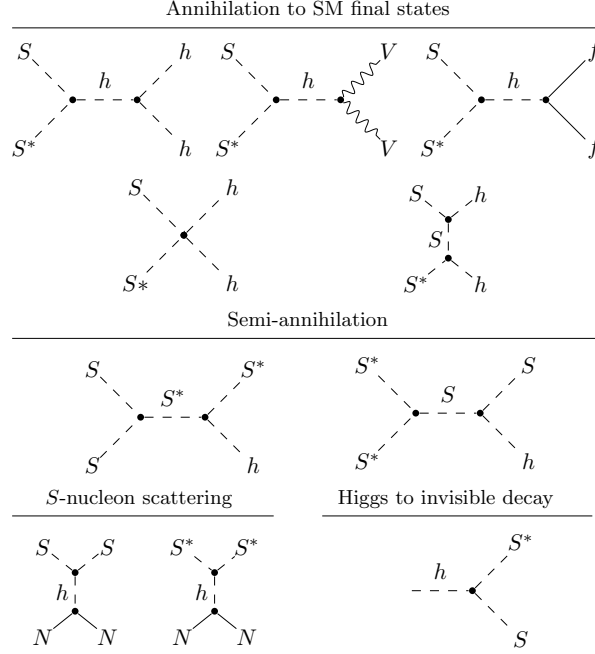


Figure 14: Feynman diagrams for annihilation, semi-annihilation, nuclear scattering and Higgs decays in scalar singlet Higgs portal models. N , f and V refer to nucleons, fermions and SM electroweak vector bosons (Z and W), respectively. Diagrams are shown for the \mathbb{Z}_3 -symmetric case, where DM exists in S and anti- S (i.e. S^*) states, but the same diagrams apply in the \mathbb{Z}_2 -symmetric case with $S = S^*$, except for semi-annihilation (which is absent in the \mathbb{Z}_2 model). The same diagrams also apply to \mathbb{Z}_2 -symmetric vector and fermionic Higgs portal models (with S replaced by the relevant DM particle and semi-annihilation also forbidden by the \mathbb{Z}_2 symmetry). From [153].

a significant role throughout the parameter space, as can be seen in Fig. 16. Except for the very bottom of the resonance region, the entirety of the model will soon be probed by direct detection.

Gamma-ray lines do not provide any meaningful constraint, as the partial annihilation cross-section for $SS \rightarrow \gamma\gamma$ is only appreciable in parts of the parameter space where the relic density is significantly suppressed. Likewise, monojet searches only constrain very large values of λ_{hS} already excluded by other constraints or expected to lead to new strong dynamics. Indeed, both these points also apply to all other Higgs portal models that we discuss in this review.

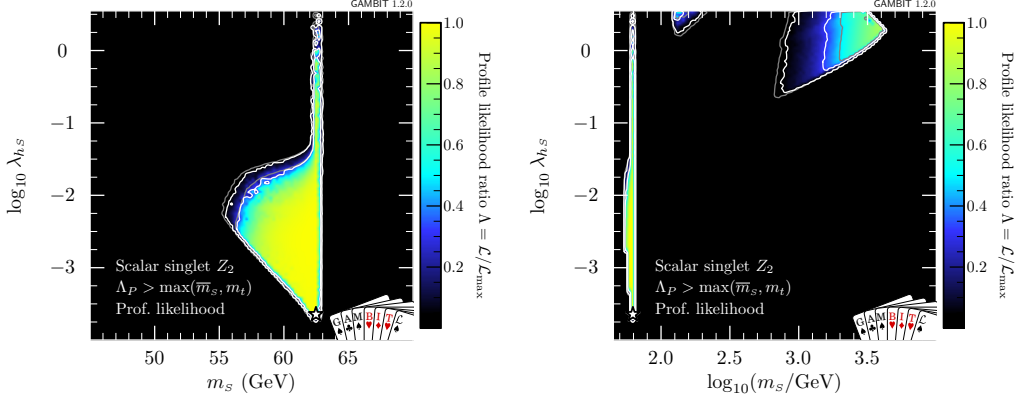


Figure 15: Profile likelihoods of parameters in the \mathbb{Z}_2 -symmetric scalar singlet Higgs portal dark matter model, including constraints from direct and indirect detection, the relic density of dark matter and LHC searches for invisible decays of the Higgs boson, along with various Standard Model, dark matter halo and nuclear uncertainties. *Left:* the low-mass resonance region. *Right:* the full mass range. Contours show 1 and 2σ confidence regions, with white corresponding to the main scan (including the 2018 XENON1T direct search [324]) and grey to a secondary scan using the 2017 XENON1T result [325]. White stars indicate the location of the best-fit point. From [153].

Given that the Higgs portal operator is not just an effective interaction, but a fully renormalisable operator in this model, it is also important to consider the UV behaviour of the theory. Due to the observed values of the top and Higgs masses, the SM possesses a second minimum in its scalar potential at $\gtrsim \mathcal{O}(10^{15})$ GeV, causing the low-scale vacuum in which we reside to be metastable. Adding an additional scalar to the SM impacts the running of the Higgs quartic coupling, raising its value at high scales. This can prevent the quartic coupling from running negative, and make the low-scale minimum a global rather than a local one. The catch is that λ_s must be relatively large in order to achieve this effect. Fig. 17 shows the parts of the parameter space, consistent with all experimental constraints, where λ_s can be pushed high enough to stabilise the SM vacuum, but without pushing any of the couplings non-perturbative below a scale of 10^{15} GeV. Clearly, the \mathbb{Z}_2 -symmetric scalar singlet can solve the vacuum stability problem without introducing new strong dynamics, and satisfy all experimental constraints, but only in a region around $m_s = 1\text{--}2$ TeV and $\sigma_{\text{SI}} \sim 10^{-45} \text{ cm}^2$. Curiously, this is also in

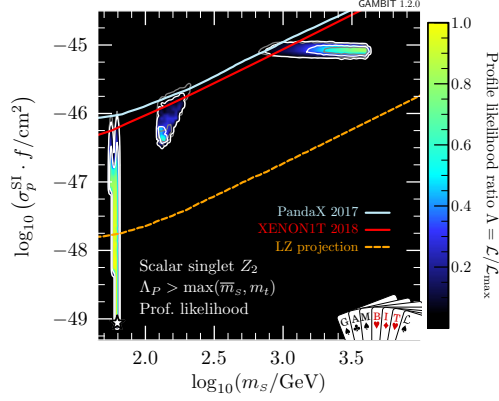


Figure 16: Results from the same analysis of the \mathbb{Z}_2 -symmetric scalar singlet Higgs portal dark matter model as shown in Fig. 15, but plotted in the plane of the effective spin-independent nuclear scattering cross-section and the scalar mass, in order to compare directly to the sensitivity of direct detection experiments. All models have their effective cross-section defined as $f\sigma_{\text{SI}}$, where $f \equiv \Omega_S/\Omega_{\text{DM}}$ is the fraction of the relic density constituted by the scalar singlet. Experiments assume $f = 1$ when publishing their results. Contours show 1 and 2σ confidence regions, and stars best fits. From [153].

the region consistent with the (admittedly very small) excess seen in the most recent XENON1T results [324]. In any case, this hypothesis will clearly be tested very quickly in the upcoming runs of the LZ and XENONnT [249, 329] experiments.

The results in Figs. 15–17 are based on profile likelihood analyses, and illustrate what is possible in each parameter plane, were one able to freely vary the other parameters of the theory (including nuisance parameters) in order to achieve the best possible fit to all available data. If one instead carries out a Bayesian analysis, looking instead at the posterior probability density for these parameters, a different picture emerges. In this case, parameter combinations become more likely if they can provide a good fit for a broader range of values of the other parameters of the theory, i.e. if they can fit the data with less fine tuning. In this case, the low-mass resonance region is strongly disfavoured, as ‘hitting’ the resonance and avoiding the relic density constraint for a given value of m_s requires some fine-tuning of various SM nuisance parameters such as m_h ; the same is true to a lesser extent for the intermediate-mass region as well. We therefore see that from a Bayesian

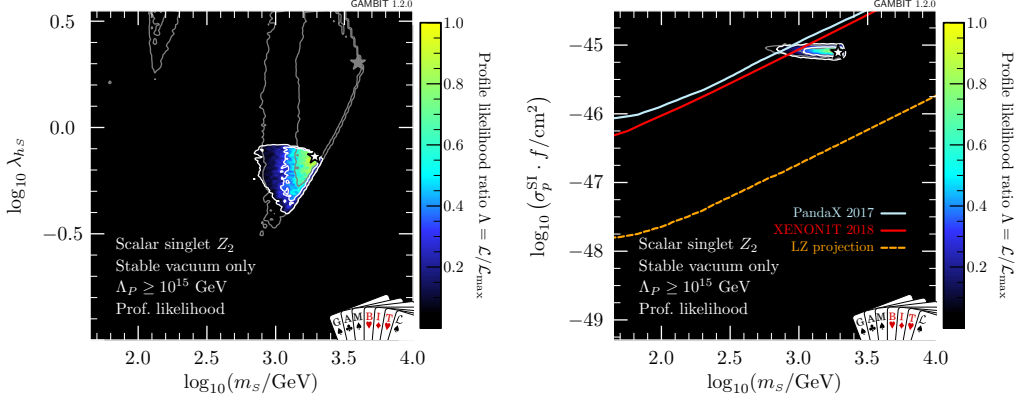


Figure 17: Regions in the \mathbb{Z}_2 -symmetric scalar singlet model that satisfy all experimental constraints, stabilise the electroweak vacuum and remain perturbative up to scales of 10^{15} GeV. Contours show 1 and 2σ confidence regions, and stars best fits. Grey contours show the allowed regions without the requirements of vacuum stability and perturbativity. From [153].

perspective, the region where the singlet model stabilises the SM vacuum is in fact favoured over the other regions of the theory, even before considering the implications for vacuum stability.

3.2.2. \mathbb{Z}_3 -symmetric scalar singlet

In contrast to the self-adjoint \mathbb{Z}_2 -symmetric scalar singlet, a \mathbb{Z}_3 symmetry leads to a complex scalar DM candidate, with both DM (S) and anti-DM (S^*) states contributing to the relic density. This symmetry also allows an additional cubic term in the Lagrangian,

$$\mathcal{L}_{\mathbb{Z}_3} = \mu_S^2 S^\dagger S + \lambda_S (S^\dagger S)^2 + \frac{\mu_3}{2} (S^{\dagger 3} + S^3) + \lambda_{hS} S^\dagger S |H|^2, \quad (7)$$

where we have introduced the new dimension-1 S cubic coupling μ_3 . This new coupling allows for so-called semi-annihilation processes $SS \rightarrow S^* h$ and $S^* S^* \rightarrow S h$, shown in Fig. 14.

Compared to the \mathbb{Z}_2 -symmetric model, semi-annihilation is able to deplete the relic density of DM at intermediate masses and open up an entirely new region of viable parameter space. This is shown in terms of the profile likelihood in Fig. 18, and highlighted in terms of the semi-annihilation fraction

$$\alpha = \frac{1}{2} \frac{\langle \sigma v_{\text{rel}} \rangle_{SS \rightarrow hS}}{\langle \sigma v_{\text{rel}} \rangle + \frac{1}{2} \langle \sigma v_{\text{rel}} \rangle_{SS \rightarrow hS}}, \quad (8)$$

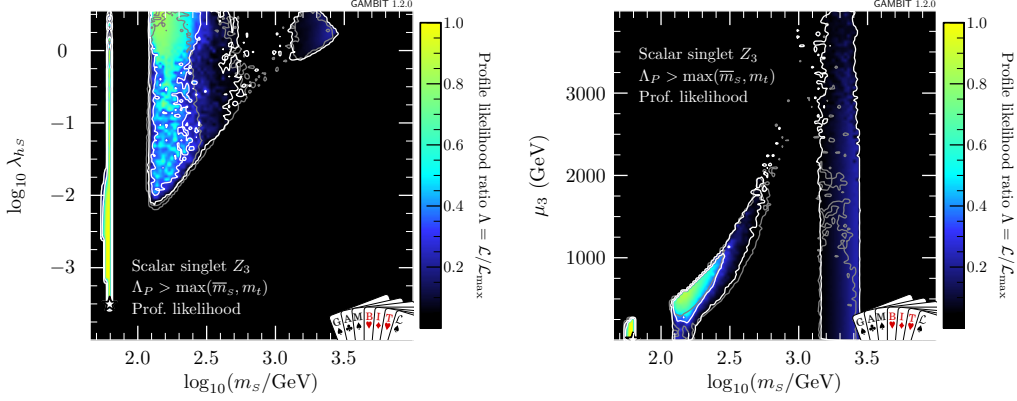


Figure 18: Profile likelihoods of parameters in the \mathbb{Z}_3 -symmetric scalar singlet Higgs portal dark matter model, including constraints from direct and indirect detection, the relic density of dark matter and LHC searches for invisible decays of the Higgs boson, along with various Standard Model, dark matter halo and nuclear uncertainties. Contours show 1 and 2σ confidence regions, with white corresponding to the main scan (including the 2018 XENON1T direct search [324]) and grey to a secondary scan using the 2017 XENON1T result [325]. White stars indicate the location of the best-fit point. From [153].

in Fig. 19. Here $\langle\sigma v_{\text{rel}}\rangle$ is the thermally averaged (semi-)annihilation cross-section weighted by the relative velocity between annihilating particles.

The vacuum structure of the theory is also more complicated than that of the \mathbb{Z}_2 -symmetric model, as regions where $\mu_3 \geq 2\sqrt{\lambda_S}m_S$ or $\mu_S^2 < 0$ and λ_{hS} is large can possess a second, \mathbb{Z}_3 -breaking minimum. The results shown in Figs. 18 and 19 avoid these regions, demanding that S does not itself obtain a VEV, and that the potential remains bounded from below.

Like the \mathbb{Z}_2 -symmetric variant, the \mathbb{Z}_3 -symmetric model can in principle completely stabilise the SM vacuum. However, because of the various factors of 2 introduced relative to the \mathbb{Z}_2 case, by virtue of DM not being self-adjoint, the region where this is possible is in fact in strong tension with the results from both XENON1T [324] and PandaX [326]. \mathbb{Z}_3 -symmetric models that stabilise the SM vacuum and produce the entire observed DM relic density are ruled out at 99% confidence; those constituting only a fraction of DM are ruled out at 98% confidence. The same is expected of other \mathbb{Z}_N -symmetric models with $N > 3$, which also feature non-self-adjoint DM.

As in the \mathbb{Z}_2 -symmetric case, a Bayesian analysis prefers the higher-mass

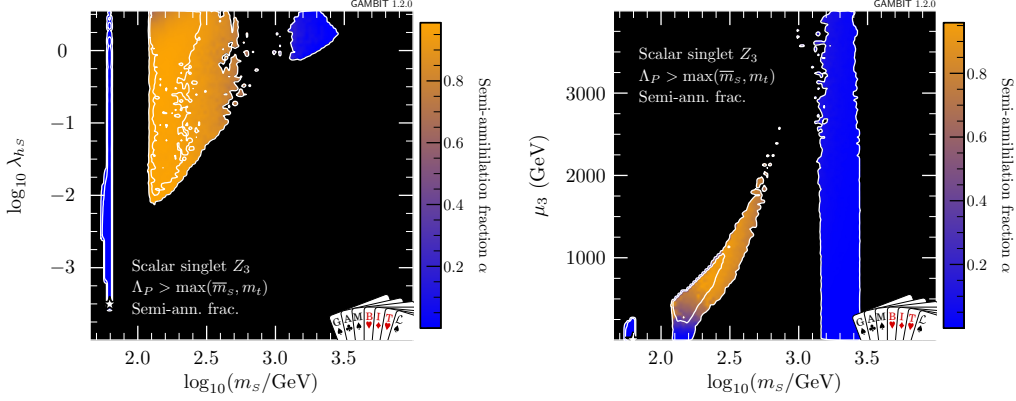


Figure 19: Results from the same analysis of the \mathbb{Z}_3 -symmetric scalar singlet Higgs portal dark matter model as shown in Fig. 18, but shaded according to the semi-annihilation fraction α (Eq. 8). From [153].

part of the parameter space, due to the fine-tuning needed to achieve agreement with all experimental data in both the resonance and semi-annihilation (intermediate mass) regions. In this case, the additional tuning in μ_3 required to satisfy the condition $\mu_3 \leq 2\sqrt{\lambda_s}m_s$ – and to achieve sufficient semi-annihilation in the intermediate-mass region – further penalises these regions.

3.2.3. \mathbb{Z}_2 -symmetric vector singlet

If DM is a \mathbb{Z}_2 -symmetric vector singlet V_μ interacting with the SM via the Higgs portal, its effective Lagrangian takes the form

$$\mathcal{L}_V = -\frac{1}{4}W_{\mu\nu}W^{\mu\nu} + \frac{1}{2}\mu_V^2 V_\mu V^\mu - \frac{1}{4!}\lambda_V(V_\mu V^\mu)^2 + \frac{1}{2}\lambda_{hV}V_\mu V^\mu H^\dagger H. \quad (9)$$

Here $W_{\mu\nu} \equiv \partial_\mu V_\nu - \partial_\nu V_\mu$ is the field strength tensor for the new vector. The tree-level DM mass has exactly the same form as Eq. 6. Although all terms here are dimension 4, the theory is not renormalisable, as it possesses an explicit mass term for V_μ . Perturbative unitarity is violated at energies above this mass. In the GAMBIT analysis [112], this issue was avoided by excluding the region of parameter space

$$0 \leq \lambda_{hV} \leq 2m_V^2/v_0^2 \quad (10)$$

from the analysis.

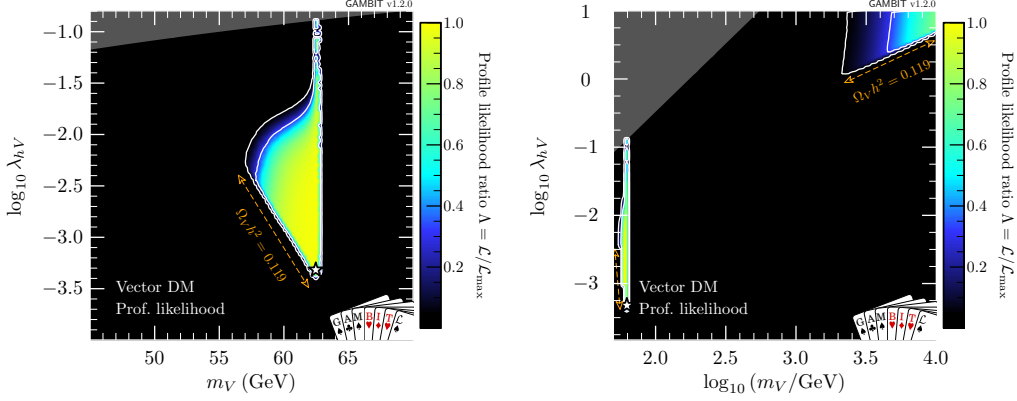


Figure 20: Profile likelihoods of parameters in the \mathbb{Z}_2 -symmetric vector singlet Higgs portal dark matter model, including constraints from direct and indirect detection, the relic density of dark matter and LHC searches for invisible decays of the Higgs boson, along with various Standard Model, dark matter halo and nuclear uncertainties. *Left:* the low-mass resonance region. *Right:* the full mass range. Grey shading indicates the area that fails the unitarity cut (Eq. 10). Orange annotations indicate the edge of the allowed parameter space along which the model reproduces the entire cosmological abundance of dark matter. Contours show 1 and 2σ confidence regions. White stars indicate the location of the best-fit point. From [112].

The phenomenology of the vector model is very similar to that of the \mathbb{Z}_2 -symmetric scalar variant, with the only major difference being the absence of the intermediate-mass solution due to the unitarity requirement (Fig. 20; the region excluded from the analysis due to the unitarity condition is shown in grey). The Bayesian analysis once again prefers the high-mass region due to the fine-tuning of nuisance parameters required in the resonance region.

3.2.4. \mathbb{Z}_2 -symmetric Dirac & Majorana fermionic singlets

The Lagrangians of the fermionic singlet Higgs portal models are

$$\begin{aligned}\mathcal{L}_\chi &= \frac{1}{2}\bar{\chi}(i\not{\partial} - \mu_\chi)\chi - \frac{1}{2}\frac{\lambda_{h\chi}}{\Lambda_\chi}\left(\cos\theta\bar{\chi}\chi + \sin\theta\bar{\chi}i\gamma_5\chi\right)H^\dagger H, \\ \mathcal{L}_\psi &= \bar{\psi}(i\not{\partial} - \mu_\psi)\psi - \frac{\lambda_{h\psi}}{\Lambda_\psi}\left(\cos\theta\bar{\psi}\psi + \sin\theta\bar{\psi}i\gamma_5\psi\right)H^\dagger H,\end{aligned}\quad (11)$$

with the Majorana variant denoted χ and the Dirac variant ψ . These noticeably possess dimension-5 effective portal operators suppressed by the scale

of new physics Λ , with both scalar (CP -even) and pseudoscalar (CP -odd) couplings. The degree to which the portal interaction violates CP is dictated by the mixing angle θ , where $\theta = 0$ corresponds to pure CP conservation and $\theta = \frac{\pi}{2}$ to maximal CP violation.

As in the scalar and vector models, the portal interaction produces terms quadratic in the DM field following electroweak symmetry breaking. The pseudoscalar coupling leads to an imaginary mass term, which must be rotated away with the field transformation $X \rightarrow e^{i\gamma_5\alpha/2}X$ for $X \in \{\chi, \psi\}$, in order to arrive at the physical (real) mass. This introduces a new parameter α . The physical masses are then

$$m_X^2 = \left(\mu_X + \frac{1}{2} \frac{\lambda_{hX}}{\Lambda_X} v_0^2 \cos \theta \right)^2 + \left(\frac{1}{2} \frac{\lambda_X}{\Lambda_X} v_0^2 \sin \theta \right)^2. \quad (12)$$

The rotation parameter α is fixed by the requirement that the mass be real, so all phenomenology can be described by three parameters: m_X , λ_X/Λ_X and $\xi \equiv \theta + \alpha$. Notably, the pure CP -conserving theory ($\theta = 0$) remains CP -conserving after electroweak symmetry breaking ($\xi = 0$), but maximal CP violation before electroweak symmetry breaking does not correspond to maximal violation after the symmetry is broken (i.e. $\theta = \frac{\pi}{2} \not\Rightarrow \xi = \frac{\pi}{2}$).

Whilst the CP -even Higgs portal coupling leads to the familiar velocity and momentum-independent nuclear scattering cross-section, the CP -odd coupling gives rise to an interaction suppressed by q^2 , the square of the momentum exchanged in the scattering event. This leads to an overall suppression of direct detection signals and corresponding constraints for $\xi \rightarrow \frac{\pi}{2}$. Conversely, the CP -odd coupling produces a velocity and momentum-independent annihilation cross-section, whereas the CP -even coupling gives rise to a velocity-suppressed annihilation cross-section.

Profile likelihoods from the global fit to the Majorana fermion model are shown in Fig. 21. Results for Dirac fermion dark matter are broadly very similar, and differ from the Majorana case only in the exact location of the border of the allowed parameter space, reflecting the essentially inconsequential nature of the relative factors of 2 between the two Lagrangians. Grey regions correspond to the regime

$$\lambda_{hX}/\Lambda_X \geq 2\pi/m_X, \quad (13)$$

where the validity of the EFT becomes questionable. Further discussion on this issue can be found in Ref. [112]; it would also be possible to unitarise

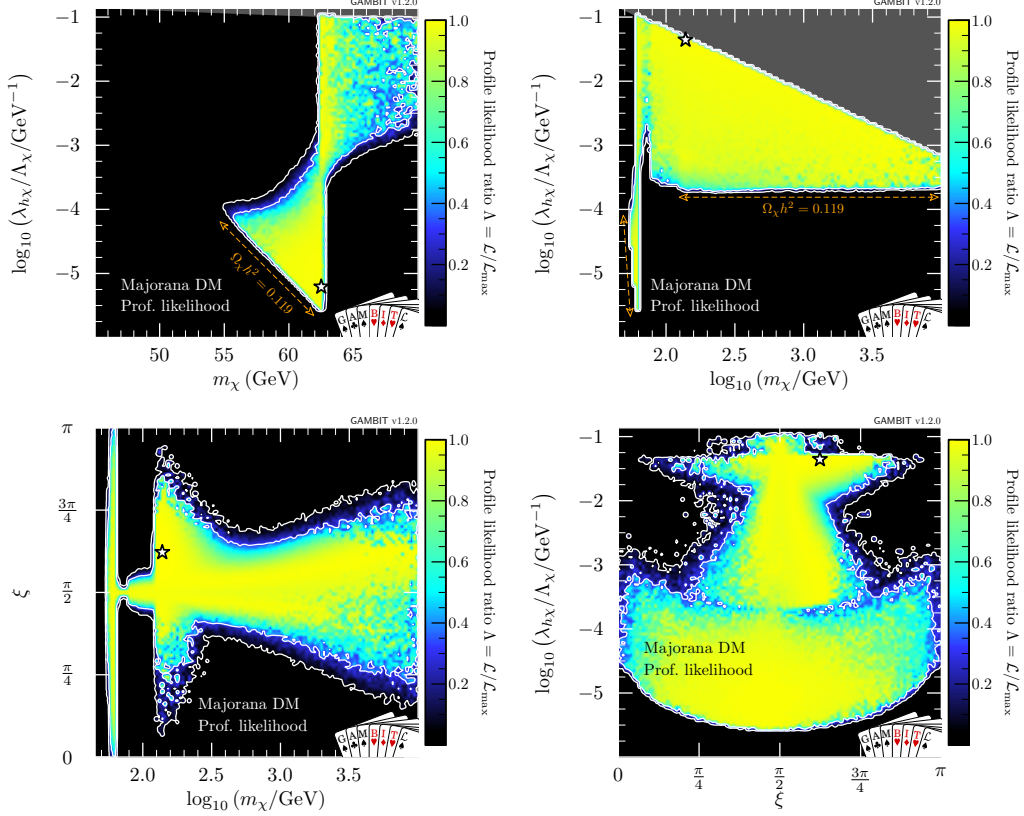


Figure 21: Profile likelihoods of parameters in the \mathbb{Z}_2 -symmetric Majorana fermion singlet Higgs portal dark matter model, including constraints from direct and indirect detection, the relic density of dark matter and LHC searches for invisible decays of the Higgs boson, along with various Standard Model, dark matter halo and nuclear uncertainties. The upper-left panel shows a zoomed-in view of the low-mass resonance region. Grey shading indicates the area that fails the unitarity cut (Eq. 13). Orange annotations indicate the edge of the allowed parameter space along which the model reproduces the entire cosmological abundance of dark matter. Contours show 1 and 2 σ confidence regions. White stars indicate the location of the best-fit point. From [112].

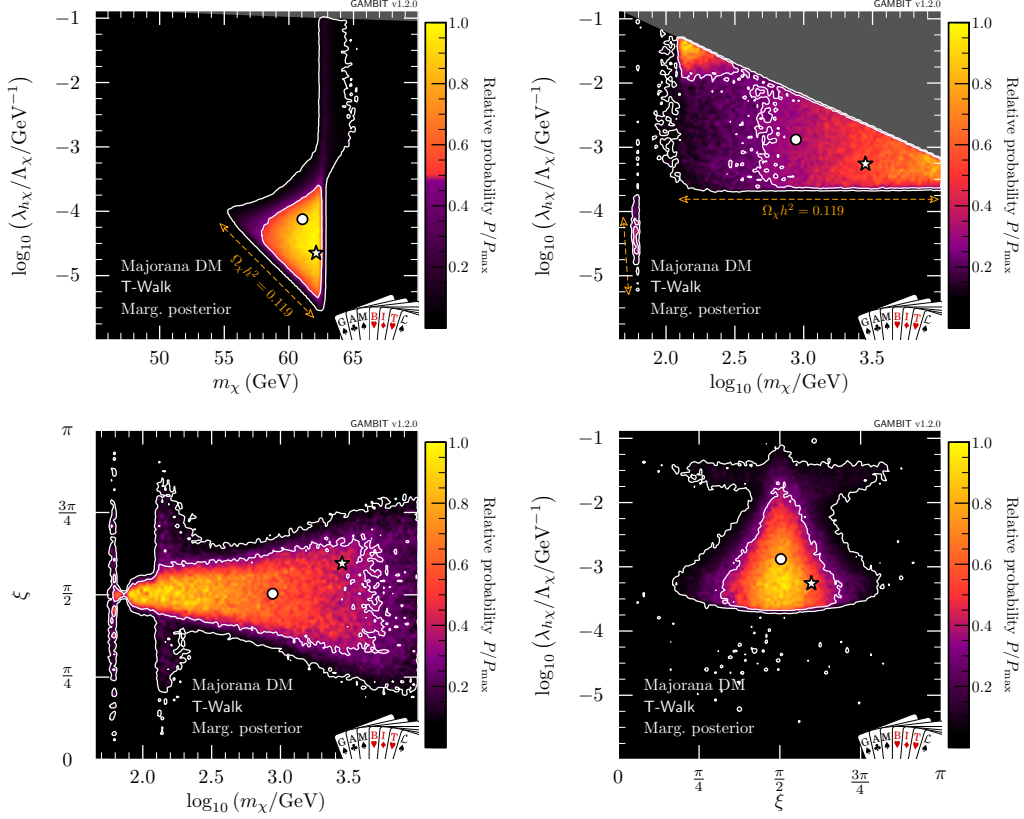


Figure 22: Posterior probability densities from a Bayesian analysis of the \mathbb{Z}_2 -symmetric Majorana fermion singlet Higgs portal dark matter model, using the same likelihood functions as Fig. 21. White bullets indicate posterior means; other annotations are as in Fig. 21. From [112].

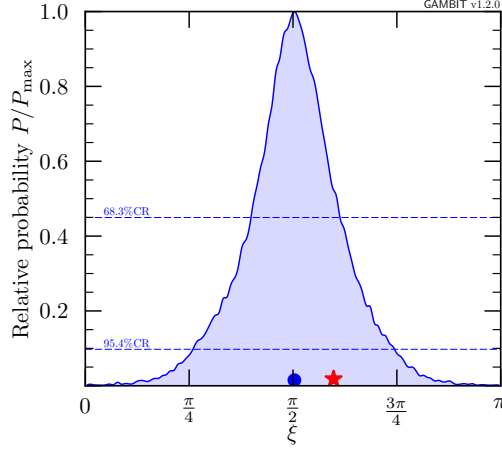


Figure 23: Marginalised one-dimensional posterior probability density for the CP -mixing parameter ξ in the \mathbb{Z}_2 -symmetric Majorana fermion singlet Higgs portal dark matter model. This result has been extracted from the same analysis as that shown in Fig. 22. The value $\xi = 0 = \pi$ corresponds to CP conservation; a clear preference for violation of CP symmetry is evident. The blue bullet indicates the posterior mean value of ξ , and the red star the value of ξ at the best-fit sample. From [112].

the theory, and draw further constraints in this region, using the K -matrix formalism [330, 331].

The preferred regions in the mass-coupling plane (upper panels of Fig. 21) include the now-familiar resonance and high-mass regions. However, unlike the vector and scalar models, these are fully connected by valid models at all masses, with the preferred region bounded from below mostly by the relic density constraint, supported by indirect detection. This is because profiling over ξ allows for the selection of CP -violating couplings in order to avoid constraints from direct detection. The degree of tuning in ξ required to achieve this is apparent in the lower panels of Fig. 21, where it is clear that good fits can be found for any value of ξ in the resonance region, but that higher masses require some degree of CP violation in order to avoid direct detection. This becomes even clearer in the equivalent Bayesian results shown in Fig. 22, where intermediate masses and couplings are disfavoured relative to other regions, due to the need to make CP violation nearly maximal in order to avoid direct detection.

Integrating the posterior over all parameters other than ξ (Fig. 23), there

is a clear preference for CP violation. This reflects the fact that the more CP violation permitted, the broader the range of other parameters able to give good fits to the combined data of all experiments. Performing Bayesian model comparison between the full model and its pure CP -conserving subspace (i.e. $\xi = 0$) results in Bayes factors of between 70:1 and 140:1, depending on the adopted priors. This indicates a strong preference for CP violation in fermionic Higgs portal models. Bayesian model comparison between the scalar, vector and fermionic variants of the Higgs portal DM model reveals essentially equal odds for each of the scalar and fermionic models, but a 6:1 preference for all of these models over the vector variant.

3.3. Axions

3.3.1. Axion models and their implementation in *GAMBIT*

Axions are an intriguing theoretical possibility due to their ability to solve the strong- CP problem of the SM whilst providing a credible DM candidate [332–335]. One can also use axion-like particles to reconcile various tensions between astrophysical observations and theory, including the cooling of white dwarfs [336–342], and the transparency of the Universe to gamma rays [343–348].

The strong- CP problem is ultimately a fine-tuning problem, arising from the fact that the SM symmetries permit a CP -odd term in the SM Lagrangian density of the form:

$$\mathcal{L}_{\text{QCD}} \supset -\frac{\alpha_S}{8\pi} \theta_{\text{QCD}} G_{\mu\nu}^a \tilde{G}^{\mu\nu,a}, \quad (14)$$

where $G_{\mu\nu}^a$ is the gluon field strength tensor, $\tilde{G}^{\mu\nu,a}$ is its dual (both of which have the $SU(3)$ gauge index a explicitly shown), and α_S is the strong coupling constant. The angle $\theta_{\text{QCD}} \in [-\pi, \pi]$ is a free parameter. In the SM, the term also receives a contribution from the chiral anomaly which, for down- and up-type Yukawa matrices Y_d and Y_u , replaces θ_{QCD} by the effective angle

$$\theta_{\text{eff}} \equiv \theta_{\text{QCD}} - \arg[\det(Y_d Y_u)] . \quad (15)$$

A non-zero θ_{eff} would result in CP -violating effects in strong interactions, which are severely constrained by observed upper limits on the electric dipole moment of the neutron, demanding $|\theta_{\text{eff}}| \lesssim 10^{-10}$ [349]. Naively, this can only be avoided in the SM by fine-tuning the value of θ_{QCD} to cancel the contribution from the chiral anomaly.

An alternative solution, first proposed by Peccei and Quinn [350, 351], is to add a new global, axial $U(1)$ symmetry spontaneously broken by the vacuum expectation value v of a complex scalar field. This breaking has an associated pseudoscalar Nambu-Goldstone boson, $a(x)$, which supplements θ_{eff} by a new term $Na(x)/v$, where the non-zero integer N is the colour anomaly of the added symmetry. The Vafa-Witten theorem [352, 353] can then be used to show that $\theta_{\text{eff}} + Na(x)/v$ is dynamically driven to zero, solving the strong CP problem.

In the resulting theory of the QCD axion, the axion is practically massless until the time of the QCD phase transition, due to a shift symmetry of the $U(1)$ phase, which prevents a mass term in the Lagrangian. After this, however, it picks up a small, temperature-dependent mass due to breaking of the continuous shift symmetry by fluctuations of the gluon fields. This gives rise to an effective axion potential

$$V(a) = f_a^2 m_a^2 [1 - \cos(a/f_a)] , \quad (16)$$

where m_a is the temperature-dependent axion mass and $f_a \equiv v/N$. The zero-temperature axion mass, $m_{a,0}$, can be calculated using next-to-leading order chiral perturbation theory, and it turns out to be inversely proportional to f_a for the QCD axion. At higher temperatures, numerical estimates of the mass are available from lattice QCD results, which can be described to a good approximation by

$$m_a(T) = m_{a,0} \begin{cases} 1 & \text{if } T \leq T_\chi \\ \left(\frac{T_\chi}{T}\right)^{\beta/2} & \text{otherwise} \end{cases} . \quad (17)$$

T_χ and β are in principle calculable, but can be left as nuisance parameters in order to account for systematic uncertainties in the calculations.

In fact, QCD axions are only one instance of a general class of *axion-like particles* (ALPs), which could generally result from the breaking of a $U(1)$ symmetry at some scale f_a , with mass generation occurring via the explicit breaking of the residual symmetry at some lower scale Λ [354–356]. It can be shown that in a Friedmann-Robertson-Walker-Lemaître universe, a QCD axion or ALP field $\theta(t) = a(t)/f_a$ satisfies the equation of motion

$$\ddot{\theta} + 3H(t)\dot{\theta} + m_a^2(t) \sin(\theta) = 0, \quad (18)$$

where we have assumed the canonical axion potential of

$$V(\theta) = f_a^2 m_a^2 [1 - \cos(\theta)] . \quad (19)$$

This is subject to the boundary condition $\theta(t_i) = \theta_i$ and $\dot{\theta}(t_i) = 0$, where θ_i is called the *initial misalignment angle*.

The **GAMBIT** collaboration completed a comprehensive study of axion and broader ALP theories in 2018 [113], using an extensive list of experimental constraints. These rely on the interactions of ALPs with SM matter, which can be studied in an effective field theory framework [357–359].

The most general axion/ALP model in **GAMBIT** assumes the effective Lagrangian density to take the form

$$\mathcal{L}_a^{\text{int}} = -\frac{f_a g_{a\gamma\gamma}}{4} \theta F_{\mu\nu} \tilde{F}^{\mu\nu} - \frac{f_a g_{aee}}{2m_e} \bar{e} \gamma^\mu \gamma_5 e \partial_\mu \theta. \quad (20)$$

Note that this provides for possible axion-photon and axion-electron interactions, whilst ignoring terms for other interactions that do not currently give rise to interesting experimental observables. The complete family tree of **GAMBIT** axion/ALP models is shown in Fig. 24, headed by the **GeneralALP** model, whose parameters have all now been defined. This provides a phenomenological description of axion physics that is not constrained to give physical solutions, as the couplings are not inversely proportional to f_a .

The **QCDAxion** model appears as a child model, and differs from the more general case by having tight constraints on some parameters, arising from the known relationships with the QCD scale. The axion-electron coupling is traded for the model-dependent form factor C_{aee}

$$g_{aee} = \frac{m_e}{f_a} C_{aee}, \quad (21)$$

whilst the axion-photon coupling is replaced by the model-dependent ratio of the electromagnetic and colour anomalies E/N

$$g_{a\gamma\gamma} = \frac{\alpha_{\text{EM}}}{2\pi f_a} \left(\frac{E}{N} - \tilde{C}_{a\gamma\gamma} \right). \quad (22)$$

$\tilde{C}_{a\gamma\gamma}$ is a model-independent contribution from axion-pion mixing, which is taken from Ref. [360], and assigned a nuisance likelihood with a relevant uncertainty. Note that the ratio E/N should in principle take discrete values, but it is sampled as a continuous parameter for convenience, seeing as the possible rational values that it can take are close together. The final nuisance parameter of the **QCDAxion** model is Λ_χ , which results from replacing the parameter $m_{a,0}$ of the **GeneralALP** model by an energy scale such that

$$m_{a,0} \equiv \frac{\Lambda_\chi^2}{f_a}. \quad (23)$$

The value of Λ_χ is taken from first-principle calculations of the zero-temperature axion mass provided in Ref. [360],⁷ and it is subject to a Gaussian nuisance likelihood.

The other models of interest for this review are the **KSVZA**xion and **DFSZA**xion model variants, which involve further field content being added to the SM. In **KSVZA**xion models [362, 363], the SM is supplemented by one or more electrically neutral, heavy quarks, and there are no tree-level interactions between the axion and SM fermions. There is, however, still an axion-photon interaction, which generates an axion-electron interaction at one loop. The **GAMBIT** study investigated four different **KSVZA**xion models, distinguished only by the choice of E/N from the set 0, 2/3, 5/3 and 8/3.

DFSZAxion models supplement the SM by an additional Higgs doublet [364, 365], which results in direct axion-electron interactions. Defining the ratio of the two Higgs vacuum expectation values to be $\tan(\beta')$, one can write two variants of the **DFSZA**xion scenario as

$$\begin{aligned} C_{aee} &= \sin^2(\beta')/3, & E/N &= 8/3 & (\text{DFSZA}x\text{ion-I}) \\ C_{aee} &= [1 - \sin^2(\beta')]/3, & E/N &= 2/3 & (\text{DFSZA}x\text{ion-II}) \end{aligned} \quad (24)$$

It is thus convenient to replace the parameter C_{aee} in the **QCD**Axion model by $\tan(\beta')$.

3.3.2. Experimental constraints on axions

Many experiments are sensitive to the axion theories described here, and current null results place tight constraints on axions for specific combinations of masses and coupling strengths. Here we provide a brief review of those constraints, referring the reader to Ref. [113] for a detailed description of the experimental likelihoods.

- **Light-shining-through-wall (LSW) experiments:** Photon-axion interactions would allow photons to pass through a wall by becoming an axion, only to convert back to a photon on the other side. LSW experiments attempt to observe this by shining laser light onto an opaque material in the presence of a strong magnetic field. The **GAMBIT** LSW likelihood uses the results from the **ALPS-I** experiment, using data for both evacuated and gas-filled magnets [366].

⁷This value was later updated in [361], after the appearance of Ref. [113].

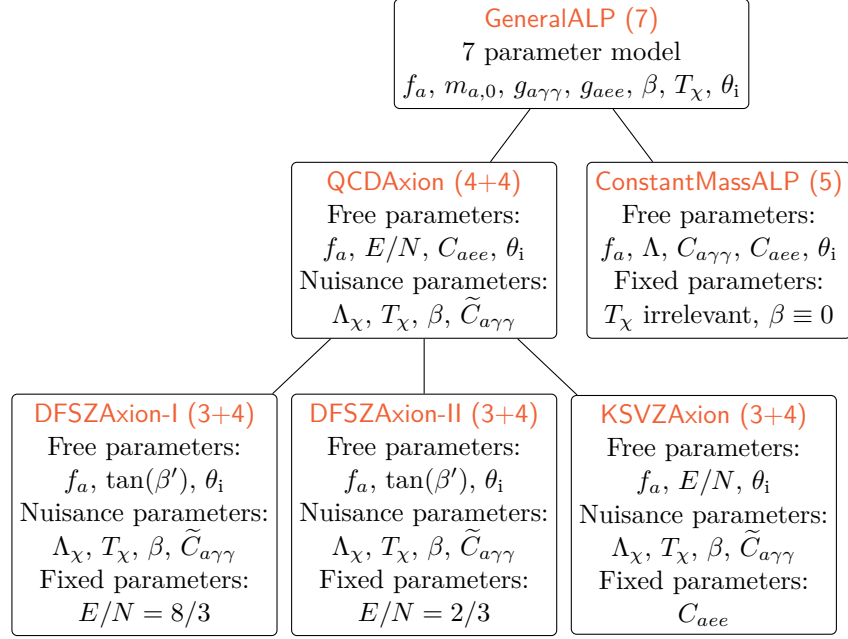


Figure 24: Family tree of axion models in GAMBIT. The numbers in brackets refer to the number of model parameters; $(n + m)$ indicates n (largely unconstrained) fundamental parameters of the model and m (typically well-constrained) nuisance parameters. From [113].

- **Helioscopes:** Axion production in the Sun can be probed by observing the solar disc with a long magnet contained in an opaque casing. Any axions produced in the Sun that made it to Earth would pass through the exterior, and potentially convert to photons within the magnetic field in the interior. The details of solar axion production depend on the solar model, in addition to the axion-photon and axion-electron couplings. The GAMBIT axion studies utilise the AGSS09met solar model [367, 368] and its more recent iteration [369], and utilise two separate likelihoods for the 2007 and 2017 results of the CAST experiment [370, 371].
- **Haloscopes (cavity experiments):** Axion haloscopes aim to detect resonant axion-photon conversion inside a tunable cavity [372, 373], with microwave cavities providing the greatest current sensitivity to axions. Unfortunately, the resonant nature of the experiment means that one obtains highly sensitive constraints only within a very narrow mass range. The ability of haloscope experiments to detect axions depends

on their cosmological abundance, as well as the galactic DM velocity distribution [374]. The **GAMBIT** study combines separate likelihood terms for the Rochester-Brookhaven-Fermi (RBF) [375, 376], University of Florida (UF) [377], ADMX 1998-2009 [378–382] and ADMX 2018 [383] datasets.

- **Dark matter relic density:** Although axions are not a thermal relic such as those encountered in WIMP models, the relic abundance of axion DM is calculable numerically via the details of the realignment mechanism that follow from the equation of motion given in Eq 18. This can be compared with the observed value from the most recent *Planck* analysis [19]. The **GAMBIT** axion study applied this as both an upper limit (in which case axions are allowed to provide only a component of DM) and, in separate analyses of each model, a measurement. In the former case, anticipated yields in experiments that rely on the local DM density were scaled accordingly.
- **Distortions of gamma-ray spectra:** Axion-photon conversions could occur in strong galactic or inter-galactic magnetic fields, resulting in a distortion of the spectra of distant sources [384–387]. There is a critical energy scale E_{crit} at which photons will efficiently convert into axions, and it can be shown that spectral distortions only occur in real measurements when the critical energy lies within the spectral window of the instrument [388, 389]. This has the effect of localising constraints from spectral distortion measurements to specific ranges of the axion mass. The **GAMBIT** axion study utilises a likelihood based on H.E.S.S studies of the active galactic nucleus PKS 2155-304 [390].
- **Supernova 1987A:** If axions had been produced in the SN1987A supernova explosion, they could have been converted to photons in the Galactic magnetic field, and detected as a coincident gamma ray burst by the Solar Maximum Mission [391]. The absence of this observation has been used to constrain axion properties. The **GAMBIT** study uses a likelihood based on Ref. [392].
- **Horizontal Branch stars and the R parameter:** The existence of axions would provide an extra mechanism of energy loss for stars, causing them to cool faster [393–395]. This would affect the relative time that stars spend on the Horizontal Branch (HB) and upper Red

Giant Branch (RGB), which in turn sets the observed ratio of the numbers of stars on these branches ($R = N_{\text{HB}}/N_{\text{RGB}}$). Theory suggests that axions would have the most significant impact on the lifetimes of HB stars, leading to a reduction in R . The **GAMBIT** R parameter likelihood is based on the comparison of a calculation of the R parameter for axion theories [339, 396–399] with the observed value of $R_{\text{obs}} = 1.39 \pm 0.03$ [399], which is based on a weighted average of cluster count observations [400].

- **White Dwarf cooling hints:** White dwarfs (WDs) are intriguing axion laboratories for several reasons. The first is that energy loss via axion production in WDs can be probed experimentally by using measurements of the oscillations of their radii and luminosities. These can be related to their internal structure via astroseismology, and measurements of the decrease in the oscillation periods can be related to energy loss. The second reason is that WDs have electron-degenerate cores, allowing us to probe the axion-electron coupling rather than the electron-photon coupling. A number of previous studies have calculated the expected period decrease in the presence of axions. The **GAMBIT** WD cooling likelihood is based on interpolation of the results and uncertainties found in Refs. [337, 338, 340, 341]. Current evidence suggests that WDs actually require an additional cooling mechanism relative to standard models, but this remains controversial due to a number of experimental and theoretical issues. The **GAMBIT** axion paper thus contains studies generated both with and without WD cooling hints added to the combined likelihood.

3.3.3. *GAMBIT results for the QCDAxion model*

Although the **GAMBIT** axion paper contained results for all of the models described above, we will here concentrate on the **QCDAxion** results in the interests of brevity. The various parameters (including nuisance parameters) are shown in Table 1, along with the chosen priors and prior ranges. For each of the nuisance parameters, the prior range is chosen to cover a range of approximately -5σ to $+5\sigma$ around the known central value, where σ is the known uncertainty. The range of E/N values is selected to encompass those encountered in a broad range of previous axion model studies, whilst the range on f_a is driven by the requirement that the range of possible axion masses reaches from very small masses to the the largest mass allowed by

Table 1: Prior choices for QCDAxion models in [113].

Model	Parameter range/value		Prior type
QCDAxion	f_a [GeV]	$[10^6, 10^{16}]$	log
	Λ_χ [MeV]	$[73, 78]$	flat
	$\tilde{C}_{a\gamma\gamma}$	$[1.72, 2.12]$	flat
	E/N	$[-1.333\,33, 174.667]$	flat
	C_{aee}	$[10^{-4}, 10^4]$	log
	θ_i	$[-3.141\,59, 3.141\,59]$	flat
	β	$[7.7, 8.2]$	flat
	T_χ [MeV]	$[143, 151]$	flat
Local DM density	ρ_0 [GeV/cm ³]	$[0.2, 0.8]$	flat

bounds on hot DM. Our choice of a log prior for f_a is motivated by the fact that the scale is unknown. C_{aee} is explored in a generous range around 1, whilst the causal structure of the early Universe motivates our use of a flat prior on the initial misalignment angle θ_i . The local DM density ρ_0 is given the same treatment as in previous GAMBIT studies.

Fig. 25 shows profile likelihood distributions in various planes of the QCDAxion parameters, obtained without the presence of WD cooling hints in the combined likelihood. The left panels show the result of imposing the relic density constraint as an upper limit. The exclusion of the low- f_a (high mass) region, except at very low values of the axion-photon coupling (which is related to E/N), arises from the R parameter and CAST results. The slight reduction in the profile likelihood for masses lower than approximately 0.1 μeV also comes from the R parameter likelihood; for such masses, the maximum allowed value for the axion-electron coupling ($C_{aee} \leq 10^4$) is not large enough to perfectly satisfy the R -parameter constraint. If axions are assumed to saturate the relic abundance of DM (right top panel), the high-mass region is excluded entirely due to the fact that the realignment mechanism cannot produce enough DM. The bottom row of Fig. 25 shows the allowed values for the initial misalignment angle. In the case that axions supply all of DM, we recover the familiar result that $|\theta_i| \ll 1$, for QCD axion masses of $m_{a,0} \lesssim 0.1 \mu\text{eV}$, a fine-tuning that we will discuss further in the context of a Bayesian analysis.

In the left panel of Fig. 26, we show the marginalised Bayesian posterior in the $\Omega_a h^2 - m_{a,0}$ plane without WD cooling hints, demonstrating that the scan can find viable parts of the parameter space where axions consistent

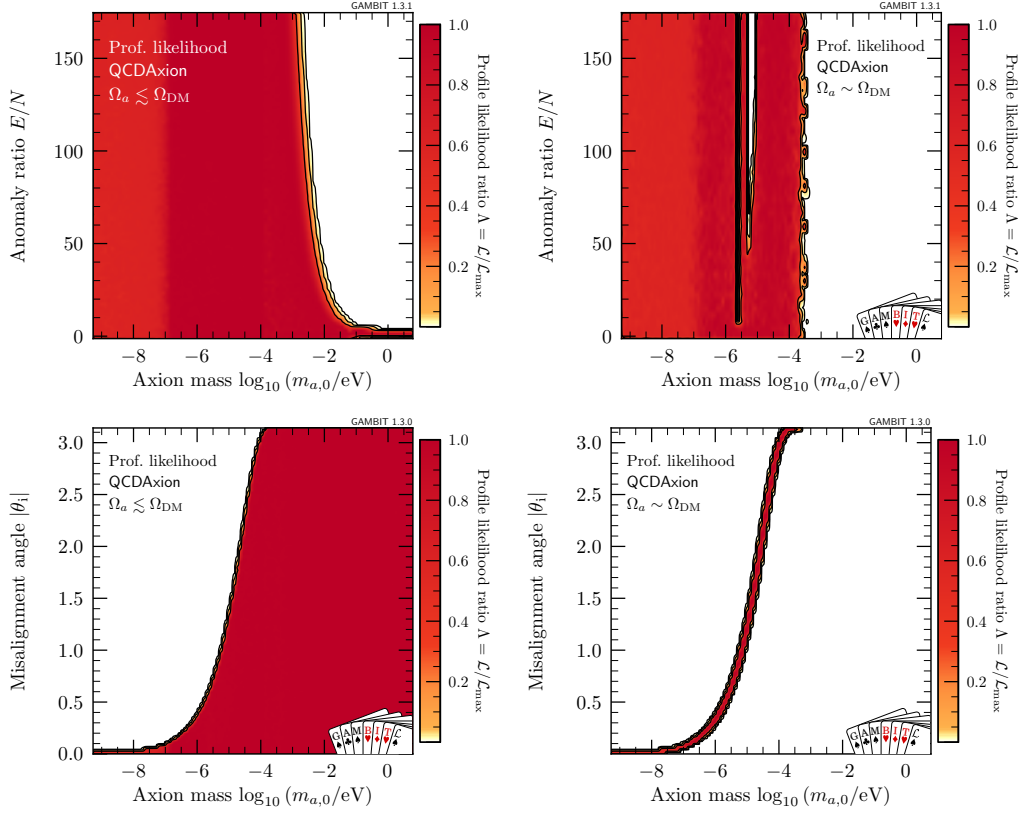


Figure 25: Profile likelihoods (from Diver) for QCD Axion models with upper limits (*left*) and matching condition (*right*) for the observed DM relic density. The upper and lower panels show the constraints on the anomaly ratio, E/N , and the absolute value of the initial misalignment angle, $|\theta_1|$, respectively. From [113].

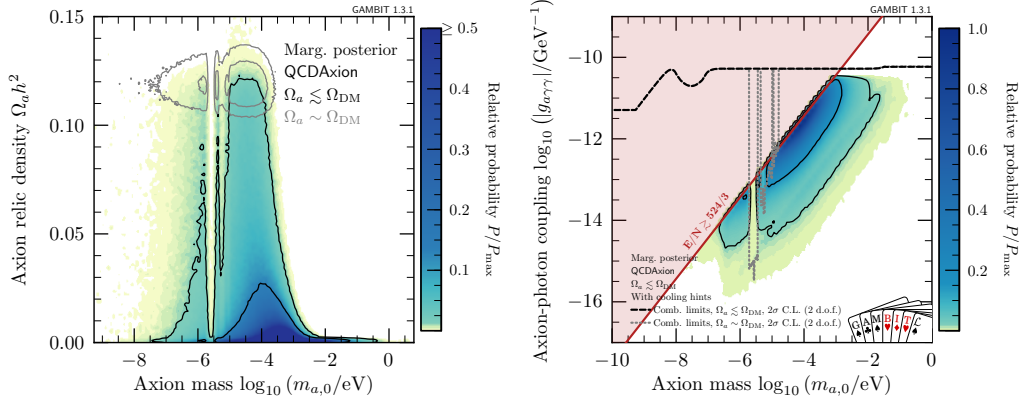


Figure 26: Marginalised posterior for QCDAxion models with the DM relic density constraint treated as an upper limit. *Left:* constraints on the energy density in axions today, $\Omega_a h^2$, without the inclusion of WD cooling hints. *Right:* constraints on the absolute value of the axion-photon coupling, $|g_{a\gamma\gamma}|$. This panel also includes WD cooling hints, but they have little impact on the result. For comparison, the right panel also shows the region for which QCD axions are not theoretically possible (red line and shading), as well as the frequentist 2σ C.L. constraints on more general ALP models (dashed lines). From [113].

with all current experimental observations can account for a sizable fraction of dark matter. The situation is similar even when WD cooling hints are included (not shown). One can also observe an interesting bound on the axion mass. If the DM relic density constraint is applied as an upper limit, we find $0.73 \mu\text{eV} \leq m_{a,0} \leq 6.1 \text{ meV}$ at 95% credibility (equal-tailed interval). Meanwhile, if axions must provide all of the observed dark matter, this changes to $0.53 \mu\text{eV} \leq m_{a,0} \leq 0.13 \text{ meV}$.

In the right panel of Fig. 26, we show the marginalised posterior in the $|g_{a\gamma\gamma}| - m_{a,0}$ plane with the DM relic density constraint applied as an upper limit, and with WD cooling hints included. Also shown are the naïve bounds on the parameter space that result from phenomenological constraints on GeneralALP models and the maximum value of E/N . The shape of the preferred region is partly formed by the effect of fine-tuning. At low axion masses, this is required to avoid dark matter overproduction, whilst at large axion masses it is required to achieve low values of $|g_{a\gamma\gamma}|$ through cancellations between E/N and $\tilde{C}_{a\gamma\gamma}$. The preferred parameter region is localised within a few orders of magnitude in mass around $m_{a,0} \sim 100 \mu\text{eV}$

Table 2: Prior choices for DFSZAxion-I, DFSZAxion-II and KSVZAxion models in [113]. Note that the priors listed in the first section of the table apply to all three models.

Model	Parameter range/value		Prior type	Comments
	f_a [GeV]	$[10^6, 10^{16}]$	log	Applies to all
	Λ_χ [MeV]	$[73, 78]$	flat	Applies to all
	$\tilde{C}_{a\gamma\gamma}$	$[1.72, 2.12]$	flat	Applies to all
	θ_i	$[-3.141\,59, 3.141\,59]$	flat	Applies to all
	β	$[7.7, 8.2]$	flat	Applies to all
	T_χ [MeV]	$[143, 151]$	flat	Applies to all
DFSZAxion-I	E/N	$8/3$	delta	
	$\tan(\beta')$	$[0.28, 140.0]$	log	
DFSZAxion-II	E/N	$2/3$	delta	
	$\tan(\beta')$	$[0.28, 140.0]$	log	
KSVZAxion	E/N	$0, 2/3, 5/3, 8/3$	delta	Discrete
Local DM density	ρ_0 [GeV/cm ³]	$[0.2, 0.8]$	flat	

and $g_{a\gamma\gamma} \sim 10^{-12} \text{ GeV}^{-1}$.

The GAMBIT Bayesian analysis of axion models also includes a model comparison of the QCDAxion, DFSZAxion-I, DFSZAxion-II and KSVZAxion, based on scans of the latter models that use the priors defined in Table 2. Bayesian evidence values $\mathbb{Z}(\mathcal{M})$ for each model \mathcal{M} were calculated using the MultiNest nested sampling package, before constructing the Bayes factor [401–403]

$$\mathcal{B} \equiv \frac{\mathbb{Z}(\mathcal{M}_1)}{\mathbb{Z}(\mathcal{M}_2)} \equiv \frac{\int \mathcal{L}(\text{data} | \boldsymbol{\theta}_1) \pi_1(\boldsymbol{\theta}_1) d\boldsymbol{\theta}_1}{\int \mathcal{L}(\text{data} | \boldsymbol{\theta}_2) \pi_2(\boldsymbol{\theta}_2) d\boldsymbol{\theta}_2}, \quad (25)$$

which relates two models \mathcal{M}_1 and \mathcal{M}_2 with parameters $\boldsymbol{\theta}_1$ and $\boldsymbol{\theta}_2$. π_1 and π_2 are the priors on the parameters of the two models, and \mathcal{L} is the likelihood. The Bayes factor is connected to the ratio of posterior probabilities of the models being correct

$$\frac{\mathcal{P}(\mathcal{M}_1 | \text{data})}{\mathcal{P}(\mathcal{M}_2 | \text{data})} = \mathcal{B} \frac{\pi(\mathcal{M}_1)}{\pi(\mathcal{M}_2)}, \quad (26)$$

where the prior probabilities of the models themselves being correct are given by $\pi(\mathcal{M}_1)$ and $\pi(\mathcal{M}_2)$. In the following, it is assumed that $\pi(\mathcal{M}_1) = \pi(\mathcal{M}_2)$, causing the the posterior odds ratio to be equal to the Bayes factor.

Without cooling hints, the odds ratios for pairs of models provide insufficient evidence to favour any particular scenario. However, if it is demanded that axions solve the DM and WD cooling problems simultaneously, there is a positive preference for the **QCDAxion** model over the DFSZ- and KSVZ-type models, at a level of about 5:1. This results from the larger C_{aee} values allowed in the **QCDAxion** model, which peaks at $C_{aee} \approx 100$ in the one-dimensional marginalised posterior. Such a large coupling may cause a problem for model building. A frequentist analysis of the same scenario allows both the **DFSZAxion** and **KSVZAxion** models to be rejected with respect to the **QCDAxion** model with better than 99% confidence; if DM is instead allowed to consist only partially of axions, only **KSVZAxion** models can be rejected in this way.

3.4. Right-handed neutrinos

3.4.1. Model definition

The addition of right-handed “sterile” neutrinos to the SM has been proposed to explain the existence of neutrino flavour oscillations, which imply a non-zero neutrino mass. They also serve an aesthetic theoretical purpose, as neutrinos are the only elementary fermions in the SM to not have both left- and right-handed incarnations. Moreover, sterile neutrinos are permitted to have both a Dirac mass term $\bar{\nu}_L M_D \nu_R$ and a Majorana mass term $\bar{\nu}_R M_M \nu_R^c$, and specific choices of the latter allow sterile neutrinos to solve cosmological problems such as the baryon asymmetry of the Universe [404–406], and the DM problem [407, 408].

A convenient parameterisation of a right-handed neutrino sector is the Casas-Ibarra parametrisation, amended to include 1-loop corrections to the left-handed neutrino mass matrix [409, 410]. This involves writing a matrix that encodes the mixing among left-handed neutrinos (LHNs) and right-handed neutrinos (RHNs) as

$$\Theta = iU_\nu \sqrt{m_\nu^{\text{diag}}} \mathcal{R} \sqrt{\tilde{M}^{\text{diag}}}^{-1}, \quad (27)$$

where U_ν is the PMNS matrix, m_ν^{diag} is a diagonalised, one-loop-corrected LHN mass matrix and \tilde{M}^{diag} is the analogous RHN mass matrix. \mathcal{R} is a complex, orthogonal matrix written as the product

$$\mathcal{R} = \mathcal{R}^{23} \mathcal{R}^{13} \mathcal{R}^{12}, \quad (28)$$

where the \mathcal{R}^{ij} can, in turn, be parameterised by complex angles ω_{ij} with

$$\mathcal{R}_{ii}^{ij} = \mathcal{R}_{jj}^{ij} = \cos \omega_{ij}, \quad (29)$$

Parameter
Active neutrino parameters
θ_{12} [rad]
θ_{23} [rad]
θ_{13} [rad]
m_{ν_0} [eV]
Δm_{21}^2 [10^{-5} eV ²]
Δm_{3l}^2 [10^{-3} eV ²]
α_1, α_2 [rad]
Sterile neutrino parameters
δ [rad]
Re ω_{ij} [rad]
Im ω_{ij}
M_I [GeV]
R_{order}
Nuisance parameters
m_h [GeV]

Table 3: The full list of scanned parameters for the GAMBIT right-handed neutrino study [114].

$$\mathcal{R}_{ij}^{ij} = -\mathcal{R}_{ji}^{ij} = \sin \omega_{ij}, \quad (30)$$

$$\mathcal{R}_{kk}^{ij} = 1; k \neq i, j. \quad (31)$$

Working in the flavour basis in which the Yukawa couplings of the charged leptons are diagonal by construction, the PMNS matrix U_ν can be written as

$$U_\nu = V^{23} U_\delta V^{13} U_{-\delta} V^{12} \text{diag}(e^{i\alpha_1/2}, e^{i\alpha_2/2}, 1), \quad (32)$$

where $U_{\pm\delta} = \text{diag}(e^{\mp i\delta/2}, 1, e^{\pm i\delta/2})$ and V^{ij} is parameterised by the LHN mixing angles θ_{ij} . The non-zero elements of V^{ij} are analogous to those of \mathcal{R} . α_1, α_2 and δ are CP -violating phases that are not excluded *a priori*.

A comprehensive, frequentist GAMBIT study of this scenario has recently been completed [114]. The full list of parameters considered in the GAMBIT RHN study is given in Table 3. Separate scans were done for the cases of a normal and an inverted mass hierarchy, and the scanning strategy used a number of carefully targeted scans to ensure that the regions near the

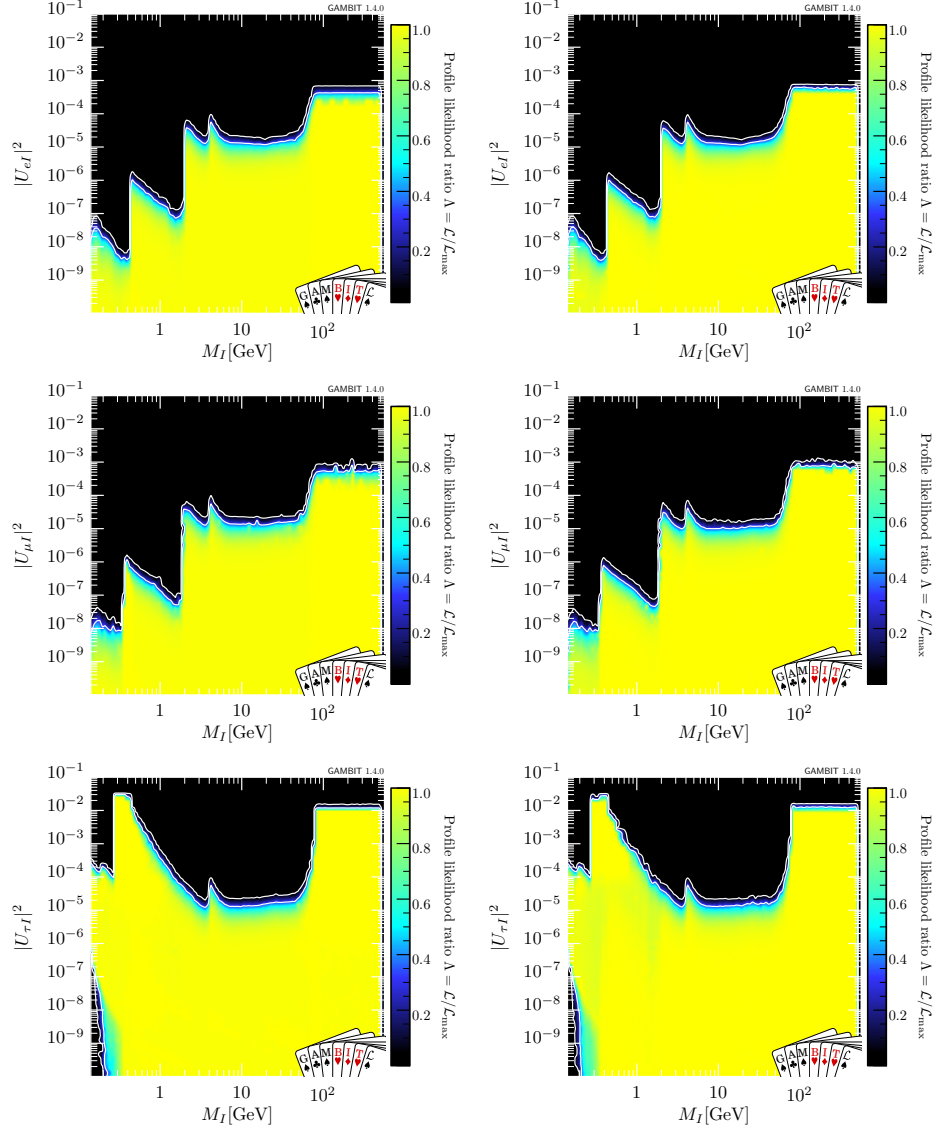


Figure 27: Profile likelihoods of right-handed neutrino models in the M_I vs U_{eI}^2 (top), M_I vs $U_{\mu I}^2$ (middle) and M_I vs $U_{\tau I}^2$ (bottom) planes. Results are shown for normal (left) and inverted (right) neutrino mass ordering. From [114].

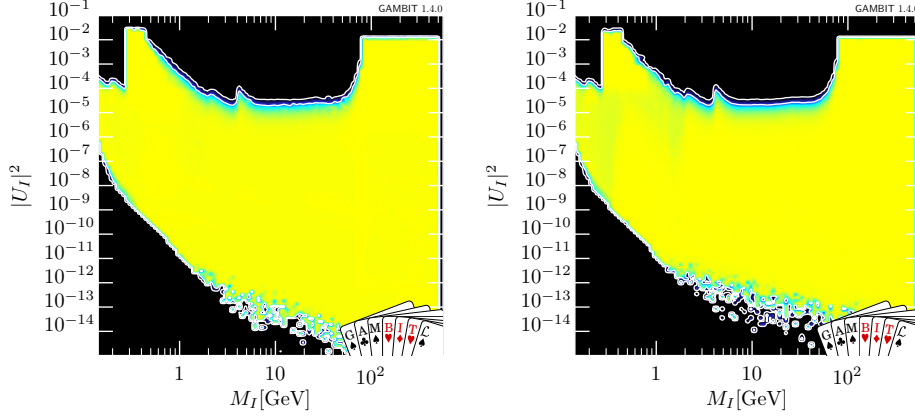


Figure 28: Profile likelihood of right-handed neutrino models in the M_I vs U_I^2 plane for normal (left) and inverted (right) neutrino mass ordering. From [114].

various experimental bounds were convergently sampled. The scans used the full range of likelihoods implemented in **NeutrinoBit**, documented in Section 2.4.7, in addition to the extra routines described in **FlavBit**, **DecayBit** and **PrecisionBit**. The main analysis used a capped likelihood, in which each point is forced to have a likelihood which is equal to or worse than the SM ($\mathcal{L} = \min[\mathcal{L}_{\text{SM}}, \mathcal{L}_{\text{RHN}}]$). This is due to a number of excesses in individual experimental observations that — although combining to give a small overall significance — would bias the presentation of exclusion limits on RHN parameters. In this review, we concentrate on the resulting limits on RHNs, and direct the reader to the original study [114] for a detailed discussion of the excesses.

The 1-loop Casas-Ibarra parameterisation used in the GAMBIT analysis [114] is valid for seesaw scenarios where the active-sterile mixing, $|\Theta|^2$, is small. In principle, additional $|\Theta|^4$ corrections could be expected in low-scale seesaw scenarios, and could only be captured by an exact expansion (e.g. Schechter-Valle [411]). Nevertheless, the loss of generality in the Casa-Ibarra approximation is outweighed by its numerical and computational benefits. This parameterisation allows one to explicitly choose the masses of both active and sterile neutrinos, and is automatically consistent with oscillation data, allowing oscillation parameters to be easily treated as Gaussian nuisances. Alternative parameterisations would constitute a different effective prior on both the sterile and active neutrino parameters. Because the GAMBIT

analysis is based on profile likelihoods, which are by construction prior-independent, switching parameterisation would only have the impact of making sampling less efficient, rather than causing any physical or statistical effect.

3.4.2. *RHN results*

In Fig. 27, we show, as functions of the heavy neutrino masses M_I , the constraints on the couplings $U_{\alpha I}^2$ to the active neutrino flavours $\alpha = (e, \mu, \tau)$; in Fig. 28 we also show the overall constraints on their combination $U_I^2 = \sum_{\alpha} U_{\alpha I}^2$. The index I can refer to any of the heavy neutrino flavours $I = (1, 2, 3)$, as their labelling has no physical significance. The profile likelihood is mostly flat at low values of the couplings, but exhibits characteristic drop-offs at higher values that result from specific experimental observations. The most dominant constraint varies with the RHN mass.

Above the masses of the weak gauge bosons, direct searches at colliders are not relevant, and the leading constraints on the RHN properties come from electroweak precision observables, CKM measurements and searches for lepton flavour violation (LFV). The upper limits on the τ couplings are much larger than on the e and μ couplings, due to the fact that the EWPO and LFV limits are stronger for the e and μ flavours.

When M_I is between the D meson and W boson masses, direct search experiments dominate, as RHNs are efficiently produced via the s -channel exchange of on-shell W bosons. The DELPHI and CMS results compete to impose the strongest bound in this region.

Below the D meson mass, the dominant constraints come from direct searches at beam-dump experiments, in particular CHARM and NuTeV (above the kaon mass), PS-191 and E949 (between the pion and the kaon mass), and pion decay experiments at even lower mass. In the case of the τ couplings, the direct search constraints are much weaker, and the most significant constraint instead comes from DELPHI searches for long-lived particles.

For M_I values below 0.3 GeV, the global constraints are stronger than the sum of the individual contributions, due to an interplay between the lower bound from BBN, the upper bounds from direct searches and the constraints on RHN mixing from neutrino oscillation data (which disfavour large hierarchies amongst the couplings to individual SM flavours). The BBN lifetime constraint does not have an observable effect on the individual couplings, but it does force their combination to be greater than a certain

value (as seen in Fig. 28).

Finally, we point out that although this analysis included the active neutrino oscillation likelihoods contained in **NeutrinoBit**, based on the results of **NuFit** [3], it would not change the results even slightly if one were to replace these with nuisance likelihoods from either of the other main 3-flavour neutrino fitting groups [412, 413]. This is because the results of all three groups are highly consistent, and the preferred parameter region is where the approximate $B - L$ symmetry holds and the oscillation constraints are essentially irrelevant. As the fits allow $m_{\nu_0} \rightarrow 0$, there is no lower limit implied on M_I from oscillation data, but rather only from BBN (the effects of which were modelled under the massless neutrino approximation).

4. Summary

GAMBIT is an open-source software framework for combining all relevant experimental constraints on theories for physics Beyond the Standard Model. It includes extensive libraries of theory and likelihood routines for dark matter, flavour, collider, neutrino and precision observables, along with spectrum and decay calculations, all for a range of popular and highly plausible theories of new physics. It features an array of different statistical samplers, a hierarchical model database, an automated engine for building calculations based on graph theory, and the ability to connect to external physics calculators with ease.

In the two years since its release, **GAMBIT** has produced seven global analyses of leading theories for physics beyond the Standard Model. In supersymmetry, this includes analyses of the CMSSM, NUHM1, NUHM2, a 7-parameter weak-scale MSSM, and an electroweakino effective field theory known as the EWMSSM. Results indicate a 3.3σ combined preference in LHC searches for weak production of light charginos and neutralinos. In Higgs portal dark matter, **GAMBIT** results cover \mathbb{Z}_2 and \mathbb{Z}_3 -symmetric scalar singlet models, as well as \mathbb{Z}_2 -symmetric vector and fermion models. All can provide good fits to experimental constraints, but fermionic models strongly prefer to violate CP . Scalar models can not only solve the dark matter problem, but can also stabilise the vacuum of the standard model if and only if they possess TeV-scale masses and respect a \mathbb{Z}_2 symmetry. **GAMBIT** studies indicate that QCD axions are most likely to constitute a fraction of dark matter rather than the entire amount, and to reside in a mass window between about 10^{-7} and 10^{-3} eV. Right-handed neutrinos are constrained by a wide array of different searches at different masses; interactions with

electrons and muons are the most strongly constrained, with constraints on couplings to tau leptons somewhat weaker.

GAMBIT is a powerful tool for testing theories of new physics. The code can be obtained from <https://gambit.hepforge.org>. All samples, input files and benchmark points resulting from the GAMBIT physics studies discussed in this review can also be obtained from Zenodo, by visiting <https://zenodo.org/communities/gambit-official>.

Acknowledgements

We thank our collaborators within the GAMBIT Community for their essential and extensive contributions to the work reviewed in this article, and Tomás Gonzalo in particular for comments on right-handed neutrinos. The majority of plots presented in the review were produced with `pippi` [414]. We acknowledge PRACE for awarding us access to Marconi at CINECA, Italy.

References

- [1] F. Capozzi, G. L. Fogli, *et. al.*, *Status of three-neutrino oscillation parameters, circa 2013*, *Phys. Rev. D* **89** (2014) 093018, [[arXiv:1312.2878](#)].
- [2] D. V. Forero, M. Tórtola, and J. W. F. Valle, *Neutrino oscillations refitted*, *Phys. Rev. D* **90** (2014) 093006, [[arXiv:1405.7540](#)].
- [3] J. Bergström, M. C. Gonzalez-Garcia, M. Maltoni, and T. Schwetz, *Bayesian global analysis of neutrino oscillation data*, *JHEP* **9** (2015) 200, [[arXiv:1507.04366](#)].
- [4] J. Charles, A. Höcker, *et. al.*, *CP violation and the CKM matrix: assessing the impact of the asymmetric B factories*, *Eur. Phys. J. C* **41** (2005) 1–131, [[hep-ph/0406184](#)].
- [5] A. B. Arbuzov, M. Awramik, *et. al.*, *ZFITTER: a semi-analytical program for fermion pair production in ee annihilation, from version 6.21 to version 6.42*, *Comp. Phys. Comm.* **174** (2006) 728–758, [[hep-ph/0507146](#)].

- [6] M. Baak, M. Goebel, *et. al.*, *Updated status of the global electroweak fit and constraints on new physics*, *Eur. Phys. J. C* **72** (2012) 2003, [[arXiv:1107.0975](#)].
- [7] ATLAS Collaboration, *Search for resonances decaying to photon pairs in 3.2 fb^{-1} of pp collisions at $\sqrt{s} = 13\text{ TeV}$ with the ATLAS detector*, *ATLAS-CONF-2015-081* (2015).
- [8] ATLAS Collaboration: ATLAS Collaboration, *Summary of the ATLAS experiment's sensitivity to supersymmetry after LHC Run 1 – interpreted in the phenomenological MSSM*, *JHEP* **10** (2015) 134, [[arXiv:1508.06608](#)].
- [9] CMS Collaboration: CMS Collaboration, *Search for supersymmetry in the multijet and missing transverse momentum final state in pp collisions at 13 TeV* , *Phys. Lett. B* **758** (2016) 152–180, [[arXiv:1602.06581](#)].
- [10] G. W. Bennett, B. Bousquet, *et. al.*, *Final report of the E821 muon anomalous magnetic moment measurement at BNL*, *Phys. Rev. D* **73** (2006) 072003, [[hep-ex/0602035](#)].
- [11] T. Abe, I. Adachi, *et. al.*, *Belle II Technical Design Report*, [[arXiv:1011.0352](#)].
- [12] CMS and LHCb Collaborations, *Observation of the rare $B_s^0 \rightarrow \mu^+ \mu^-$ decay from the combined analysis of CMS and LHCb data*, *Nature* **522** (2015) 68–72, [[arXiv:1411.4413](#)].
- [13] XENON100 Collaboration: E. Aprile, M. Alfonsi, *et. al.*, *Dark Matter Results from 225 Live Days of XENON100 Data*, *Phys. Rev. Lett.* **109** (2012) 181301, [[arXiv:1207.5988](#)].
- [14] C. Amole, M. Ardid, *et. al.*, *Dark matter search results from the PICO-60 CF_3 I bubble chamber*, *Phys. Rev. D* **93** (2016) 052014, [[arXiv:1510.07754](#)].
- [15] D. S. Akerib, H. M. Araújo, *et. al.*, *Improved Limits on Scattering of Weakly Interacting Massive Particles from Reanalysis of 2013 LUX Data*, *Phys. Rev. Lett.* **116** (2016) 161301, [[arXiv:1512.03506](#)].

- [16] T. Bringmann and C. Weniger, *Gamma ray signals from dark matter: Concepts, status and prospects*, *Physics of the Dark Universe* **1** (2012) 194–217, [[arXiv:1208.5481](#)].
- [17] Fermi-LAT Collaboration: M. Ackermann, A. Albert, *et. al.*, *Searching for Dark Matter Annihilation from Milky Way Dwarf Spheroidal Galaxies with Six Years of Fermi Large Area Telescope Data*, *Phys. Rev. Lett.* **115** (2015) 231301, [[arXiv:1503.02641](#)].
- [18] IceCube Collaboration: M. G. Aartsen *et. al.*, *Improved limits on dark matter annihilation in the Sun with the 79-string IceCube detector and implications for supersymmetry*, *JCAP* **04** (2016) 022, [[arXiv:1601.00653](#)].
- [19] Planck Collaboration, P. A. R. Ade, *et. al.*, *Planck 2015 results. XIII. Cosmological parameters*, *A&A* **594** (2016) A13, [[arXiv:1502.01589](#)].
- [20] T. R. Slatyer, *Indirect dark matter signatures in the cosmic dark ages. I. Generalizing the bound on s -wave dark matter annihilation from Planck results*, *Phys. Rev. D* **93** (2016) 023527, [[arXiv:1506.03811](#)].
- [21] R. Adhikari, M. Agostini, *et. al.*, *A White Paper on keV Sterile Neutrino Dark Matter*, [arXiv:1602.04816](#).
- [22] E. A. Baltz and P. Gondolo, *Markov Chain Monte Carlo Exploration of Minimal Supergravity with Implications for Dark Matter*, *JHEP* **10** (2004) 52, [[hep-ph/0407039](#)].
- [23] B. C. Allanach and C. G. Lester, *Multidimensional $mSUGRA$ likelihood maps*, *Phys. Rev. D* **73** (2006) 015013, [[hep-ph/0507283](#)].
- [24] R. Lafaye, T. Plehn, and D. Zerwas, *SFITTER: SUSY Parameter Analysis at LHC and LC*, [hep-ph/0404282](#).
- [25] R. Ruiz de Austri, R. Trotta, and L. Roszkowski, *A Markov chain Monte Carlo analysis of CMSSM*, *JHEP* **5** (2006) 2, [[hep-ph/0602028](#)].
- [26] C. Stenge, G. Bertone, *et. al.*, *Profile likelihood maps of a 15-dimensional MSSM*, *JHEP* **9** (2014) 81, [[arXiv:1405.0622](#)].
- [27] P. Bechtle, J. E. Camargo-Molina, *et. al.*, *Killing the $cMSSM$ softly*, *Eur. Phys. J. C* **76** (2016) 96, [[arXiv:1508.05951](#)].

- [28] M. E. Cabrera-Catalan, S. Ando, C. Weniger, and F. Zandanel, *Indirect and direct detection prospect for TeV dark matter in the nine parameter MSSM*, *Phys. Rev. D* **92** (2015) 035018, [[arXiv:1503.00599](#)].
- [29] K. J. de Vries, E. A. Bagnaschi, *et. al.*, *The pMSSM10 after LHC run 1*, *Eur. Phys. J. C* **75** (2015) 422, [[arXiv:1504.03260](#)].
- [30] R. Trotta, R. R. de Austri, and L. Roszkowski, *Prospects for direct dark matter detection in the constrained MSSM*, *New Astronomy Review* **51** (2007) 316–320, [[astro-ph/0609126](#)].
- [31] L. Roszkowski, R. Ruiz de Austri, and R. Trotta, *Implications for the Constrained MSSM from a new prediction for $b \rightarrow s\gamma$* , *JHEP* **7** (2007) 75, [[0705.2012](#)].
- [32] L. Roszkowski, R. Ruiz de Austri, J. Silk, and R. Trotta, *On prospects for dark matter indirect detection in the Constrained MSSM*, *Phys. Lett. B* **671** (2009) 10–14, [[0707.0622](#)].
- [33] G. D. Martinez, J. S. Bullock, M. Kaplinghat, L. E. Strigari, and R. Trotta, *Indirect Dark Matter detection from Dwarf satellites: joint expectations from astrophysics and supersymmetry*, *JCAP* **6** (2009) 14, [[0902.4715](#)].
- [34] L. Roszkowski, R. Ruiz de Austri, R. Trotta, Y.-L. S. Tsai, and T. A. Varley, *Global fits of the nonuniversal Higgs model*, *Phys. Rev. D* **83** (2011) 015014, [[arXiv:0903.1279](#)].
- [35] L. Roszkowski, R. Ruiz de Austri, and R. Trotta, *Efficient reconstruction of constrained MSSM parameters from LHC data: A case study*, *Phys. Rev. D* **82** (2010) 055003, [[arXiv:0907.0594](#)].
- [36] P. Scott, J. Conrad, *et. al.*, *Direct constraints on minimal supersymmetry from Fermi-LAT observations of the dwarf galaxy Segue 1*, *JCAP* **1** (2010) 31, [[arXiv:0909.3300](#)].
- [37] G. Bertone, D. G. Cerdeño, M. Fornasa, R. Ruiz de Austri, and R. Trotta, *Identification of dark matter particles with LHC and direct detection data*, *Phys. Rev. D* **82** (2010) 055008, [[arXiv:1005.4280](#)].

- [38] M. Bridges, K. Cranmer, *et. al.*, *A coverage study of CMSSM based on ATLAS sensitivity using fast neural networks techniques*, *JHEP* **3** (2011) 12, [[arXiv:1011.4306](#)].
- [39] G. Bertone, D. Cumberbatch, R. Ruiz de Austri, and R. Trotta, *Dark Matter searches: the nightmare scenario*, *JCAP* **1** (2012) 4, [[arXiv:1107.5813](#)].
- [40] G. Bertone, D. G. Cerdeño, *et. al.*, *Complementarity of indirect and accelerator dark matter searches*, *Phys. Rev. D* **85** (2012) 055014, [[arXiv:1111.2607](#)].
- [41] P. Scott, C. Savage, J. Edsjö, and the IceCube Collaboration: R. Abbasi *et al.*, *Use of event-level neutrino telescope data in global fits for theories of new physics*, *JCAP* **11** (2012) 57, [[arXiv:1207.0810](#)].
- [42] G. Bertone, D. G. Cerdeño, *et. al.*, *Global fits of the cMSSM including the first LHC and XENON100 data*, *JCAP* **1** (2012) 15, [[arXiv:1107.1715](#)].
- [43] G. Bertone, F. Calore, *et. al.*, *Global analysis of the pMSSM in light of the Fermi GeV excess: prospects for the LHC Run-II and astroparticle experiments*, *JCAP* **2016** (2016) 037, [[arXiv:1507.07008](#)].
- [44] O. Buchmueller, R. Cavanaugh, *et. al.*, *Predictions for supersymmetric particle masses using indirect experimental and cosmological constraints*, *JHEP* **9** (2008) 117, [[arXiv:0808.4128](#)].
- [45] O. Buchmueller, R. Cavanaugh, *et. al.*, *Likelihood functions for supersymmetric observables in frequentist analyses of the CMSSM and NUHM1*, *Eur. Phys. J. C* **64** (2009) 391–415, [[arXiv:0907.5568](#)].
- [46] O. Buchmueller, R. Cavanaugh, *et. al.*, *Frequentist analysis of the parameter space of minimal supergravity*, *Eur. Phys. J. C* **71** (2011) 1583, [[arXiv:1011.6118](#)].
- [47] O. Buchmueller, R. Cavanaugh, *et. al.*, *Implications of initial LHC searches for supersymmetry*, *Eur. Phys. J. C* **71** (2011) 1634, [[arXiv:1102.4585](#)].

- [48] O. Buchmueller, R. Cavanaugh, *et. al.*, *Supersymmetry and dark matter in light of LHC 2010 and XENON100 data*, *Eur. Phys. J. C* **71** (2011) 1722, [[arXiv:1106.2529](#)].
- [49] O. Buchmueller, R. Cavanaugh, *et. al.*, *Higgs and supersymmetry*, *Eur. Phys. J. C* **72** (2012) 2020, [[arXiv:1112.3564](#)].
- [50] O. Buchmueller *et. al.*, *The NUHM2 after LHC Run 1*, *Eur. Phys. J. C* **74** (2014) 3212, [[arXiv:1408.4060](#)].
- [51] E. Bagnaschi *et. al.*, *Likelihood Analysis of Supersymmetric $SU(5)$ GUTs*, *Eur. Phys. J. C* **77** (2017) 104, [[arXiv:1610.10084](#)].
- [52] E. Bagnaschi *et. al.*, *Likelihood Analysis of the Minimal AMSB Model*, *Eur. Phys. J. C* **77** (2017) 268, [[arXiv:1612.05210](#)].
- [53] B. C. Allanach, K. Cranmer, C. G. Lester, and A. M. Weber, *Natural priors, CMSSM fits and LHC weather forecasts*, *JHEP* **08** (2007) 023, [[arXiv:0705.0487](#)].
- [54] S. S. Abdussalam, B. C. Allanach, F. Quevedo, F. Feroz, and M. Hobson, *Fitting the phenomenological MSSM*, *Phys. Rev. D* **81** (2010) 095012, [[arXiv:0904.2548](#)].
- [55] S. S. Abdussalam, B. C. Allanach, M. J. Dolan, F. Feroz, and M. P. Hobson, *Selecting a model of supersymmetry breaking mediation*, *Phys. Rev. D* **80** (2009) 035017, [[arXiv:0906.0957](#)].
- [56] B. C. Allanach, *Impact of CMS Multi-jets and Missing Energy Search on CMSSM Fits*, *Phys. Rev. D* **83** (2011) 095019, [[arXiv:1102.3149](#)].
- [57] B. C. Allanach, T. J. Khoo, C. G. Lester, and S. L. Williams, *The impact of ATLAS zero-lepton, jets and missing momentum search on a CMSSM fit*, *JHEP* **6** (2011) 35, [[arXiv:1103.0969](#)].
- [58] C. Balázs, A. Buckley, D. Carter, B. Farmer, and M. White, *Should we still believe in constrained supersymmetry?*, *Eur. Phys. J. C* **73** (2013) 2563, [[arXiv:1205.1568](#)].
- [59] M. E. Cabrera, J. A. Casas, and R. Ruiz de Austri, *The health of SUSY after the Higgs discovery and the XENON100 data*, *JHEP* **07** (2013) 182, [[arXiv:1212.4821](#)].

- [60] A. Fowlie, K. Kowalska, L. Roszkowski, E. M. Sessolo, and Y.-L. S. Tsai, *Dark matter and collider signatures of the MSSM*, *Phys. Rev. D* **88** (2013) 055012, [[arXiv:1306.1567](#)].
- [61] S. Henrot-Versillé, R. Lafaye, *et. al.*, *Constraining supersymmetry using the relic density and the Higgs boson*, *Phys. Rev. D* **89** (2014) 055017, [[arXiv:1309.6958](#)].
- [62] D. Kim, P. Athron, C. Balázs, B. Farmer, and E. Hutchison, *Bayesian naturalness of the CMSSM and CNMSSM*, *Phys. Rev. D* **90** (2014) 055008, [[arXiv:1312.4150](#)].
- [63] K. Kowalska, L. Roszkowski, E. M. Sessolo, and A. J. Williams, *GUT-inspired SUSY and the muon $g - 2$ anomaly: prospects for LHC 14 TeV*, *JHEP* **06** (2015) 020, [[arXiv:1503.08219](#)].
- [64] M. E. Cabrera, J. A. Casas, A. Delgado, S. Robles, and R. Ruiz de Austri, *Naturalness of MSSM dark matter*, *JHEP* **08** (2016) 058, [[arXiv:1604.02102](#)].
- [65] C. Han, K.-i. Hikasa, L. Wu, J. M. Yang, and Y. Zhang, *Status of CMSSM in light of current LHC Run-2 and LUX data*, *Phys. Lett. B* **769** (2017) 470–476, [[arXiv:1612.02296](#)].
- [66] P. Bechtle *et. al.*, *How alive is constrained SUSY really?*, in *Proceedings, 37th International Conference on High Energy Physics (ICHEP 2014): Valencia, Spain, July 2-9, 2014* (2016) [[arXiv:1410.6035](#)].
- [67] L. Roszkowski, E. M. Sessolo, and A. J. Williams, *What next for the CMSSM and the NUHM: Improved prospects for superpartner and dark matter detection*, *JHEP* **08** (2014) 067, [[arXiv:1405.4289](#)].
- [68] A. Fowlie and M. Raidal, *Prospects for constrained supersymmetry at $\sqrt{s} = 33$ TeV and $\sqrt{s} = 100$ TeV proton-proton super-colliders*, *Eur. Phys. J. C* **74** (2014) 2948, [[arXiv:1402.5419](#)].
- [69] O. Buchmueller *et. al.*, *The CMSSM and NUHM1 after LHC Run 1*, *Eur. Phys. J. C* **74** (2014) 2922, [[arXiv:1312.5250](#)].
- [70] O. Buchmueller *et. al.*, *Implications of Improved Higgs Mass Calculations for Supersymmetric Models*, *Eur. Phys. J. C* **74** (2014) 2809, [[arXiv:1312.5233](#)].

- [71] P. Bechtle *et. al.*, *Constrained Supersymmetry after the Higgs Boson Discovery: A global analysis with Fittino*, *PoS EPS-HEP2013* (2013) 313, [[arXiv:1310.3045](#)].
- [72] S. Henrot-Versillé, R. Lafaye, *et. al.*, *Constraining Supersymmetry using the relic density and the Higgs boson*, *Phys. Rev. D* **89** (2014) 055017, [[arXiv:1309.6958](#)].
- [73] N. Bornhauser and M. Drees, *Determination of the CMSSM Parameters using Neural Networks*, *Phys. Rev. D* **88** (2013) 075016, [[arXiv:1307.3383](#)].
- [74] S. Akula and P. Nath, *Gluino-driven radiative breaking, Higgs boson mass, muon $g-2$, and the Higgs diphoton decay in supergravity unification*, *Phys. Rev. D* **87** (2013) 115022, [[arXiv:1304.5526](#)].
- [75] M. Citron, J. Ellis, *et. al.*, *End of the CMSSM coannihilation strip is nigh*, *Phys. Rev. D* **87** (2013) 036012, [[arXiv:1212.2886](#)].
- [76] C. Strobe, G. Bertone, *et. al.*, *Global fits of the cMSSM and NUHM including the LHC Higgs discovery and new XENON100 constraints*, *JCAP* **4** (2013) 13, [[arXiv:1212.2636](#)].
- [77] A. V. Gladyshev and D. I. Kazakov, *Is (Low Energy) SUSY Still Alive?*, in *Proceedings, 2012 European School of High-Energy Physics (ESHEP 2012): La Pommeraye, Anjou, France, June 06-19, 2012* (2014) 107–159, [[arXiv:1212.2548](#)].
- [78] K. Kowalska, S. Munir, *et. al.*, *Constrained next-to-minimal supersymmetric standard model with a 126 GeV Higgs boson: A global analysis*, *Phys. Rev. D* **87** (2013) 115010, [[arXiv:1211.1693](#)].
- [79] O. Buchmueller, R. Cavanaugh, *et. al.*, *The CMSSM and NUHM1 in light of 7 TeV LHC, $B_s \rightarrow \mu^+ \mu^-$ and XENON100 data*, *Eur. Phys. J. C* **72** (2012) 2243, [[arXiv:1207.7315](#)].
- [80] S. Akula, P. Nath, and G. Peim, *Implications of the Higgs Boson Discovery for mSUGRA*, *Phys. Lett. B* **717** (2012) 188–192, [[arXiv:1207.1839](#)].

- [81] H. Baer, V. Barger, A. Lessa, and X. Tata, *Discovery potential for SUSY at a high luminosity upgrade of LHC14*, *Phys. Rev. D* **86** (2012) 117701, [[arXiv:1207.4846](#)].
- [82] L. Roszkowski, E. M. Sessolo, and Y.-L. S. Tsai, *Bayesian implications of current LHC supersymmetry and dark matter detection searches for the constrained MSSM*, *Phys. Rev. D* **86** (2012) 095005, [[arXiv:1202.1503](#)].
- [83] C. Streve, G. Bertone, *et. al.*, *Updated global fits of the cMSSM including the latest LHC SUSY and Higgs searches and XENON100 data*, *JCAP* **3** (2012) 30, [[arXiv:1112.4192](#)].
- [84] P. Bechtle, T. Bringmann, *et. al.*, *Constrained supersymmetry after two years of LHC data: a global view with Fittino*, *JHEP* **6** (2012) 98, [[arXiv:1204.4199](#)].
- [85] O. Buchmueller, R. Cavanaugh, *et. al.*, *Supersymmetry in light of 1/fb of LHC data*, *Eur. Phys. J. C* **72** (2012) 1878, [[arXiv:1110.3568](#)].
- [86] A. Fowlie, A. Kalinowski, M. Kazana, L. Roszkowski, and Y. L. S. Tsai, *Bayesian Implications of Current LHC and XENON100 Search Limits for the Constrained MSSM*, *Phys. Rev. D* **85** (2012) 075012, [[arXiv:1111.6098](#)].
- [87] P. Bechtle, K. Desch, M. Uhlenbrock, and P. Wienemann, *Constraining SUSY models with Fittino using measurements before, with and beyond the LHC*, *Eur. Phys. J. C* **66** (2010) 215–259, [[arXiv:0907.2589](#)].
- [88] R. Trotta, F. Feroz, M. Hobson, L. Roszkowski, and R. Ruiz de Austri, *The impact of priors and observables on parameter inferences in the constrained MSSM*, *JHEP* **12** (2008) 24, [[arXiv:0809.3792](#)].
- [89] P. Bechtle, K. Desch, and P. Wienemann, *Fittino, a program for determining MSSM parameters from collider observables using an iterative method*, *Comp. Phys. Comm.* **174** (2006) 47–70, [[hep-ph/0412012](#)].
- [90] K. Kowalska, *Phenomenological MSSM in light of new 13 TeV LHC data*, *Eur. Phys. J. C* **76** (2016) 684, [[arXiv:1608.02489](#)].

- [91] G. Bertone, F. Calore, *et. al.*, *Global analysis of the pMSSM in light of the Fermi GeV excess: prospects for the LHC Run-II and astroparticle experiments*, *JCAP* **1604** (2016) 037, [[arXiv:1507.07008](#)].
- [92] E. A. Bagnaschi, O. Buchmueller, *et. al.*, *Supersymmetric dark matter after LHC run 1*, *Eur. Phys. J. C* **75** (2015) 500, [[arXiv:1508.01173](#)].
- [93] S. S. AbdusSalam and L. Velasco-Sevilla, *Where to look for natural supersymmetry*, *Phys. Rev. D* **94** (2016) 035026, [[arXiv:1506.02499](#)].
- [94] K. J. de Vries *et. al.*, *The pMSSM10 after LHC Run 1*, *Eur. Phys. J. C* **75** (2015) 422, [[arXiv:1504.03260](#)].
- [95] E. Bagnaschi *et. al.*, *Likelihood Analysis of the pMSSM11 in Light of LHC 13-TeV Data*, *Eur. Phys. J. C* **78** (2018) 256, [[arXiv:1710.11091](#)].
- [96] K. Cheung, Y.-L. S. Tsai, P.-Y. Tseng, T.-C. Yuan, and A. Zee, *Global Study of the Simplest Scalar Phantom Dark Matter Model*, *JCAP* **1210** (2012) 042, [[arXiv:1207.4930](#)].
- [97] A. Arhrib, Y.-L. S. Tsai, Q. Yuan, and T.-C. Yuan, *An Updated Analysis of Inert Higgs Doublet Model in light of the Recent Results from LUX, PLANCK, AMS-02 and LHC*, *JCAP* **1406** (2014) 030, [[arXiv:1310.0358](#)].
- [98] S. Matsumoto, S. Mukhopadhyay, and Y.-L. S. Tsai, *Singlet Majorana fermion dark matter: a comprehensive analysis in effective field theory*, *JHEP* **10** (2014) 155, [[arXiv:1407.1859](#)].
- [99] D. Chowdhury and O. Eberhardt, *Global fits of the two-loop renormalized Two-Higgs-Doublet model with soft Z_2 breaking*, *JHEP* **11** (2015) 52, [[arXiv:1503.08216](#)].
- [100] S. Liem, G. Bertone, *et. al.*, *Effective field theory of dark matter: a global analysis*, *JHEP* **9** (2016) 77, [[arXiv:1603.05994](#)].
- [101] X. Huang, Y.-L. S. Tsai, and Q. Yuan, *LikeDM: likelihood calculator of dark matter detection*, *Comp. Phys. Comm.* **213** (2017) 252–263, [[arXiv:1603.07119](#)].

- [102] S. Banerjee, S. Matsumoto, K. Mukaida, and Y.-L. S. Tsai, *WIMP Dark Matter in a Well-Tempered Regime: A case study on Singlet-Doublets Fermionic WIMP*, *JHEP* **11** (2016) 070, [[arXiv:1603.07387](#)].
- [103] S. Matsumoto, S. Mukhopadhyay, and Y.-L. S. Tsai, *Effective Theory of WIMP Dark Matter supplemented by Simplified Models: Singlet-like Majorana fermion case*, *Phys. Rev. D* **94** (2016) 065034, [[arXiv:1604.02230](#)].
- [104] A. Cuoco, B. Eiteneuer, J. Heisig, and M. Krämer, *A global fit of the γ -ray galactic center excess within the scalar singlet Higgs portal model*, *JCAP* **6** (2016) 050, [[arXiv:1603.08228](#)].
- [105] V. Cacchio, D. Chowdhury, O. Eberhardt, and C. W. Murphy, *Next-to-leading order unitarity fits in Two-Higgs-Doublet models with soft \mathbb{Z}_2 breaking*, *JHEP* **11** (2016) 026, [[arXiv:1609.01290](#)].
- [106] G. Bertone, K. Kong, R. R. de Austri, and R. Trotta, *Global fits of the minimal universal extra dimensions scenario*, *Phys. Rev. D* **83** (2011) 036008, [[arXiv:1010.2023](#)].
- [107] C.-W. Chiang, G. Cottin, and O. Eberhardt, *Global fits in the Georgi-Machacek model*, *Phys. Rev. D* **99** (2019) 015001, [[arXiv:1807.10660](#)].
- [108] J. De Blas *et. al.*, *HEPfit: a Code for the Combination of Indirect and Direct Constraints on High Energy Physics Models*, [arXiv:1910.14012](#).
- [109] S. Matsumoto, Y.-L. S. Tsai, and P.-Y. Tseng, *Light Fermionic WIMP Dark Matter with Light Scalar Mediator*, *JHEP* **07** (2019) 050, [[arXiv:1811.03292](#)].
- [110] GAMBIT Collaboration: P. Athron, C. Balázs, *et. al.*, *GAMBIT: The Global and Modular Beyond-the-Standard-Model Inference Tool*, *Eur. Phys. J. C* **77** (2017) 784, [[arXiv:1705.07908](#)]. Addendum in [[111](#)].
- [111] GAMBIT Collaboration: P. Athron, C. Balázs, *et. al.*, *GAMBIT: The Global and Modular Beyond-the-Standard-Model Inference Tool*.

Addendum for GAMBIT 1.1: Mathematica backends, SUSYHD interface and updated likelihoods, *Eur. Phys. J. C* **xx** (2017) xx, [[arXiv:1705.07908](#)]. Addendum to [110].

- [112] GAMBIT Collaboration: P. Athron *et. al.*, *Global analyses of Higgs portal singlet dark matter models using GAMBIT*, *Eur. Phys. J. C* **79** (2019) 38, [[arXiv:1808.10465](#)].
- [113] S. Hoof, F. Kahlhoefer, P. Scott, C. Weniger, and M. White, *Axion global fits with Peccei-Quinn symmetry breaking before inflation using GAMBIT*, *JHEP* **03** (2019) 191, [[arXiv:1810.07192](#)].
- [114] M. Chruszcz, M. Drewes, *et. al.*, *A frequentist analysis of three right-handed neutrinos with GAMBIT*, [arXiv:1908.02302](#).
- [115] F. Mahmoudi, *SuperIso: A Program for calculating the isospin asymmetry of $B \rightarrow K^* \gamma$ in the MSSM*, *Comp. Phys. Comm.* **178** (2008) 745, [[arXiv:0710.2067](#)].
- [116] F. Mahmoudi, *SuperIso v2.3: A Program for calculating flavor physics observables in Supersymmetry*, *Comp. Phys. Comm.* **180** (2009) 1579, [[arXiv:0808.3144](#)].
- [117] F. Mahmoudi, *SuperIso v3.0, flavor physics observables calculations: Extension to NMSSM*, *Comp. Phys. Comm.* **180** (2009) 1718.
- [118] P. Gondolo, J. Edsjo, *et. al.*, *DarkSUSY: Computing supersymmetric dark matter properties numerically*, *JCAP* **0407** (2004) 008, [[astro-ph/0406204](#)].
- [119] T. Bringmann, J. Edsjö, P. Gondolo, P. Ullio, and L. Bergström, *DarkSUSY 6 : An Advanced Tool to Compute Dark Matter Properties Numerically*, *JCAP* **1807** (2018) 033, [[arXiv:1802.03399](#)].
- [120] GAMBIT Dark Matter Workgroup: T. Bringmann, J. Conrad, *et. al.*, *DarkBit: A GAMBIT module for computing dark matter observables and likelihoods*, *Eur. Phys. J. C* **77** (2017) 831, [[arXiv:1705.07920](#)].
- [121] S. Heinemeyer, W. Hollik, and G. Weiglein, *FeynHiggs: A Program for the calculation of the masses of the neutral CP even Higgs bosons in the MSSM*, *Comp. Phys. Comm.* **124** (2000) 76–89, [[hep-ph/9812320](#)].

- [122] S. Heinemeyer, W. Hollik, and G. Weiglein, *The Masses of the neutral CP - even Higgs bosons in the MSSM: Accurate analysis at the two loop level*, *Eur. Phys. J. C* **9** (1999) 343–366, [[hep-ph/9812472](#)].
- [123] G. Degrandi, S. Heinemeyer, W. Hollik, P. Slavich, and G. Weiglein, *Towards high precision predictions for the MSSM Higgs sector*, *Eur. Phys. J. C* **28** (2003) 133–143, [[hep-ph/0212020](#)].
- [124] M. Frank, T. Hahn, *et. al.*, *The Higgs Boson Masses and Mixings of the Complex MSSM in the Feynman-Diagrammatic Approach*, *JHEP* **02** (2007) 047, [[hep-ph/0611326](#)].
- [125] T. Hahn, S. Heinemeyer, W. Hollik, H. Rzehak, and G. Weiglein, *High-Precision Predictions for the Light CP -Even Higgs Boson Mass of the Minimal Supersymmetric Standard Model*, *Phys. Rev. Lett.* **112** (2014) 141801, [[arXiv:1312.4937](#)].
- [126] P. Athron, M. Bach, *et. al.*, *GM2Calc: precise MSSM prediction for (g-2) of the muon*, *Eur. Phys. J. C* **76** (2016) 62, [[arXiv:1510.08071](#)].
- [127] P. Bechtle, O. Brein, S. Heinemeyer, G. Weiglein, and K. E. Williams, *HiggsBounds: Confronting Arbitrary Higgs Sectors with Exclusion Bounds from LEP and the Tevatron*, *Comp. Phys. Comm.* **181** (2010) 138–167, [[arXiv:0811.4169](#)].
- [128] P. Bechtle, O. Brein, S. Heinemeyer, G. Weiglein, and K. E. Williams, *HiggsBounds 2.0.0: Confronting Neutral and Charged Higgs Sector Predictions with Exclusion Bounds from LEP and the Tevatron*, *Comp. Phys. Comm.* **182** (2011) 2605–2631, [[arXiv:1102.1898](#)].
- [129] P. Bechtle, O. Brein, *et. al.*, *HiggsBounds – 4: Improved Tests of Extended Higgs Sectors against Exclusion Bounds from LEP, the Tevatron and the LHC*, *Eur. Phys. J. C* **74** (2014) 2693, [[arXiv:1311.0055](#)].
- [130] P. Bechtle, S. Heinemeyer, O. Stål, T. Stefaniak, and G. Weiglein, *HiggsSignals: Confronting arbitrary Higgs sectors with measurements at the Tevatron and the LHC*, *Eur. Phys. J. C* **74** (2014) 2711, [[arXiv:1305.1933](#)].

- [131] G. Bélanger, F. Boudjema, A. Pukhov, and A. Semenov, *MicrOMEGAs: A Program for calculating the relic density in the MSSM*, *Comp. Phys. Comm.* **149** (2002) 103–120, [[hep-ph/0112278](#)].
- [132] G. Bélanger, F. Boudjema, A. Pukhov, and A. Semenov, *micrOMEGAs: Version 1.3*, *Comp. Phys. Comm.* **174** (2006) 577–604, [[hep-ph/0405253](#)].
- [133] G. Bélanger, F. Boudjema, A. Pukhov, and A. Semenov, *MicrOMEGAs 2.0: A Program to calculate the relic density of dark matter in a generic model*, *Comp. Phys. Comm.* **176** (2007) 367–382, [[hep-ph/0607059](#)].
- [134] G. Bélanger, F. Boudjema, A. Pukhov, and A. Semenov, *Dark matter direct detection rate in a generic model with micrOMEGAs 2.2*, *Comp. Phys. Comm.* **180** (2009) 747–767, [[arXiv:0803.2360](#)].
- [135] G. Bélanger, F. Boudjema, *et. al.*, *Indirect search for dark matter with micrOMEGAs2.4*, *Comp. Phys. Comm.* **182** (2011) 842–856, [[arXiv:1004.1092](#)].
- [136] G. Bélanger, F. Boudjema, A. Pukhov, and A. Semenov, *micrOMEGAs 3: A program for calculating dark matter observables*, *Comp. Phys. Comm.* **185** (2014) 960–985, [[arXiv:1305.0237](#)].
- [137] G. Bélanger, F. Boudjema, A. Pukhov, and A. Semenov, *micrOMEGAs4.1: Two dark matter candidates*, *Comp. Phys. Comm.* **192** (2015) 322–329, [[arXiv:1407.6129](#)].
- [138] T. Sjöstrand, S. Mrenna, and P. Z. Skands, *PYTHIA 6.4 Physics and Manual*, *JHEP* **05** (2006) 026, [[hep-ph/0603175](#)].
- [139] T. Sjostrand, S. Ask, *et. al.*, *An Introduction to PYTHIA 8.2*, *Comp. Phys. Comm.* **191** (2015) 159–177, [[arXiv:1410.3012](#)].
- [140] W. Porod, *SPheno, a program for calculating supersymmetric spectra, SUSY particle decays and SUSY particle production at e^+e^- colliders*, *Comp. Phys. Comm.* **153** (2003) 275–315, [[hep-ph/0301101](#)].
- [141] W. Porod and F. Staub, *SPheno 3.1: Extensions including flavour, CP-phases and models beyond the MSSM*, *Comp. Phys. Comm.* **183** (2012) 2458–2469, [[arXiv:1104.1573](#)].

- [142] J. P. Vega and G. Villadoro, *SusyHD: Higgs mass Determination in Supersymmetry*, *JHEP* **07** (2015) 159, [[arXiv:1504.05200](#)].
- [143] A. Djouadi, M. M. Mühlleitner, and M. Spira, *Decays of supersymmetric particles: The Program SUSY-HIT (SUspect-SdecaY-Hdecay-InTerface)*, *Acta Phys. Polon.* **38** (2007) 635–644, [[hep-ph/0609292](#)].
- [144] GAMBIT Scanner Workgroup: G. D. Martinez, J. McKay, *et. al.*, *Comparison of statistical sampling methods with ScannerBit, the GAMBIT scanning module*, *Eur. Phys. J. C* **77** (2017) 761, [[arXiv:1705.07959](#)].
- [145] GAMBIT Collaboration: P. Athron *et. al.*, *Combined collider constraints on neutralinos and charginos*, *Eur. Phys. J. C* **79** (2019) 395, [[arXiv:1809.02097](#)].
- [146] A. Putze and L. Derome, *The Grenoble Analysis Toolkit (GreAT)-A statistical analysis framework*, *Physics of the Dark Universe* **5** (2014) 29–34.
- [147] F. Feroz and M. Hobson, *Multimodal nested sampling: an efficient and robust alternative to MCMC methods for astronomical data analysis*, *Mon.Not.Roy.Astron.Soc.* **384** (2008) 449, [[arXiv:0704.3704](#)].
- [148] F. Feroz, M. Hobson, and M. Bridges, *MultiNest: an efficient and robust Bayesian inference tool for cosmology and particle physics*, *Mon.Not.Roy.Astron.Soc.* **398** (2009) 1601–1614, [[arXiv:0809.3437](#)].
- [149] W. J. Handley, M. P. Hobson, and A. N. Lasenby, *POLYCHORD: next-generation nested sampling*, *MNRAS* **453** (2015) 4384–4398, [[arXiv:1506.00171](#)].
- [150] GAMBIT Collaboration: P. Athron, C. Balázs, *et. al.*, *Global fits of GUT-scale SUSY models with GAMBIT*, *Eur. Phys. J. C* **77** (2017) 824, [[arXiv:1705.07935](#)].
- [151] GAMBIT Collaboration: P. Athron, C. Balázs, *et. al.*, *A global fit of the MSSM with GAMBIT*, *Eur. Phys. J. C* **77** (2017) 879, [[arXiv:1705.07917](#)].

- [152] GAMBIT Collaboration: P. Athron, C. Balázs, *et. al.*, *Status of the scalar singlet dark matter model*, *Eur. Phys. J. C* **77** (2017) 568, [[arXiv:1705.07931](#)].
- [153] P. Athron, J. M. Cornell, *et. al.*, *Impact of vacuum stability, perturbativity and XENON1T on global fits of \mathbb{Z}_2 and \mathbb{Z}_3 scalar singlet dark matter*, *Eur. Phys. J. C* **78** (2018) 830, [[arXiv:1806.11281](#)].
- [154] J. McKay, P. Scott, and P. Athron, *Pitfalls of iterative pole mass calculation in electroweak multiplets*, *Eur. Phys. J. Plus* **133** (2018) 444, [[arXiv:1710.01511](#)].
- [155] J. McKay and P. Scott, *Two-loop mass splittings in electroweak multiplets: Winos and minimal dark matter*, *Phys. Rev. D* **97** (2018) 055049, [[arXiv:1712.00968](#)].
- [156] P. Athron, J.-h. Park, D. Stöckinger, and A. Voigt, *FlexibleSUSY - A spectrum generator for supersymmetric models*, *Comp. Phys. Comm.* **190** (2015) 139–172, [[arXiv:1406.2319](#)].
- [157] H. Bahl and W. Hollik, *Precise prediction for the light MSSM Higgs boson mass combining effective field theory and fixed-order calculations*, *Eur. Phys. J. C* **76** (2016) 499, [[arXiv:1608.01880](#)].
- [158] Particle Data Group: K. A. Olive *et. al.*, *Review of Particle Physics*, *Chin. Phys. C* **38** (2014) 090001.
- [159] LHC Higgs Cross Section Working Group: J. R. Andersen *et. al.*, *Handbook of LHC Higgs Cross Sections: 3. Higgs Properties*, [[arXiv:1307.1347](#)].
- [160] GAMBIT Models Workgroup: P. Athron, C. Balázs, *et. al.*, *SpecBit, DecayBit and PrecisionBit: GAMBIT modules for computing mass spectra, particle decay rates and precision observables*, *Eur. Phys. J. C* **78** (2018) 22, [[arXiv:1705.07936](#)].
- [161] Particle Data Group: K. A. Olive *et. al.*, *Review of Particle Physics*, update to Ref. [[415](#)] (2017).
- [162] M. Drewes and B. Garbrecht, *Combining experimental and cosmological constraints on heavy neutrinos*, *Nucl. Phys.* **B921** (2017) 250–315, [[arXiv:1502.00477](#)].

- [163] S. Antusch and O. Fischer, *Non-unitarity of the leptonic mixing matrix: Present bounds and future sensitivities*, *JHEP* **10** (2014) 094, [[arXiv:1407.6607](#)].
- [164] S. Antusch and O. Fischer, *Testing sterile neutrino extensions of the Standard Model at future lepton colliders*, *JHEP* **05** (2015) 053, [[arXiv:1502.05915](#)].
- [165] A. Ferroglia and A. Sirlin, *Comparison of the standard theory predictions of M_W and $\sin^2 \theta_{eff}^{lept}$ with their experimental values*, *Phys. Rev. D* **87** (2013) 037501, [[arXiv:1211.1864](#)].
- [166] E. Fernandez-Martinez, J. Hernandez-Garcia, J. Lopez-Pavon, and M. Lucente, *Loop level constraints on Seesaw neutrino mixing*, *JHEP* **10** (2015) 130, [[arXiv:1508.03051](#)].
- [167] A. Abada, A. M. Teixeira, A. Vicente, and C. Weiland, *Sterile neutrinos in leptonic and semileptonic decays*, *JHEP* **02** (2014) 091, [[arXiv:1311.2830](#)].
- [168] I. Dubovyk, A. Freitas, J. Gluza, T. Riemann, and J. Usovitsch, *Complete electroweak two-loop corrections to Z boson production and decay*, *Phys. Lett. B* **783** (2018) 86–94, [[arXiv:1804.10236](#)].
- [169] G. Bélanger, J. Da Silva, T. Perrillat-Bottonet, and A. Pukhov, *Limits on dark matter proton scattering from neutrino telescopes using micrOMEGAs*, *JCAP* **12** (2015) 036, [[arXiv:1507.07987](#)].
- [170] Planck Collaboration, N. Aghanim, *et. al.*, *Planck 2018 results. VI. Cosmological parameters*, *arXiv e-prints* (2018) [[arXiv:1807.06209](#)].
- [171] LHCb: R. Aaij *et. al.*, *Measurements of the S -wave fraction in $B^0 \rightarrow K^+ \pi^- \mu^+ \mu^-$ decays and the $B^0 \rightarrow K^*(892)^0 \mu^+ \mu^-$ differential branching fraction*, *JHEP* **11** (2016) 047, [[arXiv:1606.04731](#)].
[Erratum: JHEP04,142(2017)].
- [172] LHCb Collaboration: R. Aaij *et. al.*, *Angular analysis and differential branching fraction of the decay $B_s^0 \rightarrow \phi \mu^+ \mu^-$* , *JHEP* **09** (2015) 179, [[arXiv:1506.08777](#)].

- [173] LHCb Collaboration: R. Aaij *et. al.*, *Measurement of the ratio of branching fractions $\mathcal{B}(\bar{B}^0 \rightarrow D^{*+}\tau^-\bar{\nu}_\tau)/\mathcal{B}(\bar{B}^0 \rightarrow D^{*+}\mu^-\bar{\nu}_\mu)$* , *Phys. Rev. Lett.* **115** (2015) 111803, [[arXiv:1506.08614](#)]. [Addendum: *Phys. Rev. Lett.* 115, no.15, 159901 (2015)].
- [174] LHCb Collaboration: R. Aaij *et. al.*, *Test of lepton universality using $B^+ \rightarrow K^+\ell^+\ell^-$ decays*, *Phys. Rev. Lett.* **113** (2014) 151601, [[arXiv:1406.6482](#)].
- [175] LHCb Collaboration: R. Aaij *et. al.*, *Measurement of Form-Factor-Independent Observables in the Decay $B^0 \rightarrow K^{*0}\mu^+\mu^-$* , *Phys. Rev. Lett.* **111** (2013) 191801, [[arXiv:1308.1707](#)].
- [176] LHCb: R. Aaij *et. al.*, *Search for lepton-universality violation in $B^+ \rightarrow K^+\ell^+\ell^-$ decays*, *Phys. Rev. Lett.* **122** (2019) 191801, [[arXiv:1903.09252](#)].
- [177] LHCb: R. Aaij *et. al.*, *Differential branching fractions and isospin asymmetries of $B \rightarrow K^{(*)}\mu^+\mu^-$ decays*, *JHEP* **06** (2014) 133, [[arXiv:1403.8044](#)].
- [178] BaBar Collaboration: J. P. Lees *et. al.*, *Evidence for an excess of $\bar{B} \rightarrow D^{(*)}\tau^-\bar{\nu}_\tau$ decays*, *Phys. Rev. Lett.* **109** (2012) 101802, [[arXiv:1205.5442](#)].
- [179] BaBar Collaboration: J. P. Lees *et. al.*, *Measurement of an Excess of $\bar{B} \rightarrow D^{(*)}\tau^-\bar{\nu}_\tau$ Decays and Implications for Charged Higgs Bosons*, *Phys. Rev. D* **88** (2013) 072012, [[arXiv:1303.0571](#)].
- [180] Belle Collaboration: M. Huschle *et. al.*, *Measurement of the branching ratio of $\bar{B} \rightarrow D^{(*)}\tau^-\bar{\nu}_\tau$ relative to $\bar{B} \rightarrow D^{(*)}\ell^-\bar{\nu}_\ell$ decays with hadronic tagging at Belle*, *Phys. Rev. D* **92** (2015) 072014, [[arXiv:1507.03233](#)].
- [181] Belle: A. Abdesselam *et. al.*, *Measurement of the branching ratio of $\bar{B}^0 \rightarrow D^{*+}\tau^-\bar{\nu}_\tau$ relative to $\bar{B}^0 \rightarrow D^{*+}\ell^-\bar{\nu}_\ell$ decays with a semileptonic tagging method*, in *Proceedings, 51st Rencontres de Moriond on Electroweak Interactions and Unified Theories: La Thuile, Italy, March 12-19, 2016* (2016) [[arXiv:1603.06711](#)].
- [182] Belle Collaboration: A. Abdesselam *et. al.*, *Angular analysis of $B^0 \rightarrow K^{*}(892)^0\ell^+\ell^-$* , in *Proceedings, LHCSki 2016 - A First*

Discussion of 13 TeV Results: Obergurgl, Austria, April 10-15, 2016
(2016) [[arXiv:1604.04042](#)].

- [183] BaBar: B. Aubert *et. al.*, *Measurements of branching fractions, rate asymmetries, and angular distributions in the rare decays $B \rightarrow K\ell^+\ell^-$ and $B \rightarrow K^*\ell^+\ell^-$* , *Phys. Rev.* **D73** (2006) 092001, [[hep-ex/0604007](#)].
- [184] BaBar: J. P. Lees *et. al.*, *Measurement of angular asymmetries in the decays $B \rightarrow K^*l^+l^-$* , *Phys. Rev.* **D93** (2016) 052015, [[arXiv:1508.07960](#)].
- [185] Belle: J. T. Wei *et. al.*, *Measurement of the Differential Branching Fraction and Forward-Backward Asymmetry for $B \rightarrow K^{(*)}\ell^+\ell^-$* , *Phys. Rev. Lett.* **103** (2009) 171801, [[arXiv:0904.0770](#)].
- [186] Belle: S. Wehle *et. al.*, *Lepton-Flavor-Dependent Angular Analysis of $B \rightarrow K^*\ell^+\ell^-$* , *Phys. Rev. Lett.* **118** (2017) 111801, [[arXiv:1612.05014](#)].
- [187] GAMBIT Flavour Workgroup: F. U. Bernlochner, M. Chrzęszcz, *et. al.*, *FlavBit: A GAMBIT module for computing flavour observables and likelihoods*, *Eur. Phys. J. C* **77** (2017) 786, [[arXiv:1705.07933](#)].
- [188] MEG: A. M. Baldini *et. al.*, *Search for the lepton flavour violating decay $\mu^+ \rightarrow e^+\gamma$ with the full dataset of the MEG experiment*, *Eur. Phys. J. C* **76** (2016) 434, [[arXiv:1605.05081](#)].
- [189] BaBar: B. Aubert *et. al.*, *Searches for Lepton Flavor Violation in the Decays $\tau^{+-} \rightarrow e^{+-} \gamma$ and $\tau^{+-} \rightarrow \mu^{+-} \gamma$* , *Phys. Rev. Lett.* **104** (2010) 021802, [[arXiv:0908.2381](#)].
- [190] Belle: K. Hayasaka *et. al.*, *New Search for $\tau \rightarrow \mu \gamma$ and $\tau \rightarrow e \gamma$ Decays at Belle*, *Phys. Lett. B* **666** (2008) 16–22, [[arXiv:0705.0650](#)].
- [191] BaBar: J. P. Lees *et. al.*, *Limits on tau Lepton-Flavor Violating Decays in three charged leptons*, *Phys. Rev. D* **81** (2010) 111101, [[arXiv:1002.4550](#)].
- [192] K. Hayasaka *et. al.*, *Search for Lepton Flavor Violating Tau Decays into Three Leptons with 719 Million Produced $\tau^+\tau^-$ Pairs*, *Phys. Lett. B* **687** (2010) 139–143, [[arXiv:1001.3221](#)].

- [193] ATLAS Collaboration: G. Aad *et. al.*, *Probing lepton flavour violation via neutrinoless $\tau \rightarrow 3\mu$ decays with the ATLAS detector*, *Eur. Phys. J. C* **76** (2016) 232, [[arXiv:1601.03567](#)].
- [194] LHCb Collaboration: R. Aaij *et. al.*, *Search for the lepton flavour violating decay $\tau^- \rightarrow \mu^- \mu^+ \mu^-$* , *JHEP* **02** (2015) 121, [[arXiv:1409.8548](#)].
- [195] SINDRUM: U. Bellgardt *et. al.*, *Search for the Decay $\mu^+ \rightarrow e^+ e^+ e^-$* , *Nucl. Phys.* **B299** (1988) 1–6.
- [196] SINDRUM II: J. Kaulard *et. al.*, *Improved limit on the branching ratio of $\mu^- \rightarrow e^+$ conversion on titanium*, *Phys. Lett. B* **422** (1998) 334–338.
- [197] SINDRUM II: W. Honecker *et. al.*, *Improved limit on the branching ratio of $\mu \rightarrow e$ conversion on lead*, *Phys. Rev. Lett.* **76** (1996) 200–203.
- [198] SINDRUM II: W. H. Bertl *et. al.*, *A Search for muon to electron conversion in muonic gold*, *Eur. Phys. J. C* **47** (2006) 337–346.
- [199] LHCb: R. Aaij *et. al.*, *Test of lepton universality with $B^0 \rightarrow K^{*0} \ell^+ \ell^-$ decays*, *JHEP* **08** (2017) 055, [[arXiv:1705.05802](#)].
- [200] J. Bhom and M. Chrzaszcz, *HEPLike*, 2019.
- [201] GAMBIT Collider Workgroup: C. Balazs, A. Buckley, *et. al.*, *ColliderBit: a GAMBIT module for the calculation of high-energy collider observables and likelihoods*, *Eur. Phys. J. C* **77** (2017) 795, [[arXiv:1705.07919](#)].
- [202] S. Kraml, S. Kulkarni, *et. al.*, *SModelS: a tool for interpreting simplified-model results from the LHC and its application to supersymmetry*, *Eur. Phys. J. C* **74** (2014) 2868, [[arXiv:1312.4175](#)].
- [203] M. Papucci, K. Sakurai, A. Weiler, and L. Zeune, *Fastlim: a fast LHC limit calculator*, *Eur. Phys. J. C* **74** (2014) 3163, [[arXiv:1402.0492](#)].
- [204] I. Esteban, M. C. Gonzalez-Garcia, M. Maltoni, I. Martinez-Soler, and T. Schwetz, *Updated fit to three neutrino mixing: exploring the*

- accelerator-reactor complementarity*, *JHEP* **01** (2017) 087, [[arXiv:1611.01514](#)].
- [205] I. Esteban, M. C. Gonzalez-Garcia, M. Maltoni, I. Martinez-Soler, and T. Schwetz, “NuFit 3.2.” <http://www.nu-fit.org> (accessed 2018-05-08), 2018.
 - [206] B. T. Cleveland, T. Daily, *et. al.*, *Measurement of the solar electron neutrino flux with the Homestake chlorine detector*, *Astrophys. J.* **496** (1998) 505–526.
 - [207] F. Kaether, W. Hampel, G. Heusser, J. Kiko, and T. Kirsten, *Reanalysis of the GALLEX solar neutrino flux and source experiments*, *Phys. Lett. B* **685** (2010) 47–54, [[arXiv:1001.2731](#)].
 - [208] SAGE: J. N. Abdurashitov *et. al.*, *Measurement of the solar neutrino capture rate with gallium metal. III: Results for the 2002–2007 data-taking period*, *Phys. Rev.* **C80** (2009) 015807, [[arXiv:0901.2200](#)].
 - [209] SNO: B. Aharmim *et. al.*, *Combined Analysis of all Three Phases of Solar Neutrino Data from the Sudbury Neutrino Observatory*, *Phys. Rev.* **C88** (2013) 025501, [[arXiv:1109.0763](#)].
 - [210] Super-Kamiokande: J. Hosaka *et. al.*, *Solar neutrino measurements in super-Kamiokande-I*, *Phys. Rev. D* **73** (2006) 112001, [[hep-ex/0508053](#)].
 - [211] Super-Kamiokande: J. P. Cravens *et. al.*, *Solar neutrino measurements in Super-Kamiokande-II*, *Phys. Rev. D* **78** (2008) 032002, [[arXiv:0803.4312](#)].
 - [212] Super-Kamiokande: K. Abe *et. al.*, *Solar neutrino results in Super-Kamiokande-III*, *Phys. Rev. D* **83** (2011) 052010, [[arXiv:1010.0118](#)].
 - [213] G. Bellini *et. al.*, *Precision measurement of the ^7Be solar neutrino interaction rate in Borexino*, *Phys. Rev. Lett.* **107** (2011) 141302, [[arXiv:1104.1816](#)].
 - [214] Borexino: G. Bellini *et. al.*, *Measurement of the solar ^8B neutrino rate with a liquid scintillator target and 3 MeV energy threshold in the Borexino detector*, *Phys. Rev. D* **82** (2010) 033006, [[arXiv:0808.2868](#)].

- [215] BOREXINO: G. Bellini *et. al.*, *Neutrinos from the primary proton–proton fusion process in the Sun*, *Nature* **512** (2014) 383–386.
- [216] IceCube: M. G. Aartsen *et. al.*, *Determining neutrino oscillation parameters from atmospheric muon neutrino disappearance with three years of IceCube DeepCore data*, *Phys. Rev. D* **91** (2015) 072004, [[arXiv:1410.7227](#)].
- [217] KamLAND: A. Gando *et. al.*, *Reactor On-Off Antineutrino Measurement with KamLAND*, *Phys. Rev. D* **88** (2013) 033001, [[arXiv:1303.4667](#)].
- [218] Daya Bay: F. P. An *et. al.*, *Improved Measurement of the Reactor Antineutrino Flux and Spectrum at Daya Bay*, *Chin. Phys.* **C41** (2017) 013002, [[arXiv:1607.05378](#)].
- [219] Daya Bay: F. P. An *et. al.*, *Measurement of electron antineutrino oscillation based on 1230 days of operation of the Daya Bay experiment*, *Phys. Rev. D* **95** (2017) 072006, [[arXiv:1610.04802](#)].
- [220] H. Seo, “New Results from RENO. - 2017. Talk given at the EPS Conference on High Energy Physics, Venice, Italy, July 5-12.”
- [221] MINOS: P. Adamson *et. al.*, *Measurement of Neutrino and Antineutrino Oscillations Using Beam and Atmospheric Data in MINOS*, *Phys. Rev. Lett.* **110** (2013) 251801, [[arXiv:1304.6335](#)].
- [222] MINOS: P. Adamson *et. al.*, *Electron neutrino and antineutrino appearance in the full MINOS data sample*, *Phys. Rev. Lett.* **110** (2013) 171801, [[arXiv:1301.4581](#)].
- [223] A. Izmaylov, “T2K Neutrino Experiment. Recent Results and Plans. - 2017. Talk given at the Flavour Physics Conference, Quy Nhon, Vietnam, August 13-19..”
- [224] A. Radovic, “Latest oscillation results from NOvA. - 2018. Fermilab. Joint Experimental-Theoretical Physics Seminar USA, January 12..”
- [225] Planck Collaboration: P. A. R. Ade *et. al.*, *Planck 2015 results. XIII. Cosmological parameters*, *Astropart. Phys.* **594** (2016) A13, [[arXiv:1502.01589](#)].

- [226] M. Agostini *et. al.*, *Background-free search for neutrinoless double- β decay of ^{76}Ge with GERDA*, *Nature* **544** (2017) 47–52, [[arXiv:1703.00570](#)].
- [227] KamLAND-Zen: A. Gando *et. al.*, *Search for Majorana Neutrinos near the Inverted Mass Hierarchy Region with KamLAND-Zen*, *Phys. Rev. Lett.* **117** (2016) 082503, [[arXiv:1605.02889](#)]. [Addendum: *Phys. Rev. Lett.* **117**, 109903 (2016)].
- [228] M. Drewes and S. Eijima, *Neutrinoless double β decay and low scale leptogenesis*, *Phys. Lett. B* **763** (2016) 72–79, [[arXiv:1606.06221](#)].
- [229] A. Faessler, M. González, S. Kovalenko, and F. Šimkovic, *Arbitrary mass Majorana neutrinos in neutrinoless double beta decay*, *Phys. Rev. D* **90** (2014) 096010, [[arXiv:1408.6077](#)].
- [230] D. Gorbunov and M. Shaposhnikov, *How to find neutral leptons of the νMSM ?*, *JHEP* **10** (2007) 015, [[arXiv:0705.1729](#)]. [Erratum: *JHEP* **11**, 101(2013)].
- [231] L. Canetti, M. Drewes, T. Frossard, and M. Shaposhnikov, *Dark Matter, Baryogenesis and Neutrino Oscillations from Right Handed Neutrinos*, *Phys. Rev. D* **87** (2013) 093006, [[arXiv:1208.4607](#)].
- [232] O. Ruchayskiy and A. Ivashko, *Restrictions on the lifetime of sterile neutrinos from primordial nucleosynthesis*, *JCAP* **1210** (2012) 014, [[arXiv:1202.2841](#)].
- [233] PIENU: M. Aoki *et. al.*, *Search for Massive Neutrinos in the Decay $\pi \rightarrow e\nu$* , *Phys. Rev. D* **84** (2011) 052002, [[arXiv:1106.4055](#)].
- [234] G. Bernardi *et. al.*, *Further Limits on Heavy Neutrino Couplings*, *Phys. Lett. B* **203** (1988) 332–334.
- [235] CHARM: F. Bergsma *et. al.*, *A Search for Decays of Heavy Neutrinos in the Mass Range 0.5-GeV to 2.8-GeV*, *Phys. Lett.* **166B** (1986) 473–478.
- [236] A. T. Shaykhiev, Yu. G. Kudenko, and A. N. Khotyantsev, *Searches for heavy neutrinos in the decays of positively charged kaons*, *Phys. Atom. Nucl.* **74** (2011) 788–793. [*Yad. Fiz.* **74**, 814(2011)].

- [237] E949: A. V. Artamonov *et. al.*, *Search for heavy neutrinos in $K^+ \rightarrow \mu^+ \nu_H$ decays*, *Phys. Rev. D* **91** (2015) 052001, [[arXiv:1411.3963](#)]. [Erratum: *Phys. Rev. D* 91, no. 5, 059903 (2015)].
- [238] NuTeV, E815: A. Vaitaitis *et. al.*, *Search for neutral heavy leptons in a high-energy neutrino beam*, *Phys. Rev. Lett.* **83** (1999) 4943–4946, [[hep-ex/9908011](#)].
- [239] DELPHI: P. Abreu *et. al.*, *A Study of the reaction $e^+e^- \rightarrow \mu^+\mu^-\gamma$ (ISR) at LEP and search for new physics at annihilation energies near 80-GeV*, *Z. Phys.* **C75** (1997) 581–592.
- [240] ATLAS: G. Aad *et. al.*, *Search for heavy Majorana neutrinos with the ATLAS detector in pp collisions at $\sqrt{s} = 8$ TeV*, *JHEP* **07** (2015) 162, [[arXiv:1506.06020](#)].
- [241] CMS Collaboration: A. M. Sirunyan *et. al.*, *Search for heavy neutral leptons in events with three charged leptons in proton-proton collisions at $\sqrt{s} = 13$ TeV*, *Phys. Rev. Lett.* **120** (2018) 221801, [[arXiv:1802.02965](#)].
- [242] H. P. Nilles, *Supersymmetry, Supergravity and Particle Physics*, *Phys. Rep.* **110** (1984) 1–162.
- [243] D. Matalliotakis and H. P. Nilles, *Implications of nonuniversality of soft terms in supersymmetric grand unified theories*, *Nucl. Phys. B* **435** (1995) 115–128, [[hep-ph/9407251](#)].
- [244] M. Olechowski and S. Pokorski, *Electroweak symmetry breaking with nonuniversal scalar soft terms and large $\tan \beta$ solutions*, *Phys. Lett. B* **344** (1995) 201–210, [[hep-ph/9407404](#)].
- [245] V. Berezhinsky, A. Bottino, *et. al.*, *Neutralino dark matter in supersymmetric models with nonuniversal scalar mass terms*, *Astropart. Phys.* **5** (1996) 1–26, [[hep-ph/9508249](#)].
- [246] M. Drees, M. M. Nojiri, D. P. Roy, and Y. Yamada, *Light Higgsino dark matter*, *Phys. Rev. D* **56** (1997) 276–290, [[hep-ph/9701219](#)]. [Erratum: *Phys. Rev. D* 64, 039901 (2001)].

- [247] P. Nath and R. L. Arnowitt, *Nonuniversal soft SUSY breaking and dark matter*, *Phys. Rev. D* **56** (1997) 2820–2832, [[hep-ph/9701301](#)].
- [248] D. S. Akerib, S. Alsum, *et. al.*, *Results from a Search for Dark Matter in the Complete LUX Exposure*, *Phys. Rev. Lett.* **118** (2017) 021303, [[arXiv:1608.07648](#)].
- [249] M. Schumann, L. Baudis, L. Bütikofer, A. Kish, and M. Selvi, *Dark matter sensitivity of multi-ton liquid xenon detectors*, *JCAP* **1510** (2015) 016, [[arXiv:1506.08309](#)].
- [250] DARWIN: J. Aalbers *et. al.*, *DARWIN: towards the ultimate dark matter detector*, *JCAP* **1611** (2016) 017, [[arXiv:1606.07001](#)].
- [251] ATLAS: M. Aaboud *et. al.*, *Search for electroweak production of supersymmetric particles in final states with two or three leptons at $\sqrt{s} = 13$ TeV with the ATLAS detector*, [arXiv:1803.02762](#).
- [252] CMS: A. M. Sirunyan *et. al.*, *Search for electroweak production of charginos and neutralinos in multilepton final states in proton-proton collisions at $\sqrt{s} = 13$ TeV*, *JHEP* **03** (2018) 166, [[arXiv:1709.05406](#)].
- [253] ATLAS Collaboration: M. Aaboud *et. al.*, *Search for chargino-neutralino production using recursive jigsaw reconstruction in final states with two or three charged leptons in proton-proton collisions at $\sqrt{s} = 13$ TeV with the ATLAS detector*, *Phys. Rev. D* **98** (2018) 092012, [[arXiv:1806.02293](#)].
- [254] ATLAS Collaboration: M. Aaboud *et. al.*, *Search for pair production of higgsinos in final states with at least three b-tagged jets in $\sqrt{s} = 13$ TeV pp collisions using the ATLAS detector*, *Submitted to: Phys. Rev.* (2018) [[arXiv:1806.04030](#)].
- [255] ATLAS Collaboration: M. Aaboud *et. al.*, *Search for supersymmetry in events with four or more leptons in $\sqrt{s} = 13$ TeV pp collisions with ATLAS*, *Phys. Rev. D* **98** (2018) 032009, [[arXiv:1804.03602](#)].
- [256] CMS: C. Collaboration, *Search for electroweak production of charginos and neutralinos in the WH final state in proton-proton collisions at $\sqrt{s} = 13$ TeV*, .

- [257] CMS: A. M. Sirunyan *et. al.*, *Search for new physics in events with two soft oppositely charged leptons and missing transverse momentum in proton-proton collisions at $\sqrt{s} = 13$ TeV*, [arXiv:1801.01846](#).
- [258] CMS: A. M. Sirunyan *et. al.*, *Search for new phenomena in final states with two opposite-charge, same-flavor leptons, jets, and missing transverse momentum in pp collisions at $\sqrt{s} = 13$ TeV*, *JHEP* **03** (2018) 076, [[arXiv:1709.08908](#)].
- [259] CMS Collaboration, *Search for electroweak production of charginos and neutralinos in multilepton final states in pp collision data at $\sqrt{s} = 13$ TeV*, CMS-PAS-SUS-16-039, 2017.
- [260] ATLAS Collaboration: G. Aad *et. al.*, *Search for direct pair production of a chargino and a neutralino decaying to the 125 GeV Higgs boson in $\sqrt{s} = 8$ TeV pp collisions with the ATLAS detector*, *Eur. Phys. J. C* **75** (2015) 208, [[arXiv:1501.07110](#)].
- [261] ATLAS Collaboration: Aad, Georges and others, *Search for direct production of charginos, neutralinos and sleptons in final states with two leptons and missing transverse momentum in pp collisions at $\sqrt{s} = 8$ TeV with the ATLAS detector*, *JHEP* **05** (2014) 071, [[arXiv:1403.5294](#)].
- [262] ATLAS Collaboration: G. Aad *et. al.*, *Search for direct production of charginos and neutralinos in events with three leptons and missing transverse momentum in $\sqrt{s} = 8$ TeV pp collisions with the atlas detector*, *JHEP* **1404** (2014) 169, [[arXiv:1402.7029](#)].
- [263] CMS Collaboration: V. Khachatryan *et. al.*, *Searches for electroweak production of charginos, neutralinos, and sleptons decaying to leptons and W, Z, and Higgs bosons in pp collisions at 8 TeV*, *Eur. Phys. J. C* **74** (2014) 3036, [[arXiv:1405.7570](#)].
- [264] V. Silveira and A. Zee, *Scalar Phantoms*, *Phys. Lett. B* **161** (1985) 136–140.
- [265] J. McDonald, *Gauge singlet scalars as cold dark matter*, *Phys. Rev. D* **50** (1994) 3637–3649, [[hep-ph/0702143](#)].

- [266] C. P. Burgess, M. Pospelov, and T. ter Veldhuis, *The Minimal Model of nonbaryonic dark matter: a singlet scalar*, *Nucl. Phys. B* **619** (2001) 709–728, [[hep-ph/0011335](#)].
- [267] H. Davoudiasl, R. Kitano, T. Li, and H. Murayama, *The New minimal standard model*, *Phys. Lett. B* **609** (2005) 117–123, [[hep-ph/0405097](#)].
- [268] A. Goudelis, Y. Mambrini, and C. Yaguna, *Antimatter signals of singlet scalar dark matter*, *JCAP* **12** (2009) 008, [[arXiv:0909.2799](#)].
- [269] C. E. Yaguna, *Gamma rays from the annihilation of singlet scalar dark matter*, *JCAP* **3** (2009) 003, [[arXiv:0810.4267](#)].
- [270] S. Profumo, L. Ubaldi, and C. Wainwright, *Singlet scalar dark matter: Monochromatic gamma rays and metastable vacua*, *Phys. Rev. D* **82** (2010) 1–10, [[arXiv:1009.5377](#)].
- [271] S. Andreas, C. Arina, T. Hambye, F.-S. Ling, and M. H. G. Tytgat, *A light scalar WIMP through the Higgs portal and CoGeNT*, *Phys. Rev. D* **82** (2010) 043522, [[arXiv:1003.2595](#)].
- [272] C. Arina and M. H. G. Tytgat, *Constraints on light WIMP candidates from the isotropic diffuse gamma-ray emission*, *JCAP* **1** (2011) 011, [[arXiv:1007.2765](#)].
- [273] Y. Mambrini, *Higgs searches and singlet scalar dark matter: Combined constraints from XENON 100 and the LHC*, *Phys. Rev. D* **84** (2011) 115017, [[arXiv:1108.0671](#)].
- [274] M. Raidal and A. Strumia, *Hints for a non-standard Higgs boson from the LHC*, *Phys. Rev. D* **84** (2011) 077701, [[arXiv:1108.4903](#)].
- [275] Y. Mambrini, *Higgs searches and singlet scalar dark matter: Combined constraints from XENON 100 and the LHC*, *Phys. Rev. D* **84** (2011) 115017, [[arXiv:1108.0671](#)].
- [276] X.-G. He and J. Tandean, *Hidden Higgs Boson at the LHC and Light Dark Matter Searches*, *Phys. Rev. D* **84** (2011) 075018, [[arXiv:1109.1277](#)].

- [277] A. Drozd, B. Grzadkowski, and J. Wudka, *Multi-Scalar-Singlet Extension of the Standard Model - the Case for Dark Matter and an Invisible Higgs Boson*, *JHEP* **04** (2012) 006, [[arXiv:1112.2582](#)].
[Erratum: *JHEP*11,130(2014)].
- [278] H. Okada and T. Toma, *Can A Higgs Portal Dark Matter be Compatible with the Anti-proton Cosmic-ray?*, *Phys. Lett. B* **713** (2012) 264–269, [[arXiv:1203.3116](#)].
- [279] N. Okada and O. Seto, *Gamma ray emission in Fermi bubbles and Higgs portal dark matter*, *Phys. Rev. D* **89** (2014) 043525, [[arXiv:1310.5991](#)].
- [280] J. M. Cline, K. Kainulainen, P. Scott, and C. Weniger, *Update on scalar singlet dark matter*, *Phys. Rev. D* **88** (2013) 055025, [[arXiv:1306.4710](#)].
- [281] Z. Chacko, Y. Cui, and S. Hong, *Exploring a Dark Sector Through the Higgs Portal at a Lepton Collider*, *Phys. Lett. B* **732** (2014) 75–80, [[arXiv:1311.3306](#)].
- [282] M. Endo and Y. Takaesu, *Heavy WIMP through Higgs portal at the LHC*, *Phys. Lett. B* **743** (2015) 228–234, [[arXiv:1407.6882](#)].
- [283] N. Craig, H. K. Lou, M. McCullough, and A. Thalapillil, *The Higgs Portal Above Threshold*, *JHEP* **02** (2016) 127, [[arXiv:1412.0258](#)].
- [284] L. Feng, S. Profumo, and L. Ubaldi, *Closing in on singlet scalar dark matter: LUX, invisible Higgs decays and gamma-ray lines*, *JHEP* **3** (2015) 45, [[arXiv:1412.1105](#)].
- [285] M. Duerr, P. Fileviez Pérez, and J. Smirnov, *Scalar singlet dark matter and gamma lines*, *Phys. Lett. B* **751** (2015) 119–122, [[arXiv:1508.04418](#)].
- [286] H. Han and S. Zheng, *Higgs-portal Scalar Dark Matter: Scattering Cross Section and Observable Limits*, *Nucl. Phys.* **B914** (2017) 248–256, [[arXiv:1510.06165](#)].
- [287] M. Duerr, P. F. Pérez, and J. Smirnov, *Gamma-ray excess and the minimal dark matter model*, *JHEP* **6** (2016) 8, [[arXiv:1510.07562](#)].

- [288] X.-G. He and J. Tandean, *New LUX and PandaX-II Results Illuminating the Simplest Higgs-Portal Dark Matter Models*, *JHEP* **12** (2016) 074, [[arXiv:1609.03551](#)].
- [289] H. Han, J. M. Yang, Y. Zhang, and S. Zheng, *Collider Signatures of Higgs-portal Scalar Dark Matter*, *Phys. Lett. B* **756** (2016) 109–112, [[arXiv:1601.06232](#)].
- [290] G. Dupuis, *Collider Constraints and Prospects of a Scalar Singlet Extension to Higgs Portal Dark Matter*, *JHEP* **07** (2016) 008, [[arXiv:1604.04552](#)].
- [291] T. Binder, T. Bringmann, M. Gustafsson, and A. Hryczuk, *Early kinetic decoupling of dark matter: when the standard way of calculating the thermal relic density fails*, *Phys. Rev. D* **96** (2017) 115010, [[arXiv:1706.07433](#)].
- [292] K. Ghorbani and P. H. Ghorbani, *Strongly First-Order Phase Transition in Real Singlet Scalar Dark Matter Model*, [arXiv:1804.05798](#).
- [293] C.-W. Chiang, Y.-T. Li, and E. Senaha, *Revisiting electroweak phase transition in the standard model with a real singlet scalar*, *Phys. Lett. B* **789** (2019) 154–159, [[arXiv:1808.01098](#)].
- [294] P. Stöcker, M. Krämer, J. Lesgourgues, and V. Poulin, *Exotic energy injection with ExoCLASS: Application to the Higgs portal model and evaporating black holes*, *JCAP* **1803** (2018) 018, [[arXiv:1801.01871](#)].
- [295] E. Hardy, *Higgs portal dark matter in non-standard cosmological histories*, *JHEP* **06** (2018) 043, [[arXiv:1804.06783](#)].
- [296] N. Bernal, C. Cosme, T. Tenkanen, and V. Vaskonen, *Scalar singlet dark matter in non-standard cosmologies*, *Eur. Phys. J. C* **79** (2019) 30, [[arXiv:1806.11122](#)].
- [297] A. Glioti, R. Rattazzi, and L. Vecchi, *Electroweak Baryogenesis above the Electroweak Scale*, *JHEP* **04** (2019) 027, [[arXiv:1811.11740](#)].
- [298] A. Urbano and W. Xue, *Constraining the Higgs portal with antiprotons*, *JHEP* **03** (2015) 133, [[arXiv:1412.3798](#)].

- [299] M. Escudero, A. Berlin, D. Hooper, and M.-X. Lin, *Toward (Finally!) Ruling Out Z and Higgs Mediated Dark Matter Models*, *JCAP* **1612** (2016) 029, [[arXiv:1609.09079](#)].
- [300] S. Kanemura, S. Matsumoto, T. Nabeshima, and H. Taniguchi, *Testing Higgs portal dark matter via Z fusion at a linear collider*, *Phys. Lett. B* **701** (2011) 591–596, [[arXiv:1102.5147](#)].
- [301] A. Djouadi, O. Lebedev, Y. Mambrini, and J. Quevillon, *Implications of LHC searches for Higgs–portal dark matter*, *Phys. Lett. B* **709** (2012) 65–69, [[arXiv:1112.3299](#)].
- [302] A. Djouadi, A. Falkowski, Y. Mambrini, and J. Quevillon, *Direct Detection of Higgs-Portal Dark Matter at the LHC*, *Eur. Phys. J.* **C73** (2013) 2455, [[arXiv:1205.3169](#)].
- [303] F. Bishara, J. Brod, P. Uttayarat, and J. Zupan, *Nonstandard Yukawa Couplings and Higgs Portal Dark Matter*, *JHEP* **01** (2016) 010, [[arXiv:1504.04022](#)].
- [304] P. Ko and H. Yokoya, *Search for Higgs portal DM at the ILC*, *JHEP* **08** (2016) 109, [[arXiv:1603.04737](#)].
- [305] A. Beniwal, F. Rajec, *et. al.*, *Combined analysis of effective Higgs portal dark matter models*, *Phys. Rev. D* **93** (2016) 115016, [[arXiv:1512.06458](#)].
- [306] T. Kamon, P. Ko, and J. Li, *Characterizing Higgs portal dark matter models at the ILC*, *Eur. Phys. J.* **C77** (2017) 652, [[arXiv:1705.02149](#)].
- [307] B. Dutta, T. Kamon, P. Ko, and J. Li, *Prospects for discovery and spin discrimination of dark matter in Higgs portal DM models and their extensions at 100 TeV pp collider*, *Eur. Phys. J. C* **78** (2018) 595, [[arXiv:1712.05123](#)].
- [308] R. Dick, *Direct signals from electroweak singlets through the Higgs portal*, *Int. J. Mod. Phys. D* **27** (2018) 1830008, [[arXiv:1804.02604](#)].
- [309] C.-H. Chen and T. Nomura, *Searching for vector dark matter via Higgs portal at the LHC*, *Phys. Rev. D* **93** (2016) 074019, [[arXiv:1507.00886](#)].

- [310] A. DiFranzo, P. J. Fox, and T. M. P. Tait, *Vector Dark Matter through a Radiative Higgs Portal*, *JHEP* **04** (2016) 135, [[arXiv:1512.06853](#)].
- [311] M. Heikinheimo, T. Tenkanen, and K. Tuominen, *WIMP miracle of the second kind*, *Phys. Rev. D* **96** (2017) 023001, [[arXiv:1704.05359](#)].
- [312] S. Baek, P. Ko, and W.-I. Park, *Invisible Higgs Decay Width vs. Dark Matter Direct Detection Cross Section in Higgs Portal Dark Matter Models*, *Phys. Rev. D* **90** (2014) 055014, [[arXiv:1405.3530](#)].
- [313] L. Lopez-Honorez, T. Schwetz, and J. Zupan, *Higgs portal, fermionic dark matter, and a Standard Model like Higgs at 125 GeV*, *Phys. Lett. B* **716** (2012) 179–185, [[arXiv:1203.2064](#)].
- [314] M. A. Fedderke, J.-Y. Chen, E. W. Kolb, and L.-T. Wang, *The Fermionic Dark Matter Higgs Portal: an effective field theory approach*, *JHEP* **08** (2014) 122, [[arXiv:1404.2283](#)].
- [315] S. Matsumoto, S. Mukhopadhyay, and Y.-L. S. Tsai, *Singlet Majorana fermion dark matter: a comprehensive analysis in effective field theory*, *JHEP* **10** (2014) 155, [[arXiv:1407.1859](#)].
- [316] A. Freitas, S. Westhoff, and J. Zupan, *Integrating in the Higgs Portal to Fermion Dark Matter*, *JHEP* **09** (2015) 015, [[arXiv:1506.04149](#)].
- [317] M. Duch, B. Grzadkowski, and M. McGarrie, *A stable Higgs portal with vector dark matter*, *JHEP* **09** (2015) 162, [[arXiv:1506.08805](#)].
- [318] S. Baek, P. Ko, M. Park, W.-I. Park, and C. Yu, *Beyond the Dark matter effective field theory and a simplified model approach at colliders*, *Phys. Lett. B* **756** (2016) 289–294, [[arXiv:1506.06556](#)].
- [319] G. Bélanger, K. Kannike, A. Pukhov, and M. Raidal, *Z_3 scalar singlet dark matter*, *JCAP* **1** (2013) 022, [[arXiv:1211.1014](#)].
- [320] Z. Kang, P. Ko, and T. Matsui, *Strong first order EWPT & strong gravitational waves in Z_3 -symmetric singlet scalar extension*, *JHEP* **02** (2018) 115, [[arXiv:1706.09721](#)].
- [321] S. Bhattacharya, P. Ghosh, T. N. Maity, and T. S. Ray, *Mitigating direct detection bounds in non-minimal Higgs portal scalar dark matter models*, *JHEP* **10** (2017) 88, [[arXiv:1706.04699](#)].

- [322] A. Hektor, A. Hryczuk, and K. Kannike, *Improved bounds on \mathbb{Z}_3 singlet dark matter*, *JHEP* **03** (2019) 204, [[arXiv:1901.08074](#)].
- [323] K. Kannike, K. Loos, and M. Raidal, *Gravitational Wave Signals of Pseudo-Goldstone Dark Matter in the \mathbb{Z}_3 Complex Singlet Model*, [arXiv:1907.13136](#).
- [324] XENON: E. Aprile *et. al.*, *Dark Matter Search Results from a One Ton-Year Exposure of XENON1T*, *Phys. Rev. Lett.* **121** (2018) 111302, [[arXiv:1805.12562](#)].
- [325] XENON: E. Aprile *et. al.*, *First Dark Matter Search Results from the XENON1T Experiment*, *Phys. Rev. Lett.* **119** (2017) 181301, [[arXiv:1705.06655](#)].
- [326] PandaX-II: X. Cui *et. al.*, *Dark Matter Results From 54-Ton-Day Exposure of PandaX-II Experiment*, *Phys. Rev. Lett.* **119** (2017) 181302, [[arXiv:1708.06917](#)].
- [327] G. Belanger, B. Dumont, U. Ellwanger, J. F. Gunion, and S. Kraml, *Global fit to Higgs signal strengths and couplings and implications for extended Higgs sectors*, *Phys. Rev. D* **88** (2013) 075008, [[arXiv:1306.2941](#)].
- [328] CMS Collaboration, *Search for invisible decays of the Higgs boson produced through vector boson fusion at $\sqrt{s} = 13$ TeV*, CMS-PAS-HIG-17-023, 2018.
- [329] LZ: D. S. Akerib *et. al.*, *LUX-ZEPLIN (LZ) Conceptual Design Report*, [arXiv:1509.02910](#).
- [330] N. Bell, G. Busoni, A. Kobakhidze, D. M. Long, and M. A. Schmidt, *Unitarisation of EFT Amplitudes for Dark Matter Searches at the LHC*, *JHEP* **08** (2016) 125, [[arXiv:1606.02722](#)].
- [331] S. Balaji and A. Kobakhidze, *More stringent constraints on the unitarised fermionic dark matter Higgs portal*, [arXiv:1812.10914](#).
- [332] J. Preskill, M. B. Wise, and F. Wilczek, *Cosmology of the invisible axion*, *Phys. Lett. B* **120** (1983) 127–132.

- [333] L. F. Abbott and P. Sikivie, *A cosmological bound on the invisible axion*, *Phys. Lett. B* **120** (1983) 133–136.
- [334] M. Dine and W. Fischler, *The not-so-harmless axion*, *Phys. Lett. B* **120** (1983) 137–141.
- [335] M. S. Turner, *Cosmic and local mass density of “invisible” axions*, *Phys. Rev. D* **33** (1986) 889–896.
- [336] J. Isern, M. Hernanz, and E. Garcia-Berro, *Axion cooling of white dwarfs*, *Astrophys. J.* **392** (1992) L23.
- [337] A. H. Córscico, L. G. Althaus, *et. al.*, *The rate of cooling of the pulsating white dwarf star G117-B15A: a new asteroseismological inference of the axion mass*, *MNRAS* **424** (2012) 2792–2799, [[arXiv:1205.6180](#)].
- [338] A. H. Córscico, L. G. Althaus, *et. al.*, *An independent limit on the axion mass from the variable white dwarf star R548*, *JCAP* **12** (2012) 010, [[arXiv:1211.3389](#)].
- [339] M. Giannotti, I. Irastorza, J. Redondo, and A. Ringwald, *Cool WISPs for stellar cooling excesses*, *JCAP* **5** (2016) 057, [[arXiv:1512.08108](#)].
- [340] A. H. Córscico, A. D. Romero, *et. al.*, *An asteroseismic constraint on the mass of the axion from the period drift of the pulsating DA white dwarf star L19-2*, *JCAP* **7** (2016) 036, [[arXiv:1605.06458](#)].
- [341] T. Battich, A. H. Córscico, L. G. Althaus, and M. M. Miller Bertolami, *First axion bounds from a pulsating helium-rich white dwarf star*, *JCAP* **8** (2016) 062, [[arXiv:1605.07668](#)].
- [342] M. Giannotti, I. G. Irastorza, J. Redondo, A. Ringwald, and K. Saikawa, *Stellar recipes for axion hunters*, *JCAP* **10** (2017) 010, [[arXiv:1708.02111](#)].
- [343] A. De Angelis, M. Roncadelli, and O. Mansutti, *Evidence for a new light spin-zero boson from cosmological gamma-ray propagation?*, *Phys. Rev. D* **76** (2007) 121301, [[arXiv:0707.4312](#)].
- [344] M. Simet, D. Hooper, and P. D. Serpico, *Milky Way as a kiloparsec-scale axionscope*, *Phys. Rev. D* **77** (2008) 063001, [[arXiv:0712.2825](#)].

- [345] I. F. M. Albuquerque and A. Chou, *A faraway quasar in the direction of the highest energy Auger event*, *JCAP* **8** (2010) 016, [[arXiv:1001.0972](#)].
- [346] A. de Angelis, G. Galanti, and M. Roncadelli, *Relevance of axionlike particles for very-high-energy astrophysics*, *Phys. Rev. D* **84** (2011) 105030, [[arXiv:1106.1132](#)].
- [347] D. Horns and M. Meyer, *Indications for a pair-production anomaly from the propagation of VHE gamma-rays*, *JCAP* **1202** (2012) 033, [[arXiv:1201.4711](#)].
- [348] M. Meyer, D. Horns, and M. Raue, *First lower limits on the photon-axion-like particle coupling from very high energy gamma-ray observations*, *Phys. Rev. D* **87** (2013) 035027, [[arXiv:1302.1208](#)].
- [349] J. M. Pendlebury, S. Afach, *et. al.*, *Revised experimental upper limit on the electric dipole moment of the neutron*, *Phys. Rev. D* **92** (2015) 092003, [[arXiv:1509.04411](#)].
- [350] R. D. Peccei and H. R. Quinn, *CP conservation in the presence of pseudoparticles*, *Phys. Rev. Lett.* **38** (1977) 1440–1443.
- [351] R. D. Peccei and H. R. Quinn, *Constraints imposed by CP conservation in the presence of pseudoparticles*, *Phys. Rev. D* **16** (1977) 1791–1797.
- [352] C. Vafa and E. Witten, *Restrictions on symmetry breaking in vector-like gauge theories*, *Nuclear Physics B* **234** (1984) 173–188.
- [353] C. Vafa and E. Witten, *Parity Conservation in Quantum Chromodynamics*, *Phys. Rev. Lett.* **53** (1984) 535–536.
- [354] J. E. Kim, *Light pseudoscalars, particle physics and cosmology*, *Physics Reports* **150** (1987) 1–177.
- [355] J. Jaeckel and A. Ringwald, *The Low-Energy Frontier of Particle Physics*, *Annual Review of Nuclear and Particle Science* **60** (2010) 405–437, [[arXiv:1002.0329](#)].
- [356] I. G. Irastorza and J. Redondo, *New experimental approaches in the search for axion-like particles*, *Progress in Particle and Nuclear Physics* **102** (2018) 89–159, [[arXiv:1801.08127](#)].

- [357] D. B. Kaplan, *Opening the axion window*, *Nuclear Physics B* **260** (1985) 215–226.
- [358] M. Srednicki, *Axion couplings to matter*, *Nuclear Physics B* **260** (1985) 689–700.
- [359] H. Georgi, D. B. Kaplan, and L. Randall, *Manifesting the invisible axion at low energies*, *Phys. Lett. B* **169** (1986) 73–78.
- [360] G. Grilli di Cortona, E. Hardy, J. Pardo Vega, and G. Villadoro, *The QCD axion, precisely*, *JHEP* **01** (2016) 034, [[arXiv:1511.02867](#)].
- [361] M. Gorghetto and G. Villadoro, *Topological Susceptibility and QCD Axion Mass: QED and NNLO corrections*, *JHEP* **03** (2019) 033, [[arXiv:1812.01008](#)].
- [362] J. E. Kim, *Weak-Interaction Singlet and Strong CP Invariance*, *Phys. Rev. Lett.* **43** (1979) 103–107.
- [363] M. Shifman, A. Vainshtein, and V. Zakharov, *Can confinement ensure natural CP invariance of strong interactions?*, *Nuclear Physics B* **166** (1980) 493–506.
- [364] A. R. Zhitnitskij, *On possible suppression of the axion-hadron interactions*, *Soviet Journal of Nuclear Physics* **31** (1980) 260.
- [365] M. Dine, W. Fischler, and M. Srednicki, *A simple solution to the strong CP problem with a harmless axion*, *Phys. Lett. B* **104** (1981) 199–202.
- [366] K. Ehret, M. Frede, *et. al.*, *New ALPS results on hidden-sector lightweights*, *Phys. Lett. B* **689** (2010) 149–155, [[arXiv:1004.1313](#)].
- [367] A. M. Serenelli, S. Basu, J. W. Ferguson, and M. Asplund, *New Solar Composition: The Problem with Solar Models Revisited*, *ApJ* **705** (2009) L123–L127, [[arXiv:0909.2668](#)].
- [368] M. Asplund, N. Grevesse, A. J. Sauval, and P. Scott, *The chemical composition of the Sun*, *ARA&A* **47** (2009) 481–522, [[arXiv:0909.0948](#)].
- [369] N. Vinyoles, A. M. Serenelli, *et. al.*, *A New Generation of Standard Solar Models*, *ApJ* **835** (2017) 202, [[arXiv:1611.09867](#)].

- [370] S. Andriamonje, S. Aune, *et. al.*, *An improved limit on the axion photon coupling from the CAST experiment*, *JCAP* **4** (2007) 010, [[hep-ex/0702006](#)].
- [371] V. Anastassopoulos, S. Aune, *et. al.*, *New CAST limit on the axion-photon interaction*, *Nature Physics* **13** (2017) 584–590, [[arXiv:1705.02290](#)].
- [372] P. Sikivie, *Experimental Tests of the “Invisible” Axion*, *Phys. Rev. Lett.* **51** (1983) 1415–1417. Erratum in [[416](#)].
- [373] P. Sikivie, *Detection rates for “invisible”-axion searches*, *Phys. Rev. D* **32** (1985) 2988–2991. Erratum in [[417](#)].
- [374] J. Hoskins, J. Hwang, *et. al.*, *Search for nonvirialized axionic dark matter*, *Phys. Rev. D* **84** (2011) [[arXiv:1109.4128](#)].
- [375] S. De Panfilis, A. C. Melissinos, B. E. Moskowitz, J. T. Rogers, and Y. K. Semertzidis, *Limits on the abundance and coupling of cosmic axions at $m(a)$ of between 4.5 and 5.0 microeV*, *Phys. Rev. Lett.* **59** (1987) 839–842.
- [376] W. U. Wuensch, S. de Panfilis-Wuensch, *et. al.*, *Results of a laboratory search for cosmic axions and other weakly coupled light particles*, *Phys. Rev. D* **40** (1989) 3153–3167.
- [377] C. Hagmann, P. Sikivie, N. S. Sullivan, and D. B. Tanner, *Results from a search for cosmic axions*, *Phys. Rev. D* **42** (1990) 1297–1300.
- [378] C. Hagmann, D. Kinion, *et. al.*, *Results from a High-Sensitivity Search for Cosmic Axions*, *Phys. Rev. Lett.* **80** (1998) 2043–2046, [[astro-ph/9801286](#)].
- [379] S. Asztalos, E. Daw, *et. al.*, *Large-scale microwave cavity search for dark-matter axions*, *Phys. Rev. D* **64** (2001) 092003.
- [380] S. J. Asztalos, R. F. Bradley, *et. al.*, *Improved rf cavity search for halo axions*, *Phys. Rev. D* **69** (2004) 011101, [[astro-ph/0310042](#)].
- [381] L. D. Duffy, P. Sikivie, *et. al.*, *High resolution search for dark-matter axions*, *Phys. Rev. D* **74** (2006) 012006, [[astro-ph/0603108](#)].

- [382] S. J. Asztalos, G. Carosi, *et. al.*, *SQUID-Based Microwave Cavity Search for Dark-Matter Axions*, *Phys. Rev. Lett.* **104** (2010) 041301, [[arXiv:0910.5914](#)].
- [383] N. Du, N. Force, *et. al.*, *Search for Invisible Axion Dark Matter with the Axion Dark Matter Experiment*, *Phys. Rev. Lett.* **120** (2018) 151301, [[arXiv:1804.05750](#)].
- [384] G. Raffelt and L. Stodolsky, *Mixing of the photon with low-mass particles*, *Phys. Rev. D* **37** (1988) 1237–1249.
- [385] C. Csáki, N. Kaloper, and J. Terning, *Dimming Supernovae without Cosmic Acceleration*, *Phys. Rev. Lett.* **88** (2002) 161302, [[hep-ph/0111311](#)].
- [386] Y. Grossman, S. Roy, and J. Zupan, *Effects of initial axion production and photon-axion oscillation on type Ia supernova dimming*, *Phys. Lett. B* **543** (2002) 23–28, [[hep-ph/0204216](#)].
- [387] A. Mirizzi, G. G. Raffelt, and P. D. Serpico, *Signatures of axionlike particles in the spectra of TeV gamma-ray sources*, *Phys. Rev. D* **76** (2007) 023001, [[arXiv:0704.3044](#)].
- [388] D. Wouters and P. Brun, *Irregularity in gamma ray source spectra as a signature of axionlike particles*, *Phys. Rev. D* **86** (2012) 043005, [[arXiv:1205.6428](#)].
- [389] G. Galanti and M. Roncadelli, *Comment on “Irregularity in gamma ray source spectra as a signature of axion-like particles”*, *ArXiv e-prints* (2013) [[arXiv:1305.2114](#)].
- [390] A. Abramowski, F. Acero, *et. al.*, *Constraints on axionlike particles with H.E.S.S. from the irregularity of the PKS 2155-304 energy spectrum*, *Phys. Rev. D* **88** (2013) 102003, [[arXiv:1311.3148](#)].
- [391] E. L. Chupp, W. T. Vestrand, and C. Reppin, *Experimental limits on the radiative decay of SN 1987A neutrinos*, *Phys. Rev. Lett.* **62** (1989) 505–508.
- [392] A. Payez, C. Evoli, *et. al.*, *Revisiting the SN1987A gamma-ray limit on ultralight axion-like particles*, *JCAP* **1502** (2015) 006, [[arXiv:1410.3747](#)].

- [393] K. Sato and H. Sato, *Higgs meson emission from a star and a constraint on its mass*, *Progress of Theoretical Physics* **54** (1975) 1564.
- [394] G. G. Raffelt, *Astrophysical methods to constrain axions and other novel particle phenomena*, *Phys. Rep.* **198** (1990) 1–113.
- [395] G. G. Raffelt, *Stars as Laboratories for Fundamental Physics: The Astrophysics of Neutrinos, Axions, and Other Weakly Interacting Particles*. University Of Chicago Press, Chicago & London, 1996.
- [396] A. Buzzoni, F. F. Pecci, R. Buonanno, and C. E. Corsi, *Helium abundance in globular clusters - The R-method*, *A&A* **128** (1983) 94–101.
- [397] G. G. Raffelt, *Core mass at the helium flash from observations and a new bound on neutrino electromagnetic properties*, *ApJ* **365** (1990) 559–568.
- [398] N. Viaux, M. Catelan, *et. al.*, *Neutrino and Axion Bounds from the Globular Cluster M5 (NGC 5904)*, *Phys. Rev. Lett.* **111** (2013) 231301, [[arXiv:1311.1669](#)].
- [399] A. Ayala, I. Domínguez, M. Giannotti, A. Mirizzi, and O. Straniero, *Revisiting the Bound on Axion-Photon Coupling from Globular Clusters*, *Phys. Rev. Lett.* **113** (2014) 191302, [[arXiv:1406.6053](#)].
- [400] M. Salaris, M. Riello, S. Cassisi, and G. Piotto, *The initial helium abundance of the Galactic globular cluster system*, *A&A* **420** (2004) 911–919, [[astro-ph/0403600](#)].
- [401] H. Jeffreys, *The Theory of Probability*. Oxford Classic Texts in the Physical Sciences. Oxford University Press, 1939.
- [402] R. E. Kass and A. E. Raftery, *Bayes factors*, *Journal of the American Statistical Association* **90** (1995) 773–795.
- [403] J. O. Berger, L. R. Pericchi, *et. al.*, *Objective Bayesian Methods for Model Selection: Introduction and Comparison*, *Lecture Notes-Monograph Series* **38** (2001) 135–207.
- [404] M. Fukugita and T. Yanagida, *Baryogenesis Without Grand Unification*, *Phys. Lett. B* **174** (1986) 45–47.

- [405] E. K. Akhmedov, V. A. Rubakov, and A. Yu. Smirnov, *Baryogenesis via neutrino oscillations*, *Phys. Rev. Lett.* **81** (1998) 1359–1362, [[hep-ph/9803255](#)].
- [406] T. Asaka and M. Shaposhnikov, *The nuMSM, dark matter and baryon asymmetry of the universe*, *Phys. Lett. B* **620** (2005) 17–26, [[hep-ph/0505013](#)].
- [407] S. Dodelson and L. M. Widrow, *Sterile-neutrinos as dark matter*, *Phys. Rev. Lett.* **72** (1994) 17–20, [[hep-ph/9303287](#)].
- [408] X.-D. Shi and G. M. Fuller, *A New dark matter candidate: Nonthermal sterile neutrinos*, *Phys. Rev. Lett.* **82** (1999) 2832–2835, [[astro-ph/9810076](#)].
- [409] J. A. Casas and A. Ibarra, *Oscillating neutrinos and $\mu \rightarrow e, \gamma$* , *Nucl. Phys.* **B618** (2001) 171–204, [[hep-ph/0103065](#)].
- [410] J. Lopez-Pavon, E. Molinaro, and S. T. Petcov, *Radiative Corrections to Light Neutrino Masses in Low Scale Type I Seesaw Scenarios and Neutrinoless Double Beta Decay*, *JHEP* **11** (2015) 030, [[arXiv:1506.05296](#)].
- [411] J. Schechter and J. W. F. Valle, *Neutrino Masses in $SU(2) \times U(1)$ Theories*, *Phys. Rev.* **D22** (1980) 2227.
- [412] P. F. de Salas, D. V. Forero, C. A. Ternes, M. Tórtola, and J. W. F. Valle, *Status of neutrino oscillations 2018: 3σ hint for normal mass ordering and improved CP sensitivity*, *Phys. Lett.* **B782** (2018) 633–640, [[arXiv:1708.01186](#)].
- [413] F. Capozzi, E. Lisi, A. Marrone, and A. Palazzo, *Current unknowns in the three neutrino framework*, *Prog. Part. Nucl. Phys.* **102** (2018) 48–72, [[arXiv:1804.09678](#)].
- [414] P. Scott, *Pippi – painless parsing, post-processing and plotting of posterior and likelihood samples*, *Eur. Phys. J. Plus* **127** (2012) 138, [[arXiv:1206.2245](#)].
- [415] Particle Data Group: C. Patrignani *et. al.*, *Review of Particle Physics*, *Chin. Phys. C* **40** (2016) 100001.

- [416] P. Sikivie, *Experimental Tests of the “Invisible” Axion*, *Phys. Rev. Lett.* **52** (1984) 695. (Erratum).
- [417] P. Sikivie, *Erratum: Detection rates for “invisible”-axion searches*, *Phys. Rev. D* **36** (1987) 974.